COLUMNAS LIQUIDAS EN CONDICIONES DE INGRAVIDEZ

INFORME FINAL AÑO 1986

Lamf-ETSIA, Laboratorio de Aerodinámica

E.T.S.I. Aeronáuticos, Ciudad Universitaria

28040 Madrid

Expediente CONIE 267/86

Madrid, Diciembre de 1986

Ref.: Lamf 8612

EXPEDIENTE CONIE No. 267/86

COLUMNAS LIQUIDAS EN CONDICIONES DE INGRAVIDEZ

Convenio de Investigación entre la Comisión Nacional de Investigación del Espacio (CONIE) y la Universidad Politécnica de Madrid (UPM), desarrollado por el Laboratorio de Aerodinámica de la Escuela Técnica Superior de Ingenieros Aeronáuticos (ETSIA), durante el año 1986.

Director del trabajo: Ignacio Da Riva de la Cavada

Colaboradores: Isidoro Martínez Herranz
José Meseguer Ruiz
Angel Pedro Sanz Andrés
Damián Rivas Rivas
José Manuel Perales Perales
Jesús López Díez

MEMORIA DE ACTIVIDADES DURANTE 1986

La producción científica relacionada con el contrato de investigación entre la CONIE y la UPM para el estudio del comportamiento de las columnas líquidas en condiciones de microgravedad, ha sido prolífica durante este año, alcanzando la cifra récor de ocho artículos entre los presentados en congresos internacionales y los enviados para su publicación en revistas científicas de archivo.

Podría incluso decirse que se ha publicado demasiado, pues como fácilmente se puede apreciar, parte de la información presentada es redundante (algunas figuras se repiten en varios artículos), pero la justificación es la siguiente. Después del éxito obtenido en la realización de los experimentos a bordo del Spacelab-D1 en Noviembre de 1985, la comunidad científica está muy interesada en ir conociendo cuanto antes los resultados que se van obteniendo en el análisis de la enorme cantidad de datos recogidos en aquellas tres horas de ensayos.

Todavía hoy, un año después del vuelo, quedan por analizar algunas secuencias (las de vibración forzada, principalmente). Pero tampoco se debe concluir de este hecho que basta con una oportunidad de experimentación en el espacio cada dos años para saturar la capacidad de trabajo de un grupo de investigación como éste; se trata de un problema coyuntural. En efecto, uno de los factores determinantes de este lento desarrollo es la falta de una infraestructura moderna de tratamiento de datos, que hubiese posibilitado la recepción de esa ingente cantidad de

información proveniente del Spacelab directamente en Madrid, en formato de acceso directo por ordenador, en lugar de tener que pasar por el penoso trabajo de tener que pedir listados impresos al centro de control alemán, introducirlos manualmente en nuestros ordenadores, comprobar que nos hacían falta más detalles, volver a pedir gruesos listados, volver a introducirlos manualmente, modificar nuestras bases de datos, etc. El problema más acuciante ha sido la digitalización manual de las dos mil fotografías obtenidas de las columnas líquidas (de hecho, tan sólo se han digitalizado unas 500, las más representativas). Y tampoco debe atribuirse a una falta de planificación de recursos, ya que no hubiera resultado sensato adquirir costosos equipos de tratamiento automático de imágenes en espera del éxito de los ensayos en vuelo (los resultados del Spacelab-1 de 1983 no merecían este esfuerzo)

Así pues, el trabajo realizado durante el año 1986 está dedicado fundamentalmente al análisis de la información obtenida en el experimento "Floating Liquid Zones" (FLIZ), realizado a bordo del Spacelab-D1 (segunda misión europea de este laboratorio espacial).

Adelantando resultados que se presentan con más detalle en el informe que sigue, cabe señalar que la secuencia experimental discurrió de acuerdo con lo estipulado en los procedimientos, aunque más lentamente de lo previsto (es de destacar el interés mostrado por el astronauta Dr. R. Furrer, quien dedicó una parte importante de su tiempo libre a la repetición de aspectos del experimento FLIZ que no resultaron totalmente satisfactorios en un primer intento, dedicando algo más de tres horas a nuestro experimento frente a los 90 minutos asignados oficialmente).

La causa principal de la lenta ejecución del experimento fue el alto nivel de ruido (en comparación con los requerimientos de nuestro experimento) existente durante la misión D1, lo que ocasionó la rotura del puente líquido repetidas veces. Sin embargo, este hecho más que un inconveniente ha supueso una ventaja por cuanto que ha permitido disponer de información adicional con la que contrastar los modelos teóricos de rotura del puente líquido.

En el Volumen I de este Informe Final se presentan seis artículos que han supuesto otros tantos comunicados a la comunidad científica internacional. El primero de ellos, publicado en la revista alemana Natur Wissenschaften, es una somera descripción del experimento FLIZ y los primeros resultados. En el segundo, presentado en Norderney (Alemania) se analiza con más detalle la secuencia experimental, estableciendo las consecuencias que se derivan del experimento. Los dos siguientes están dedicados al estudio de aspectos parciales del experimento. Así, la atención del tercer artículo (presentado en el XXXVII Congreso de la Federación Astronáutica Internacional, celebrado en Insbruck, Austria) se centra fundamentalmente en los ensayos de rotación, mientras que en el cuarto (de próxima aparición en el Journal of Crystal Growth) se analizan, básicamente, los fenómenos de rotura del puente líquido.

El quinto artículo, presentado en el 6th European Symposium on Material Sciences under Microgravity Conditions, celebrado en Burdeos (Francia), ofrece una panorámica del trabajo de análisis e interpretación del experimento FLIZ realizado hasta la fecha y, por último, en el sexto artículo se presenta un estudio de la respuesta del puente líquido a

perturbaciones aleatorias, trabajo que será publicado próximamente.

En el Volumen II se incluyen resultados obtenidos en los apartados de análisis y optimización de técnicas de experimentación en microgravedad simulada y en el de análisis de transmisión de calor. En el primer capítulo ("One-dimensional linear analysis of the liquid injection or removal in a liquid bridge", enviado para su publicación en Acta Astronautica) se aborda de un modo teórico el problema de la dinámica de la inyección o succión de fluido en un puente líquido. Actualmente el estudio está limitado a un análisis lineal, paso previo para aproximaciones más exactas.

En el segundo capítulo se muestra una propuesta presentada a la Agencia Europea del Espacio (ESA) para la construcción de un equipo telemandado para la experimentación con puentes líquidos en microgravedad simulada. En el trabajo (que sería realizado en cooperación con la industria española) se identifican los parámetros a controlar, así como el rango de las diversas variables y las diversas interrelaciones entre las mismas. Desgraciadamente no parece, por el momento, que la ESA vaya a suministrar los fondos para el desarrollo del equipo, por cuanto que se piensa que tales fondos deberían ser proporcionados por la agencia nacional.

En el tercer capítulo se analiza el proceso de solidificación de una gota líquida mediante un modelo en el que los problemas térmico e interfacial resultan desacoplados. El mayor interés del trabajo (de próxima aparición en la revista Journal of Crystal Growth) es que proporciona un método para medir de un modo relativamente simple el ángulo existente entre las

entrefases sólido-gas y fundido-gas en el avance de un frente de solidificación.

En el siguiente capítulo, escrito en colaboración con el Dr. A. Eyer, de Kristallographisches Institut der Universitat (FRG), se analiza, a través de un modelo simplificado, los resultados obtenidos en un experimento de crecimiento de monocristales de silicio por la técnica de la zona flotante, realizado durante la misión Spacelab-1 en 1983.

En el quinto capítulo se presenta la descripción de un nuevo equipo para el estudio experimental, mediante la técnica de la flotabilidad neutra (tanque de Plateau), de los modos de oscilación no axilsimétricos del puente líquido.

Finalmente, en el último apartado, se recogen las nuevas propuestas de experimentación, tanto en el Spacelab como en cohetes de sondeo, remitidas a la Agencia Espacial Europea.

INDICE

VOLUMEN I

VOLUMEN II

Naturwissenschaften

Floating Liquid Zones

I. Da Rivá and I. Martínez
Universidad Politécnica de Madrid, Spain

The aim of our experiment on the Spacelab D1 Mission was to study the stability of long liquid columns under microgravity. Nominal configuration was a cylindrical liquid bridge anchored at the edges of two equal solid discs, 35 mm in diameter. Mechanical stimuli were applied through the discs and the liquid outer shape recorded for analysis.

Nominal experiment procedures [1] were similar to those proposed for Spacelab-1 (1983), where by wetting problems allowed only partial success [2]. The same Fluid Physics Module, but with corrected end discs and a manually operated syringe for liquid injection, was used.

Experiment

Payload specialist Dr. Furrer was in charge of the experiment in flight, assisted by Dr. Martínez on ground when voice and video link was available. Start time was Mission Elapsed Time 5/23:35:00 and the experiment proceeded as expected, with the following deviations:

It was soon realized that g-jitter (Fig. 1) was much higher from Spacelab-1 and Texus-12 experience [3]. Long columns were continuously trembling.

This noisy ambient stressed the operator, who on the first trial followed a slightly scarce filling law that caused the first disruption of the column (Fig. 2) soon after the nominal working length $L=$ 95 mm was reached.

Experiment reinitiation was achieved thanks to the skillful operator (and not once, but five times),

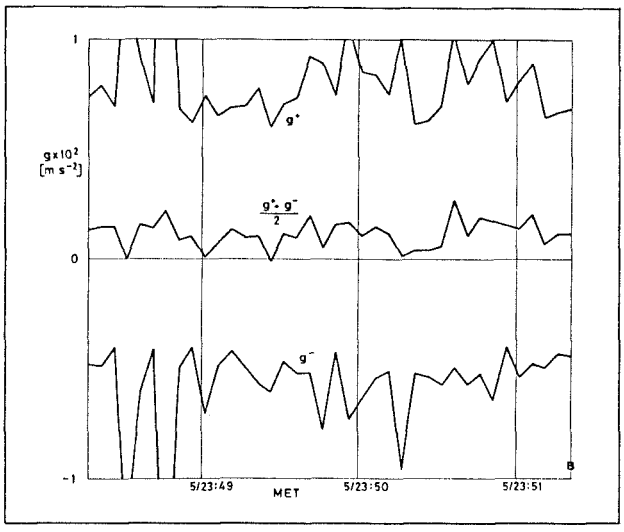

Fig. 1. Accelerometer data in the column axial direction prior to the first column breaking, at Mission Elapsed Time *B*. g^+ and g^- are the readouts of the Werkstofflabor accelerometers (maximal value sampled at 1-s interval)

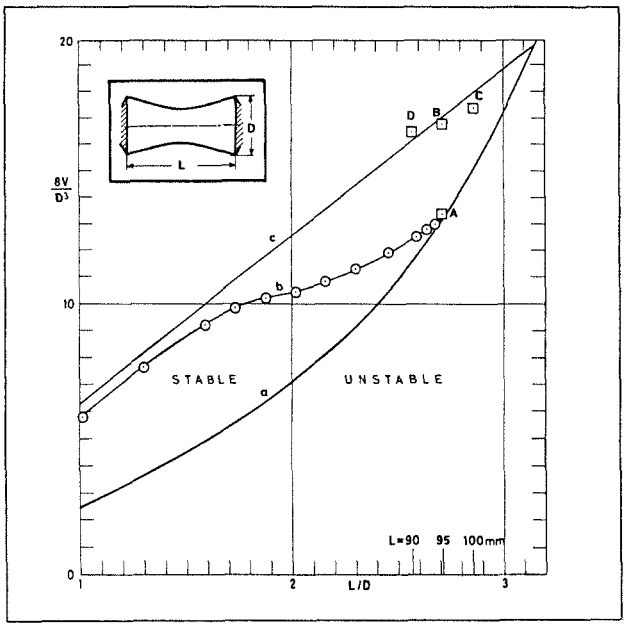

Fig. 2. Liquid bridge stability diagram. a) Minimal stable volume; b) filling law manually followed in the first trial; c) nominal cylindrical column evolution. *A*, *B*, *C* and *D* show where column breaking occurred; *B*, *C* and *D* breakings were due to isorotation at 12, 10 and 13 rpm in sequential order

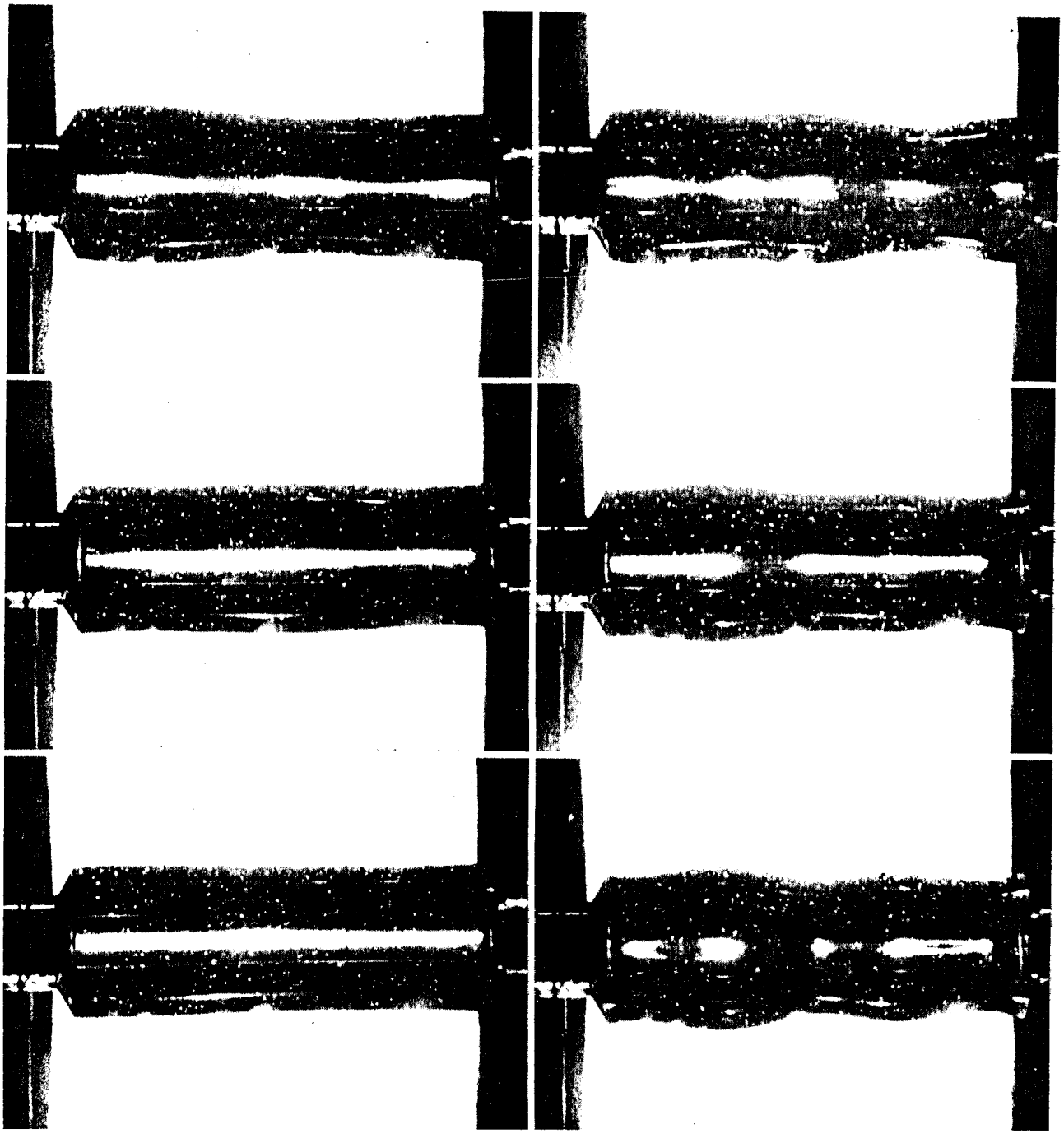

Fig. 3. Two vibration examples of a 95-mm-long cylindrical liquid column (at 0.3 and 1.1 Hz) with an amplitude of 0.5 mm. Consecutive frames at 2-s intervals

demonstrating the importance of a well-trained payload specialist on board. During a video link it was agreed to switch on background illumination in order to follow the free surface oscillations better (at the expense of a poorer tracer visualization by meridian plane lighting).

The small rotation of the discs at 3 rqm, intended for overall viewing, was switched off to diminish ambient noise (work had to be stopped several times due to the uncontrolled vibrations).

Axial oscillation of one disc at several frequencies was exercised and liquid response was as foreseen (Fig. 3) though departures from the cylinder were larger near the filling discs due to a residual accel-

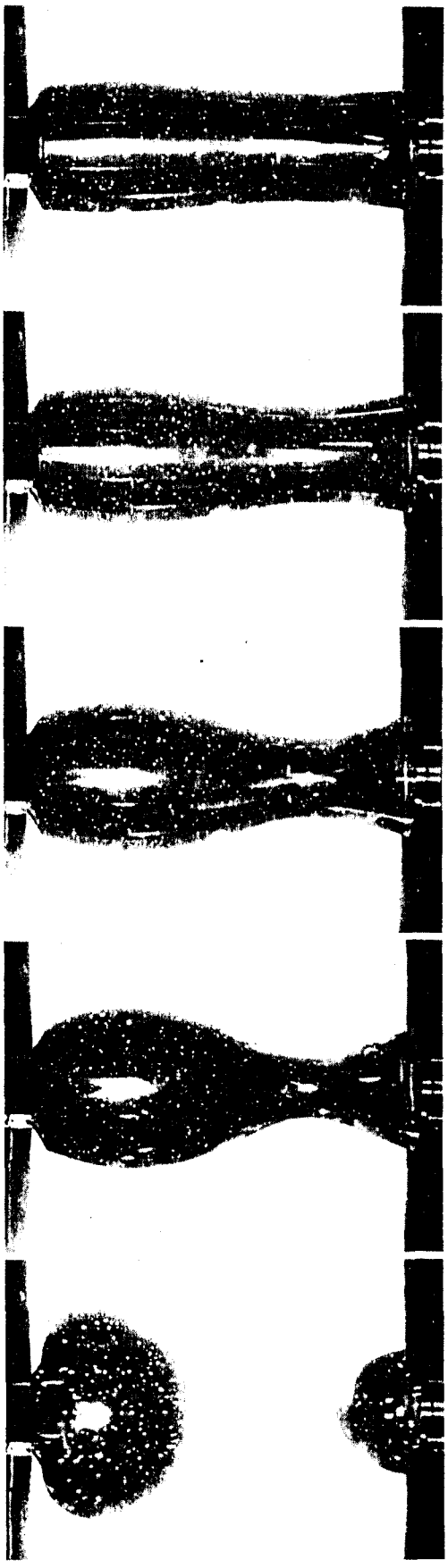

eration (Fig. 1). A second, yet unexplained breaking took place just after the axial oscillation exercise, perhaps due to some Shuttle maneuver.
Further breakings occurred at $L=95$ mm with $\Omega=$ 12 rpm, 100 mm with 10 rpm (Fig. 4) and 90 mm with 13 rpm, all in an amphora-like mode. The last breaking showed an initial C-mode deformation (like a skipping rope), but ambient noise may have changed the final breaking mode.
The last C-mode rotation trial, at $L=75$ mm with $\Omega=16$ rpm, though much less sensitive to ambient noise, was not performed due to lack of time, in spite of the generous time extensions granted to this experiment.

Perspectives

A detailed analysis of the 16-mm-film images, shot at 2-s intervals, is underway, while awaiting the on-board video recording.
The overall result was excellent and a follow-up proposal for Spacelab-D2 (1988) has already been submitted to ESA for further work on the C-mode and unequal disc stability analysis.

This project is being financed by the Spanish Commission on Space Research (CONIE).

1. Da Riva, I., Martínez, I., in: Scientific Goals of the German D1 Mission, WPF, 1985
2. Martínez, I.: Materials Science under Microgravity, ESA SP-222 (1984)
3. Martínez, I., Sanz, A.: ESA J. 9 (1985)

Fig. 4. Breaking sequence of a 100-mm-long cylindrical liquid column. Observe the middle satellite drop in the last picture. Times are, relative to the last, 0, −2, −4, −10, −50 s

FLOATING LIQUID ZONES IN MICROGRAVITY

by I. Martínez & J. Meseguer

Universidad Politécnica de Madrid, E.T.S.I.Aeronáuticos,

28040-Madrid, Spain

ABSTRACT

The preparation, performance and results of an experiment carried out in Spacelab-D1, to study the mechanical stability of long liquid columns held by surface tension between two coaxial discs, are described. The working slenderness (length/diameter) was up to 2.86. Results are in good agreement with previous theory, in spite of the relatively high level of ambient g-jitter. Some lessons learnt on logistics are summarized at the end.

1. INTRODUCTION

The experiment Floating Liquid Zone ("FLIZ" WL-FPM-04), dealing with the behaviour of long liquid bridges under mechanical disturbances in a low gravity environment, was carried out during the Spacelab-D1 Mission in November 1985.

The configuration of FLIZ experiment consisted of a near-cylindrical volume of liquid held by surface tension forces between two equal diameter coaxial solid discs at whose borders the liquid is attached (Fig. 1).

Discs were made of aluminium, with a 30^{o} receding sharp edge to avoid liquid spreading, the discs radius being R_o = 0.0175 m. Working liquid was a low viscosity dimethyl silicone oil (viscosity, $\nu = 5 \times 10^{-6}$ $m^2.s^{-1}$, density, ρ = 920 $kg.m^{-3}$ and surface tension σ = 0.02 $N.m^{-1}$) with tracers (Eccospheres, 0.15×10^{-3} m in diameter and 0.1 $kg.m^{-3}$ of concentration) to enhance inner motion visualization.

(place of Fig. 1)

The nominal experiment sequence envisaged [1] basically consists of: liquid injection, disc vibration and rotation of both discs, and was similar (slightly reduced) to the one tried on Spacelab-1 in 1983 where wetting and spreading problems with the nominal configuration allowed only partial success [2]. Although the much wanted C-mode deformation was indeed finally excited by rotating a large liquid bridges with a length to mean diameter ratio of 1.7, most of the time the liquid went out of control beyond the small mechanical and chemical (anti-spread coating) barriers. As on that occasion, the interest was to check the liquid bridge response against available theories, mainly concerning its limit of stability, a problem of practical importance in crystal growth by the floating zone technique [3].

The same Fluid Physics Module, but with corrected end-discs (more protruding and cut back) and a manually operated syringe for liquid injection (see Fig. 2) was used. A small video-camera and a 16 mm cine-camera shooting a frame every 2 seconds were the main source of data for later analysis.

(place of Fig. 2)

In the two years that separate both Spacelab flights, besides continuous effort in theoretical, numerical and ground-based experimentation, we had the opportunity to perform microgravity experiments on aircrafts in parabolic flight (NASA KC-135) and sounding rockets (German TEXUS program), in two occasions each. The short microgravity period on KC-135 (25 s) and its poor microgravity level (low frequency bumps of some 10^{-1} $m.s^{-2}$) render it useless for accurate work in FPM, although it was of great help in testing initial phase operations and for crew training. After a mechanical problem prevented any experimentation in TEXUS-10 (May 1984), the trials on TEXUS-12 (May 1985) were a big success [4]. Long (80 mm) cylindrical liquid bridges were established in less than a minute, thus, demonstrating that sounding rocket flights (6 minutes) can be used to perform experiments in microgravity with large liquid masses.

This last achievement put more confidence on the experimentation during Spacelab-D1 in November 1985. An initial assessment of the performance of FLIZ experiment [5] showed that most of the goals had been accomplished; in particular: a large liquid mass was accurately positioned in the test chamber, well anchored to the sharp edges of coaxial discs. Long cylindrical liquid columns of slenderness (length/diameter) 2.86 were easily established several times (the limit for no gravity being π). A long cylindrical liquid column subjected to axial vibrations showed a deformation with as many nodes (1, 2, 3, 4 and 5) as predicted by theory. Several (four) long cylindrical liquid columns were made to rotate at increasing rates and all them destabilized near the theoretical limit. The breaking of long cylindrical liquid bridges when subjected to

perturbations beyond the stability limit gave way to two separate drops with relative volumes as predicted by theory [6].

Nevertheless, it is a pity that the big time-constraint in Spacelab flights did not allow to finish the sequence of rotation trials and the much wanted C-mode instability could not be realized this time.

2. EXPERIMENT EXECUTION

For this research, Payload Specialist (PS) Dr. Furrer was in charge of the in-flight experimentation. Besides his training on the operation of the FPM, he closely worked with the investigators, simulating this experiment in a neutral buoyancy tank at their premises, and reviewing all the tests and results in connection with previous Spacelab, KC-135 and TEXUS flights.

Actual start time of FLIZ experiment was Mission Elapsed Time (MET) 5/23:21:00 (FPM power up), and the first picture inside the test chamber was taking 14 minutes later, already showing a liquid drop formed on the feeding disc (FD). After all the problems of handling the working liquid in Spacelab-1, there was no foreseen breakage of the liquid column until late in the experiment sequence. However, it turned out that the intended overpassing of the rotational stability limits always ended in bridge disruption. Fortunately, the PS had great dexterity in recovering back and start anew, what has served to divide the experiment in "Runs" that group all trials ended in disruption of the liquid bridge; a total of 6 such Runs have been recorded, a detailed description of which can be found in

Table 1.

(place of Table 1)

The most peculiar finding during Spacelab-D1 was that g-jitter was much higher that Spacelab-1 and TEXUS-12 experience had shown. The accelerometer data from Spacelab-1 and Spacelab-D1 show similar levels of g-jitter, namely 10^{-2} m.s^{-2} high frequency peaks, with a 10^{-3} m.s^{-2} averaged mean (Fig. 3), but the liquid column seemed to behave with a widely differently sensitivity: in Spacelab-1 interfacial deformations caused by noise were unnoticeable. The explanation may be due to the increased stability of low slender columns (1.7 against 2.86 for Spacelab-D1, the stable limit being 3.14; a steady linear theory predicts 20 to 30 times larger deformations for the same stimuli).

(place of Fig. 3)

In spite of the fact that the PS asked the other crew-members to keep quiet and got from the Shuttle crew a no-maneuvers period, the long columns achieved in Spacelab-D1 were trembling (slowly) and this noisy ambient may have contributed to premature breaking of the column. Although these breakings demanded extra crew-time for liquid recovery, they have provided additional source of information to check theoretical results on breaking dynamics.

3. RESULTS AND ANALYSIS

RUN 1

The liquid bridge disruption in Run 1 was not intentional. The idea was to establish a long cylindrical column by manual liquid injection (turning a syringe handle) while the disc separation was being automatically increased.

First, a short liquid bridge was obtained by slow injection of liquid through a 6 mm filling hole in the FD (35 mm in diameter) which remained anchored at the disc edge, growing until it came in contact with the rear disc (RD) that was 26 mm apart. At that time, some major Shuttle maneuvers happened to take place, widely deforming the bridge (which would have certainly brake, had it occurred at larger slendernesses).

During the cylindrical stretching, the PS had no experience and did not manage to follow a cylindrical evolution, following instead the path shown in Fig. 4, that eventually became unstable and the column broke in two spherical drops. This unforeseen circumstance has furnished an unexpected verification of the validity of the stability analysis of non-cylindrical liquid bridges in a real microgravity environment (this limit had been tested using neutral buoyancy simulation [7]).

(place of Fig. 4)

At that time, direct video link was available and thus, instead of some experiment sequence, a close view of the operator's hand thoroughly

cleaning the rear disc to start a new trial was transmitted. This, in fact, was a good demonstration for the safety team, who had cast doubts (and establish some hard rules) on the possibility of cleaning the FPM test chamber in flight.

RUN 2

After cleaning, injecting liquid as above and having reached a disc separation of 31 mm, the Payload Specialist started a long talk with the investigator on ground, concerning liquid visualization and ambient noise. The nominal illumination for this experiment was a meridian-cut light beam to visualize the tracers inside, combined with a background lighting (darken with a black mask with transparent square grid lines). As the mask got astray, the background illumination was dropped to avoid film overexposure. But the PS complained, and the investigator agreed when direct video link allowed to see the liquid bridge, that the background illumination would help a lot to clearly see the contour of the bridge, which was randomly oscillating and would be more difficult to handle otherway. After some trials (in real time video) it was convened that the background light should be on and the film developed accordingly, after flight. Besides, to minimize perturbations the overall 3 rpm rotation of the bridge (intended to see all around) was canceled.

In this Run, the oscillation trials were performed. The RD was set to a sinusoidal axial oscillation of 0.93 mm pick to pick at selected frequencies of 0.1, 0.3, 0.7, 1.1 and 1.6 Hz, roughly corresponding to the first natural frequencies predicted by theory for a cylindrical liquid

column of such a slenderness. During the 3 min at 0.1 Hz, the PS could not distinguish any privileged movement of the liquid (neither it is apparent on the photographs), but for the rest, standing waves with 2, 3, 4 and five inner nodes, respectively, were found, as expected (Figs. 5-6).

(place of Figs. 5-6)

Two or three minutes after the PS stopped the oscillation, the liquid column unexpectedly broke. The PS was not looking at it and no recording was on; it was attributed to Shuttle maneuvers, but the g-level recording does not show any specific jump.

RUN 3

The breaking in Run 2 left two drops well attached to the edges of the discs and thus the PS tried to approach the disc and merge the drops to re-establish the bridge. One of the most intriguing findings of this experimentation has been the fact that the two drops could not be merged, no matter how much the PS pressed one against the other by squeezing the supporting discs (rotation of the discs did not help). The only way out he could find was to remove the liquid on the FD back to the syringe and then get the FD in contact with the drop at RD (the spreading over the wet solid FD was easy and a bridge established).

In this Run the first rotation (see Fig. 7) of the column beyond the theoretical stability limit was performed and, even when the PS stopped rotation after some 30 seconds, the liquid shape deformation inevitably

grew until bridge disruption.

(place of Fig. 7)

RUN 4

The same process of drop merging of Run 3 was followed here to re-establish a bridge after the former rupture.

The PS started rotation of a 100 mm column at 10 rpm with a ramp of 9 s/rpm (second rotation trial in the procedures), but, unexpectedly, as soon as the 10 rpm were reached, he started to recover, removing liquid while approaching the discs, stopping the camera, and going out of FPM duty for about one hour.

RUN 5

The start is with a dry test chamber and the objective was to repeat Run 4 with success, what was finally achieved. The random oscillation in this column (100 mm long) were so pronounced, even when the PS managed from the Shuttle crew to have a free drift period, that at some instances it seems the column is going to break (although it stood like that for 5 minutes). When subjected to 10 rpm of isorotation, the column broke in an amphora-shape mode, as expected (Fig. 8).

(place of Fig. 8)

RUN 6

The goal of this Run was to excite a C-mode deformation in a liquid column 90 mm long. When the stability limit was surpassed at 13 rpm, the column deformed in an amphora-like mode instead of in C-mode. The explanation now given is as follows. As above mentioned, the accelerometer data indicate a residual axial acceleration of more than 10^{-3} m.s^{-2}, which tends to promote the amphora-like instability above the C-mode one by shifting the rotational stability limit to lower slendernesses, as sketched in Fig. 7.

By that time, experiment FLIZ had used resources (mostly crew-time) well above initial allocation and was concluded. Unfortunately, the only Run remaining in the nominal procedures was a last rotation trial at 16 rpm with a column of 75 mm which would have clearly shown a C-shape disruption mode.

4. LESSONS LEARNT

The details pointed out here concern marginal problems ocuured during Spacelab flight and are irrelevant to the results of the investigations, but their inclusion here may be worth regarding future space experimentation (mainly from the users point of view).

A first logistic problem arose during the setup: the background mask, intended to enhance visualization and ulterior data analysis from the images, was not found by the PS. The background mask was actually a plastic sheet of some 13x17 cm^2, a commercial photosensitive film on which

a square grid 1 cm in side had been recorded. It was properly labeled, but, in order to avoid profusion of small containers, it was decided to be included in an already available envelop which belonged to another FPM user. The ESA support team and the investigators knew these details (it seems they escaped the PS attention), but during the flight, when the PS asked for assistance to find it, the investigator (who had to talk to the PS through two or three intermediate relay personnel) realized that it had already cost several of the 90 minutes initially allocated to the whole series of experiments and instruct the PS to forget about the plastic sheet.

This multi-relay voice link caused more waste of time than the already said above. Sometimes the PS sent a message to the investigator on ground, who correctly received it and was prompt to answer, but another member in the link did not catch it and asked the PS to repeat the message or clarify some point on it. Besides, the PS was constantly requested from ground during the scarce voice-link periods to take messages for other business, what distracted him and prevented a more interactive operation.

Another weak point was connected with liquid volume recording. The FPM reservoir used in Spacelab-1 was awkward to control, but its settings were automatically recorded every second. The small manual syringe specially designed for D1 was much more handy, and helped a lot the PS to control the liquid supply and removal, but it was not connected to the data acquisition system. Training on ground was irrealisticaly optimist; once up there, the PS was so busy coping with a highly sensitive liquid column, that he had no time to keep a detailed logbook of the syringe counter. Besides, when at some point the PS measured the syringe counter it was for

instance 25.2 handle turns, instead of the 26.1 expected for a cylindrical column of that length, an error beyond normal experience on ground trials. Thus, all volumes had to be estimated from the shape on the images.

Concerning data retrieval, D1 mission was much better than Spacelab-1, but still an entangled job far from being satisfactory. The problem is that the investigator does not know before hand how much data will be needed because it all depends on the actual development of the experiment. Besides, a major impact on data requirement in these pionering space research is the relaibility of the data sources (problems with FPM cine-camera, malfunction of on board video-tape recording, possible errors in data acquisition, etc). For example, when the PS selected (according to the procedures) 12 rpm synchronously for both discs, the printout shows unrelated scatter from 11.2 to 12.7 in disc rotation rates (against an FPM accuracy of 0.1 rpm).

Even when reliable data is available, it is difficult to handle; for instance, the bulky printout of FPM housekeeping and accelerometer data. Major steps will be needed if an automated data acquisition (and image processing) capability is wanted in future (presently, the outline of some 100 enlarged pictures have been manualy digitized).

Contrary to the above drawbacks, the incorporation of a frame counter to the FPM housekeeping data for D1 mission has represented a great improvement with regard to Spacelab-1 (the FPM camera does not recors time on film).

5. CONCLUSIONS

The purpose of this experiment was to study the mechanical stability of long liquid columns under microgravity and the aim has been achieved with success.

Apart of minor details as those described on the last section, everything worked as expected: the liquid column was vibrated at the frequencies foreseen in the procedures, and the influence of rotation on the maximum stable length of the liquid bridge was checked through three different rotation tests (another rotation trial was not performed due to lack of time, in spite of the generous time extensions granted to this experiment). In particular:

- -A large liquid mass was accurately positioned in the test chamber, well anchored to the sharp edges of coaxial discs.
- -Long cylindrical liquid columns of slenderness (length/diameter) 2.86 were easily established several times (the limit for no gravity being π).
- -A long cylindrical liquid column subjected to axial vibrations showed a deformation with as many nodes (1, 2, 3, 4 and 5) as predicted by theory.
- -Several (four) long cylindrical liquid columns were made to rotate at increasing rates and all them destabilized near the theoretical limit.
- -The breaking of long cylindrical liquid bridges when subjected to perturbations beyond the stability limit gave way to two separate drops with relative volumes as predicted by theory.

-ambient noise in Spacelab seems to pose a bound on the maximum length of cylindrical columns of 35 mm in diameter that can be handled in this laboratory: around the 100 mm achieved during D1 mission.

The detailed analysis of the 16 mm film shot during FLIZ experiment is still in progress, and main results up to date are here presented. It can be anticipated that the overall result of FLIZ experiment has been excellent, and a follow-on proposal for Spacelab-D2 (1990) has already been submitted to ESA for further work.

ACKNOWLEDGEMENT

This research is being supported by founds from the Spanish Commission on Space Research (CONIE).

REFERENCES

1. Martinez, I., "Floating zone hydrodynamics", Wissenschaftliche ziele der Deutschen Spacelab mission D1, 40-41, 1985.
2. Martinez, I., "Liquid column stability", ESA SP-222, 31-36, 1984.
3. Martinez, I. & Eyer, A., "Liquid bridge analysis of silicon crystal growth experiments under microgravity", J. Crystal Growth 75, 535-544, 1986.
4. Martinez, I. & Sanz, A., "Long liquid bridges aboard sounding rockets", ESA Journal 9, 323-328, 1985.
5. Da Riva, I. & Martinez, I., "Floating liquid zones", Natur wassenschaften, Springer-Verlag, 1986.
6. Meseguer, J., Sanz, A. & López, J., "Liquid bridges breakages aboard Spacelab-D1", (to be published in J. Crystal Growth), 1986.
7. Sanz, A. & Martinez, I., "Minimum volume for a liquid bridge between equal disks", J. Colloid Interf. Sci. 93, 235-240, 1983.

FIGURE CAPTIONS

Fig. 1. Sketch of the configuration used, with details of the disc shape. FD=Front Disc (used to feed the liquid and to vary the separation L), RD=Rear disc (used to vibrate the liquid).

Fig. 2. Difference in hardware used in Spacelab-1 (1983) and Spacelab-D1 (1985).

Fig. 3. Mean value of the readings (at 5 s interval) of some accelerometers near the FPM (in the axial direction of the liquid column). Pick values have a fluctuation one order of magnitud larger. Because the caracteristic response time of the liquid column is of the order of 20 s, the averaged of five centred samples is also shown (smoother curve).

Fig. 4. Actual path (b)in the stability diagram followed by liquid column in the first Run. It is seen how it deviates from the cylindrical evolution (c) and gets unstable.

Fig. 5. Theoretical natural frequencies for axial vibration od a cylindrical column as a function of slenderness (no residual gravity and no rotation). The points correspond to the trials performed (see Fig. 6).

Fig. 6. Some consecutive film frames (at 2 s interval) showing oscillation of a 95 mm long column at 0.3 Hz (0.93 mm pick to pick amplitude).

Fig. 7. Points in the rotation-slenderness stability diagram for cylindrical liquid columns, exercised during Spacelab-D1. Dashed line intends to show the effect of an axial residual gravity on the rotational stability limit. See also Fig. 8.

Fig. 8. Breaking sequence of a 100-mm-long cylindrical liquid column. Times, relative to the last picture, are -50, -10, -4, -2 and 0 seconds, respectively.

Table 1. Description of FLIZ experiment as executed. Time (MET), column length L, rotation rate Ω and corresponding frame in the 16 mm film, are given.

MET	L [mm]	Ω [rpm]	Frame	DESCRIPTION
5/23:35:00	26.0	0	45	**Start of RUN 1.** After lead tail, first frame already shows a liquid drop on FP. Meridian plane illumination. **Tracers visible.**
5/23:35:11	26.0	0	51	Bridge formation by liquid feeding.
5/23:36:31	26.0	3	77	Start low isorotation to see all around. Barrel bridge.
5/23:36:46	26.0	3	83	Shuttle jet firings start. The experiment is paused.
5/23:48:56	26.0	3	183	Filming restart. Liquid removal to get a cylindrical bridge, followed by disc separation and simultaneous liquid injection for a cylindrical stretching.
5/23:51:16	95.0	3	253	End of disc separation. Spindle shape. Close to instability.
5/23:51:21	95.0	3	255	Breaking of the liquid bridge.
5/23:51:41	95.0	3	264	End of scene. Direct TV shows operator's hand cleaning on site the disc at RP.
6/00:28:23	26.0	3	265	**Start of RUN 2.** Drop at FP.
6/00:29:09	26.0	3	288	Drop at FP contacts RP and forms a bridge.
6/00:31:21	26.0	3	354	Start of disc separation.
6/00:31:36	31.3	3	361	Separation stops. Crewman and investigator talk. Direct TV link for some 15 min. Illumination system trials. Very large g-jitter.
6/00:33:23	31.3	3	412	From here to end, both meridian plane and background plane illumination are on.
6/00:35:56	31.3	3	418	Disc separation and simultaneous liquid injection for a cylindrical stretching.

MET	L [mm]	Ω [rpm]	Frame	DESCRIPTION
6/00:40:51	95.0	3	544	Disc separation stops. Cylindrical shape with a small random vibration.
6/00:49:11	95.0	0	794	After some 9 min of jitter, disc rotation (for visualization purpose) is stopped.
6/00:53:06	95.0	0	911	Overexposed frame to mark the start of disc oscillation experiments.
6/00:56:21	95.0	0	914	RP oscillation experiments at frequencies 0.1, 0.3, 0.7, 1.1 and 1.6 Hz (starting in frame 914, 1007, 1059, 1092 and 1117, respectively). Amplitude is 0.465 mm and frame interval 2 s.
6/01:03:51	95.0	0	1139	End of oscillation experiments (Amplit.=0).
6/01:06:21	95.0	0	1167	Liquid bridge breaking (unexpected). The 1 min 35 s prior to rupture are not filmed. Larger drop at FP. g-peak at 6/01:06:44.
6/01:07:56	95.0	0	1168	End of scene.
6/01:09:26	86.6	0	1169	**Start of RUN 3.** First, some liquid is removed from the (larger) FP drop. When both drops are equal, the discs are approached for merging.
6/01:11:01	39.1	0	1170	Both drops touching, but not merging (even when disc rotation is activated).
6/01:14:01	32.6	3	1172	Both drops heavily deformed by pushing against each other, but not merging. Small isorotation of the discs to see all around.
6/01:14:36	32.6	0	1189	End of rotation. Merging impossible. All the liquid from the FP drop is removed and the discs approached.
6/01:16:46	15.9	0	1254	The RP drop spreads over the FP disc. After that, disc separation starts, combined with liquid injection to keep a cylindrical bridge.
6/01:26:36	95.0	0	1273	After reaching the working slenderness, iso- rotation experiments start. Rotation starts.

MET	L [mm]	Ω [rpm]	Frame	DESCRIPTION
6/01:28:39	95.0	12.3	1340	Maximum rotation rate reached by the discs (the ramp was 9 s/rpm). At this time, the operator stops both disc rotation.
6/01:28:52	95.0	0	1346	Liquid bridge breaking.
6/01/29:31	95.0	0	1360	End of scene. Change of onboard videotape 6 to 7.
6/01:31:01	50.6	0	1361	**Start of RUN 4.** Two drops. The one at FP is removed and the discs are approached to spread the RP drop over the FP.
6/01:32:36	16.0	0	1362	Bridge formed. Cylindrical stretching until L=100 mm, followed by a prolonged pause to wait for a calm period (high g-jitter).
6/01:50:47	99.9	1.5	1414	Start of isorotation experiment.
6/01:51:48	99.9	8.0	1444	Unexpected start of disc approaching and liquid removal (the operator tries to avoid a breaking). Rotation speed still increasing. Manouvres.
6/01:52:06	91.9	10.0	1453	Rotation rate reached.
6/01:53:39	34.5	10.0	1499	End of scene. Filming is stopped before liquid bridge breakage. Crew reporting two minutes later.
6/03:03:06	9.2	0	1513	**Start of RUN 5.** About one hour with operator off duty. No liquid in the test chamber. Start liquid injection. Repetition of previous experiment.
6/03:04:41	56.7	0	1514	Bridge formed at this point, followed by cylindrical stretching.
6/03:10:41	100.0	0	1605	Disc separation stops. Cylindrical shape with large random oscillations. In frames number 1609 and 1636, the liquid column is near to break.
6/03:13:56	100.0	0.5	1703	Start of isorotation experiment.
6/03:16:26	100.0	10.0	1778	Rotation rate reached.

MET	L [mm]	Ω [rpm]	Frame	DESCRIPTION
6/03:16:46	100.0	10.0	1788	Disc rotation stopped.
6/03:16:53	100.0	0	1791	Liquid bridge breaking.
6/03:18:46	82.6	0	1802	End of scene.
6/03:20:31	50.5	0	1803	**Start of RUN 6.** Disc separation and liquid injection until a cylindrical column is achieved at this point.
6/03:23:45	90.0	0	1857	Disc separation stops.
6/03:26:11	90.0	1.7	1930	Disc isorotation starts.
6/03:27:56	90.0	12.7	1982	Rotation rate reached. Operator reports.
6/03:28:51	90.0	12.7	2010	Disc isorotation stopped.
6/03:29:01	90.0	0	2015	Liquid bridge breaking.
6/03:30:33	90.0	0	2035	End of scene. Operator reports ten minutes later.

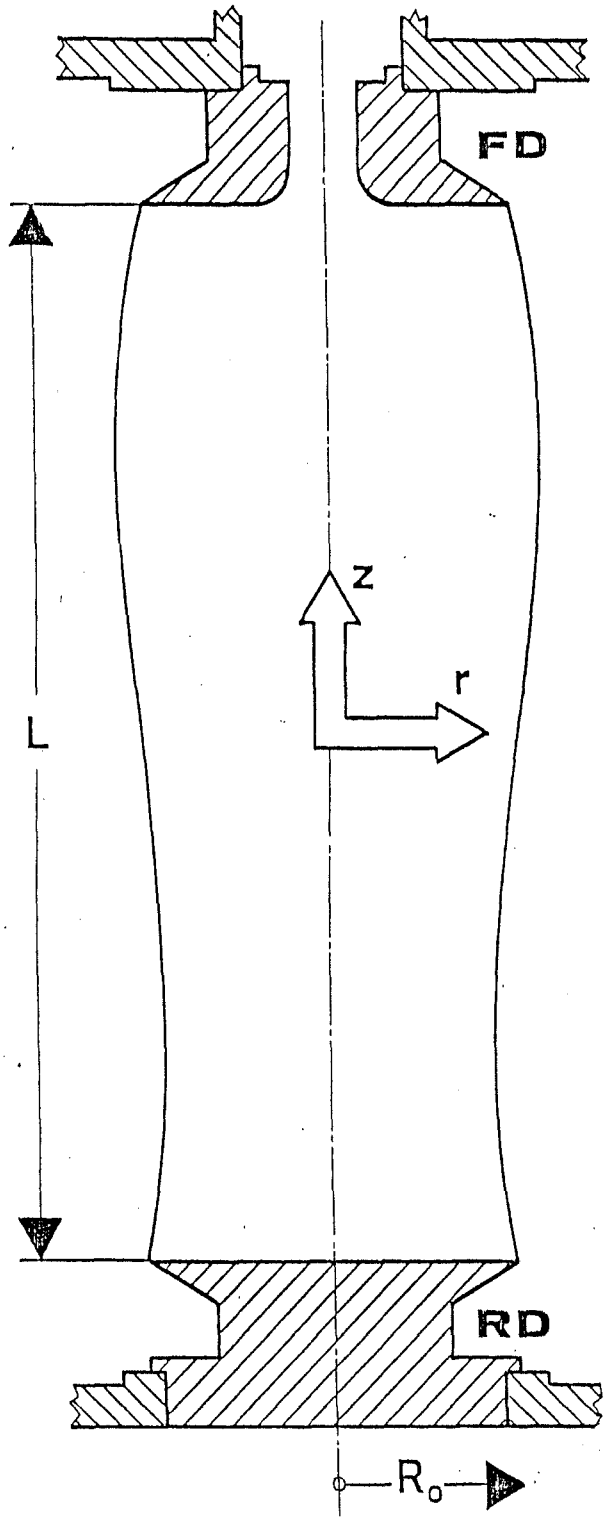

Fig. 1

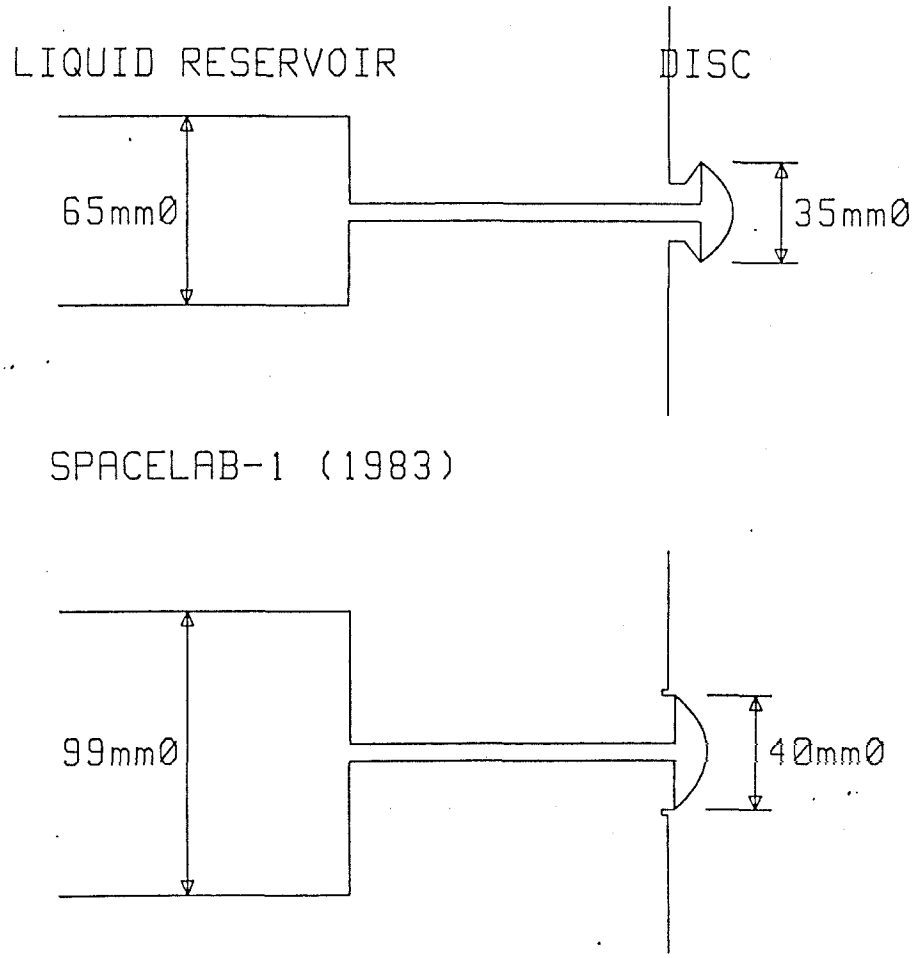
LIQUID RESERVOIR
DISC
65mmØ
35mmØ
SPACELAB-1 (1983)
99mmØ
40mmØ
SPACELAB-D1 (1985)

Fig. 2

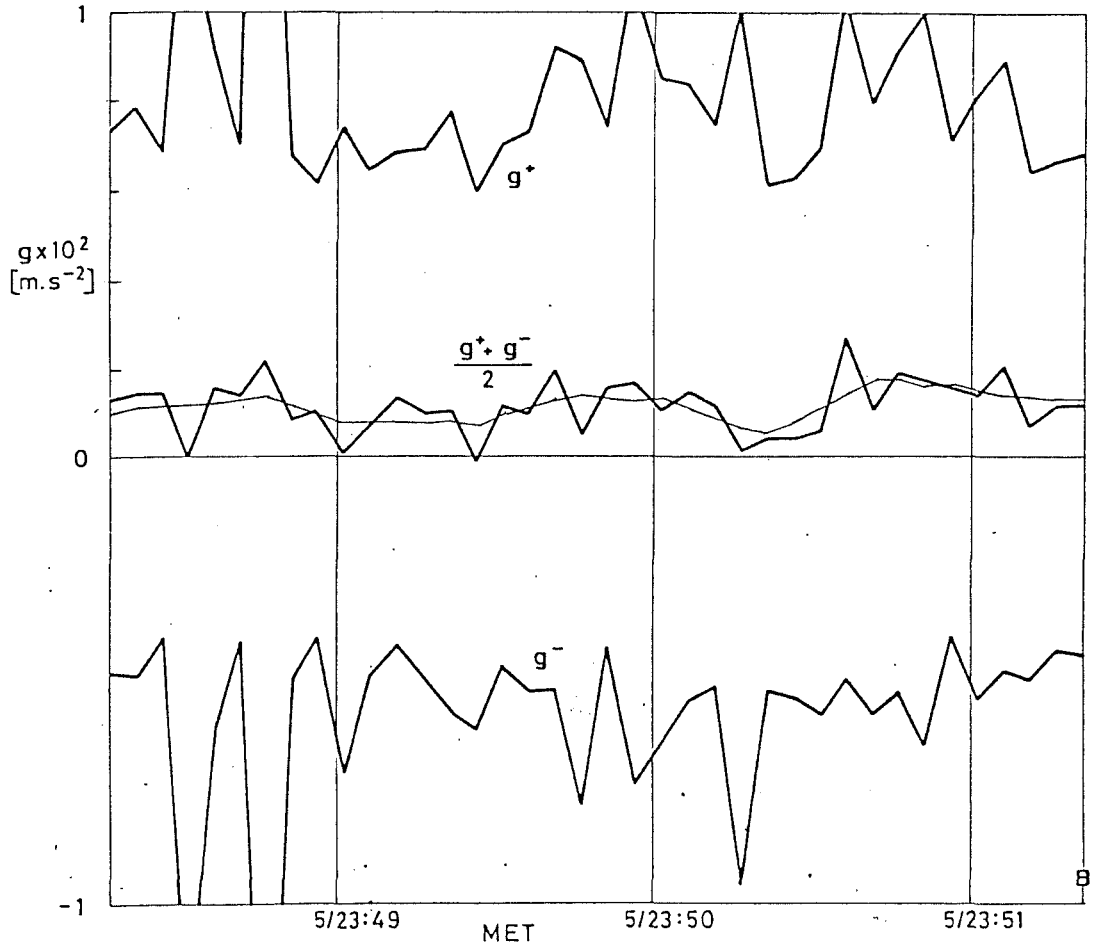

Fig. 3

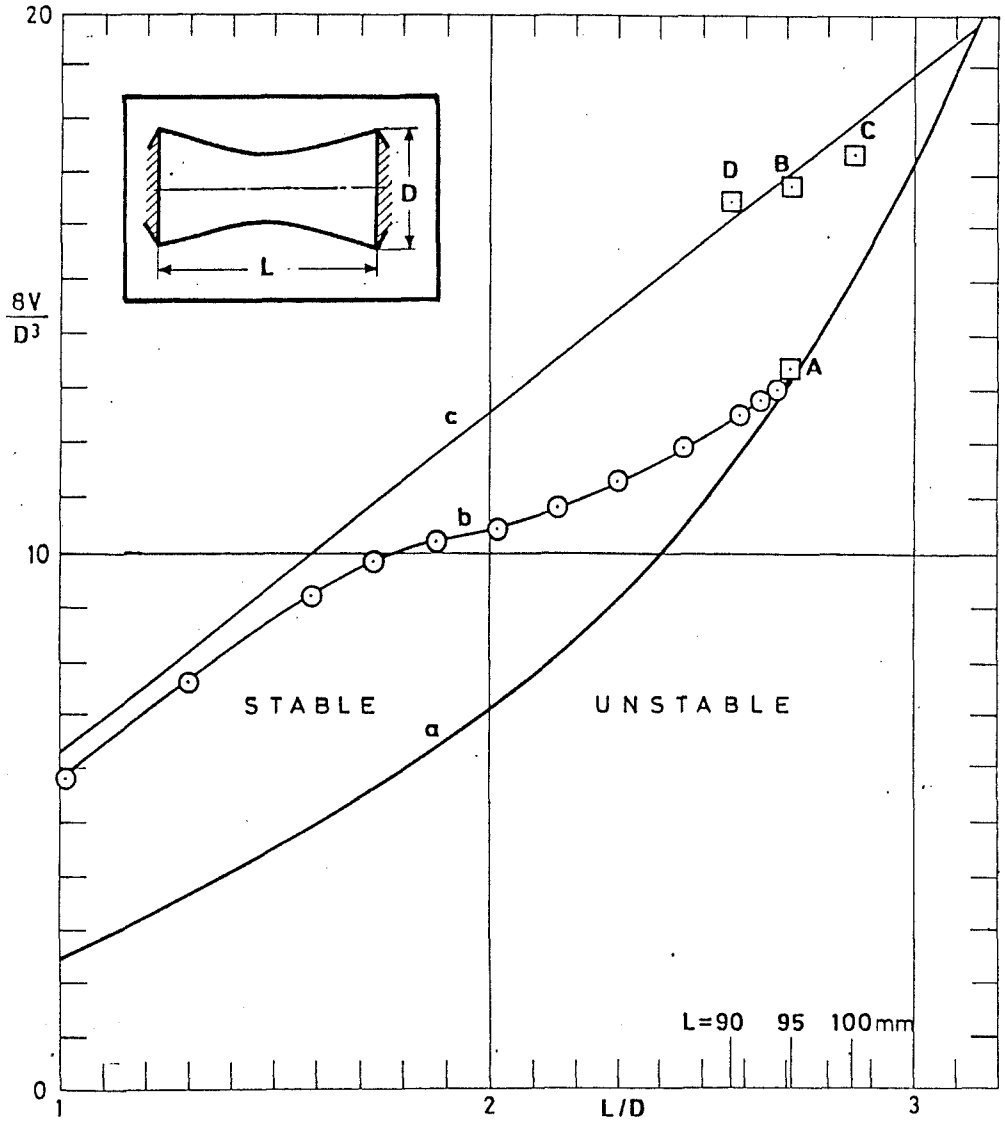

Fig. 4

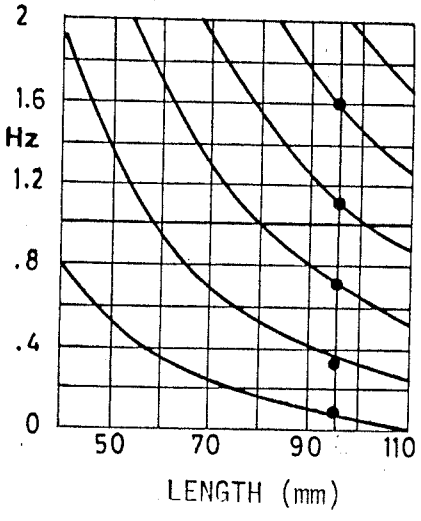

Fig. 5

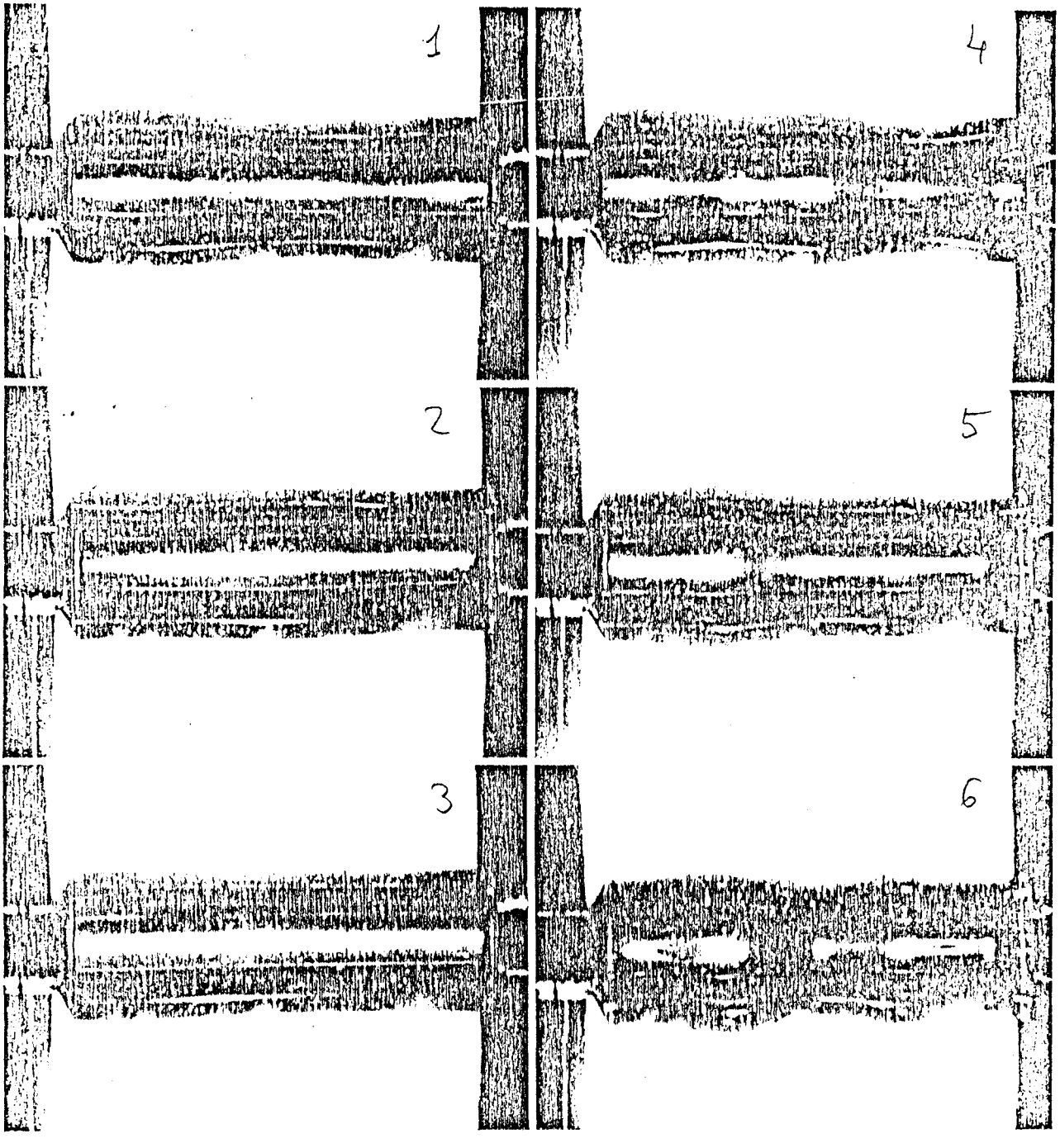

Fig. 6

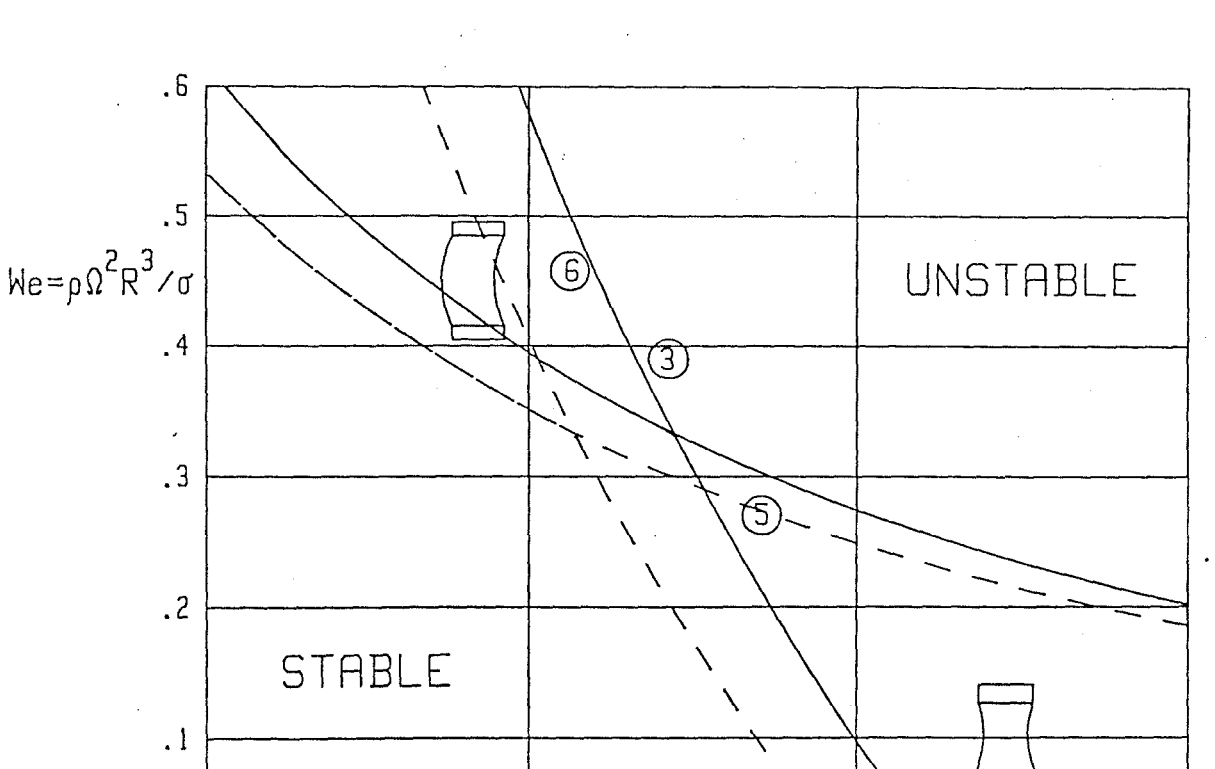

Fig. 7

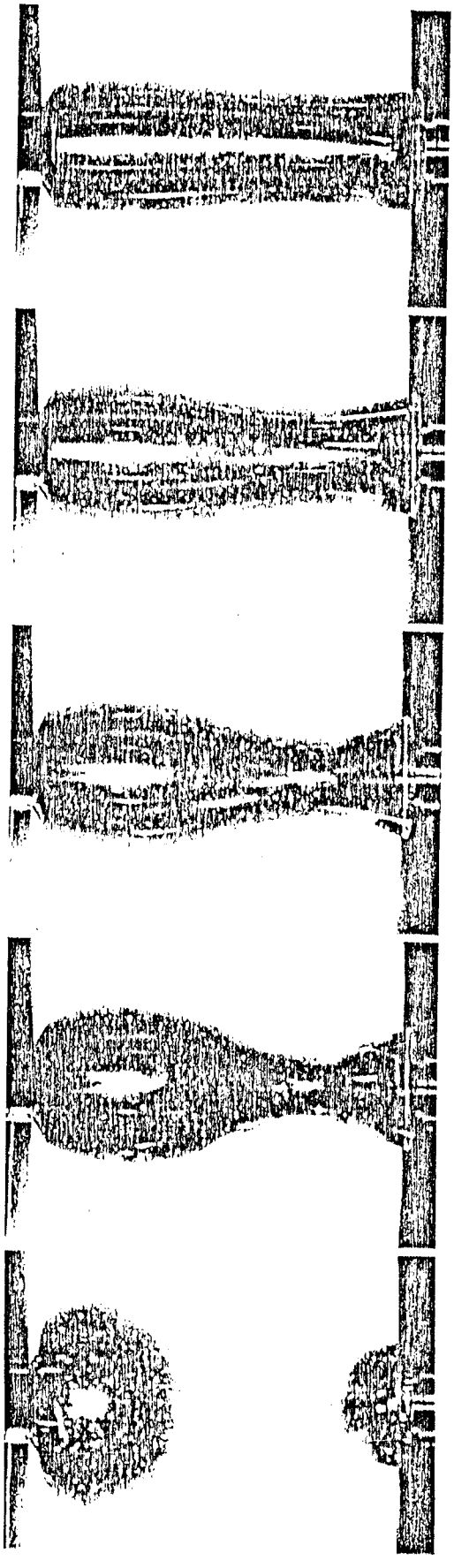

Fig. 8

IAF'86

37th CONGRESS OF THE
INTERNATIONAL ASTRONAUTICAL FEDERATION
INNSBRUCK, AUSTRIA, OCTOBER 4–11, 1986

SPACE: New Opportunities for All People

PREPRINT

Ref. No.: IAF-86-272

Title: Stability of Liquid Bridges. Results of SL-D1 Experiment

Author(s): I. Martínez

This Preprint is for distribution at the Congress only

Published for the
International Astronautical Federation
by
Pergamon Press
Oxford · New York · Beijing · Frankfurt
São Paulo · Sydney · Tokyo · Toronto

$3.00

STABILITY OF LIQUID BRIDGES
RESULTS OF SL-D1 EXPERIMENT

by I. Martinez

Universidad Politécnica de Madrid, E.T.S.I.Aeronáuticos, 28040-Madrid, Spain

ABSTRACT

An analysis is presented of an experiment aboard Spacelab-D1 on the mechanical stability of long liquid columns between coaxial equal discs. The effect of g-jitter, column slenderness, disc rotation and disc vibration upon the liquid outer shape, is studied.

KEYWORDS

Liquid bridge, floating zone, microgravity, Spacelab experiment, capillarity.

INTRODUCTION

Experiments with cylindrical liquid bridges of 35 mm in diameter and up to 100 mm in length were performed by Payload Specialist Dr. Furrer during the Spacelab-D1 mission (November 1985) to investigate the behaviour of long liquid columns when subjected to mechanical disturbances in a microgravity environment, under a wider-scope experimental project which make use of different microgravity platforms (aircraft parabolic flights, sounding rockets and Spacelab) as well as ground tests using the neutral buoyancy technique.

Apart of its own fluidmechanical interest, the behaviour of liquid bridges is of great importance in several well-known applications, among which the floating zone technique of producing high purity single-crystals of semiconductor materials can be pointed out. Even just in the mechanical behaviour of a real floating zone, there are so many factors interplaying (surface tension, gradients in surface tension caused by temperature and concentration fields, sample rotation to uniformize the heating, gravity, vibration induced by the drivers during the processing, etc) that the most suitable approach is to analyze one by one the different factors.

Thus, one tries to get rid of gravity (the dominant factor) by minimizing the Bond number $Bo = \Delta\rho g R^2/\sigma$, which measures the relative importance of gravity and capillary forces. To this aim, and taking into account that the surface tension of most suitable liquids varies scarcely, one can adopt three possible approachs: to diminish the density difference $\Delta\rho$ in a neutral buoyancy tank (as pioneered by Plateau in the XIX century), to diminish the effective gravity g by an inertial balance (drop tower, parabolic flight of airplanes and rockets, or orbital flight) or to reduce the spatial dimensions of the sample (characterized here by the disc radius R) working with microscopic zones. The latter approach brings so many experimental constrains that have not been pursued under this project.

Experimentation on ground in a Plateau Tank Facility (Martinez and Rivas, 1982) provides a simple accurate mean to perform static experiments to measure shapes and stability (Sanz and Martinez, 1983) and, if a theory for the effect of the outer bath on liquid bridge movements is developed, can also serve to investigate certain dynamic characteristics (Sanz, 1985). However, this method is not suitable to perform experiments on liquid bridge rotation, for instance.

Experimentation in microgravity platforms imposes its own constrains, as can be learnt from the experience in this project of liquid-bridge stability investigations. In 1976, an experiment proposal for SL-1 was accepted. When the nominal procedures were executed in 1983 (SL-1) the liquid went uncontroled after a few seconds from start, due to inertial spreading beyond the intended edges (Martinez, 1984). A more conservative design was then tried in 1984, within the 20 seconds of microgravity provided by NASA's KC-135 plane in parabolic flight, but the results, though encouraging, were inconclusive due to high g-jitter. Clear success came in May 1985 with an experiment on the TEXUS rocket, where cylindrical liquid columns up to 80 mm long and 30 mm in diameter were repeatedly formed in a few minutes (Martinez and Sanz, 1985). Finally, the experiments envisaged for SL-1 were successfully carried out in SL-D1 where the only problem found when working with liquid columns up to 100 mm long and 35 mm in diameter was that the residual gravity and g-jitter prevent going any further towards the cylindrical stability limit of length/diameter=π in absence of gravity (Da Riva and Martinez, 1986; Martinez and Meseguer, 1986).

The trials performed can be separated to the purpose of analysis (in chronological order) as shown in Table 1.

Table 1. Summary of trials performed (MET=Mission Elapsed Time).

From MET	to MET	Run	L_{max}[mm]	Ω_{max}[rpm]	Comments
5/23:35:00	5/23:51:41	1	95	0	Broke by volume depletion
6/00:28:23	6/01:07:56	2	95	0	Broke by jet firing from the Shuttle
6/01:09:26	6/01:29:31	3	95	12	Broke by disc spinning
6/03:03:06	6/03:18:46	4	100	10	Broke by disc spinning
6/03:20:31	6/03:30:33	5	90	13	Broke by disc spinning

The data recorded during the experiment consists of photographic images of the liquid bridge, on a 16 mm film (KODAK 2476), shot at 2 seconds per frame (f/2, 1/20 s), video images, house-keeping data of the Fluid Physics Module used, and auxiliary information (voice track and logbooks).

The analysis has concentrated on the photos because they are best suited to manual handling (the sophisticated automatic image processing needed is not available). Besides, malfunction of the on-board video tape recorded damaged the best part of the video track.

The procedure followed has been: 1) enlarge the 16 mm frames with a microfilm projector and manually draw the outline of the liquid column roughly filling an A4 sheet, 2) input that shape (some 50 points each) to a computer via a digitizing tablet, 3) smooth the shape with a Fourier series expansion (a few terms), and finally analysis the sequence of shapes. The effect of optical distortions, subjective shape-drawing, number of digitized points, number of Fourier terms, etc. has been thoroughly screened. The only artificial correction applied has been an axial compression of the digitized shape to match the known slenderness of the column (the consistent bias to values 2% or 3% larger is attributed to optical deformations in the microfilm projector).

A weak point is that the volume of liquid in the column was not measured and has to be computed from the outer shape of columns that are not perfectly axisymmetric (a characteristic type deviation of 3% has been found).

A description of the trials performed and results obtained follows.

Run 1: Non-cylindrical breaking

Bridge formation was achieved by growing a large drop anchored to the feeding disc edge until contact with the opposite disc, situated at 3/4 of diameter apart, occurred (see Fig. 1). This procedure was also used in SL-1, but there, either the first spreading wave advancing over the feeding disc, or the later spreading wave over the opposite disc when contact took place, caused the liquid to jump over the disc edge and get uncontroled. This procedure was not used in TEXUS-12, where a cylindrical filling law was followed from the initial zero-separation stage. A big jet firing occurred at this stage in SL-D1, but this short bridge withstood it easily.

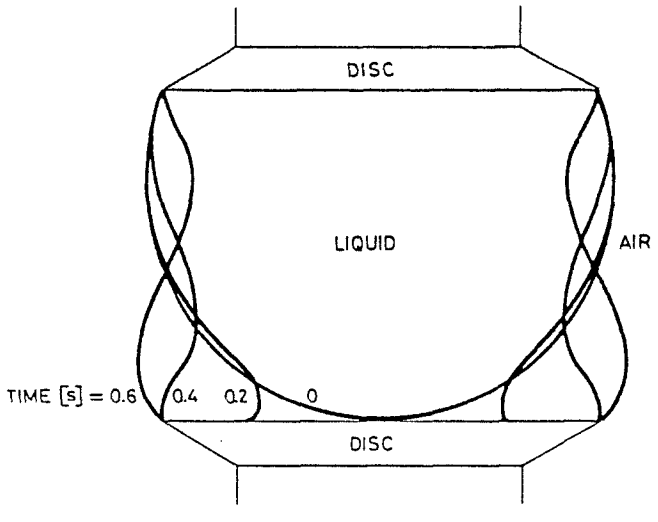

Fig. 1. Four stages in the spreading of the captive drop over the opposite disc (untreated aluminium) used in Spacelab-D1 to establish a liquid bridge (by hand from TV images).

Subsequent bridge elongation was performed setting an automatic separation speed of 1 mm/s and instructing the operator to inject liquid from a syringe, normally turning a handle (delivering 3.45 cm^3 per turn) while watching at the bridge to keep it as cylindrical as possible.

The stretching seemed to be too fast and, as soon as the intended length (95 mm) was reached, the bridge disrupted. Image analysis has allowed the reconstruction of the volume-separation history and showed that the minimum volume limit had been transpassed (Da Riva and Martinez, 1986).

Run 2: Axial oscillations

After liquid recovery, the procedure to establish a long (95 mm) liquid column was repeated (this time at 0.5 mm/s), but when the separation was 31.3 mm big, jet firings from the Shuttle (see Fig. 2) forced the operator to hold for several minutes. After that, he succeeded in applying a 0.93 mm peak-to-peak axial oscillation through one of the disc at frequencies of 0.1, 0.3, 0.7, 1.1 and 1.6 Hz that were predicted to lay near the resonances. Except for the first mode, where no deformation was apparent (over the ambient jitter) the response of the column was as expected. Unfortunately, a couple of minutes after those trials (at MET 6/01:06:44), when no monitoring or recording of the column was going on, a Shuttle jet-firing caused bridge disruption.

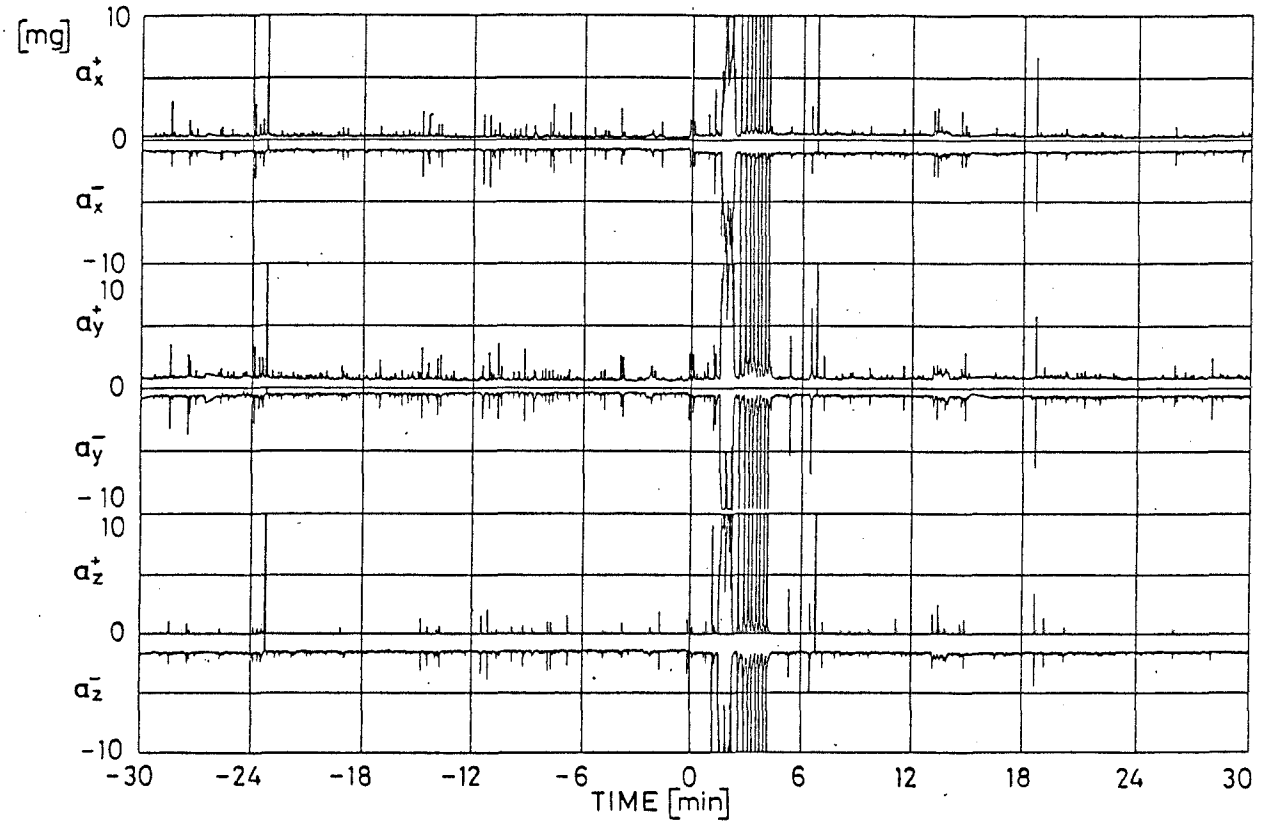

Fig. 2. Signal from accelerometers near the Fluid Physics Module in Spacelab-D1. The maximum value inside a 1 s interval, for each of the six directions, is recorded. The unit mg stands for 10^{-3} times Earth gravity. Time origin is Mission Elapsed Time (MET) 6/01:00:00.

Run 3: Disc rotation at 12 rpm

After liquid recovery and column reforming to 95 mm in length, both discs were spun up at 9 s/rpm up to 12 rpm, slightly surpassing the theoretical speed limit of zero-gravity. Although no visible effect upon the outer shape when spinning up, some tens of seconds after the speed was reached, the necking deepened until breakage. Although the column slenderness in this case was chosen to coincide with the separation between anphora-mode and C-mode instabilities at zero-gravity, the residual mean axial gravity forced an anphora-mode deformation both initially and in the subsequent breaking, but the breakage itself was triggered by rotation and not by gravity (Meseguer and colleagues, 1986).

Run 4: Disc rotation at 10 rpm

A first attempt of this trial had to be aborted because, once the 100 mm long column was established and the spin up started, high g-jitter and the announcement of forthcoming maneuvers advice the operator to close and resume one hour later.

When finally this trial was performed, the behaviour of the liquid column was as in Run 3. In fact, has the bias of residual gravity been known, this trial could have been spared, as the outcome is foreseeable. However, being the longest column ever achieved (100 mm), it has provided very valuable data (Fig. 3) on the effect of ambient g-jitter at these high slendernesses (L/D = 2.857).

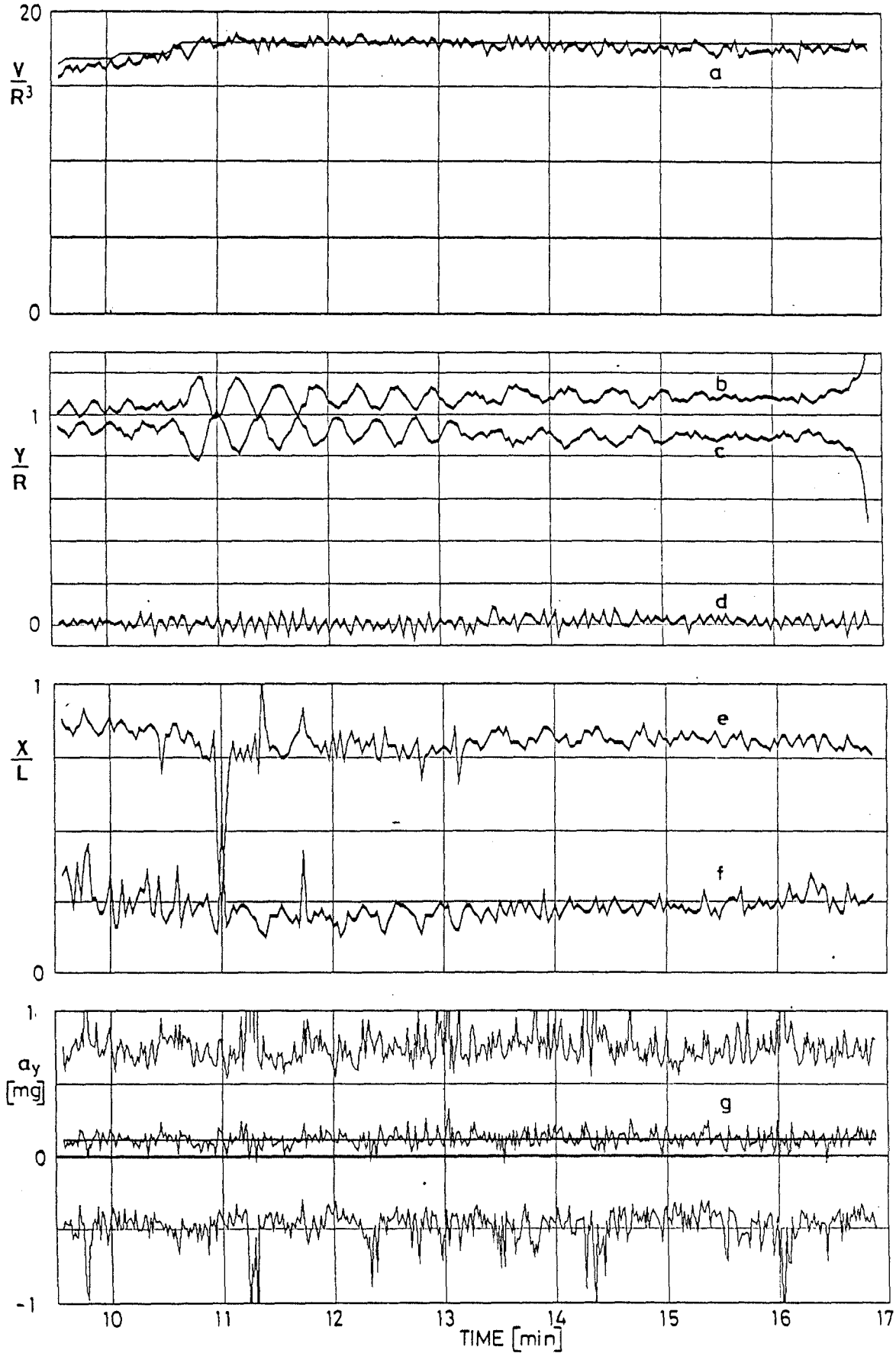

Fig. 3. Some results on time evolution of a long nearly-cylindrical liquid column. Origin is at Mission Elapsed Time (MET) 6/03:00:00. **a)** Liquid volume computed from the pictures compared with the scheduled one (cylindrical volume means $V/R^3=17.95$). **b)** and **c)** Radius at 3/4 and 1/4 of the column length, respectively (they nearly correspond to the maximum bulge and neck). **d)** Deformation of the column center-line at mid length (natural frequency is about three times that of b). **e)** and **f)** Position of maximum bulge and neck along the column, respectively. **g)** Accelerometer data in the axial direction, mean value and averaged mean (mg stands for 10^{-3} times Earth gravity).

A most puzzling finding in this respect is the apparent disagreement between actual response of the liquid column to the residual gravity and predictions, as presented in the following reasoning. From Fig. 3b and c it can be concluded that the neck and ridge oscillate relative to mean values of 1.09 and 0.90 respectively. For that geometry, a cylindrical volume ($V=\pi R^2 L$) and that deformation, theory indicates the need of a Bond number Bo = 0.010. However, from the accelerometer data (Fig. 3g) a mean value of Bo = 0.017 is deduced, that, besides being quite distinct, is beyond the maximum Bo for stability with that geometry and assumed volume, Bo_{cr} = 0.015.

If the accelerometer data is discarded, the observed behaviour is easily explained as follows: a cylindrical column 100 mm long between discs of 35 mm supports a mean residual axial acceleration equivalent to Bo = 0.010 that, in absence of any other perturbation, would give an outer shape as in Fig. 4 (Bo = 0.010). From Mission Elapsed Time (MET) 6/03:10:40 to 6/03:13:00 what is seen is that due to the effect of stopping bridge stretching, a wide oscillation was superimposed that caused the shape to nearly reach the limiting deformation (see Fig. 4).

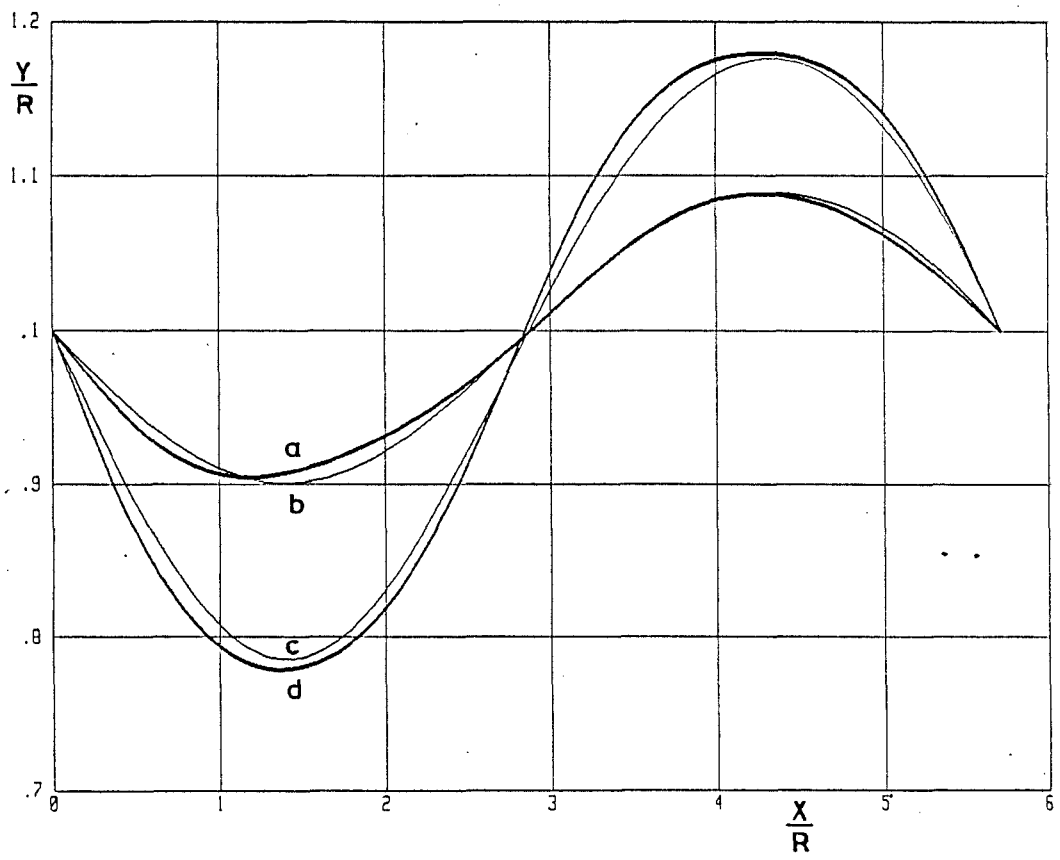

Fig. 4. Experimental (a and d) and theoretical (b and c) shapes of liquid bridges with L/D=2.857 and a cylindrical volume. From MET 6/03:10:40 to 6/03:13:00 the shape shows damped oscillations around shape a, going from a nearly cylindrical form to shape d. For that slenderness and volume, the maximum axial gravity allowed would correspond to a deformation as c. Thus, if the mean axial gravity were 7.10^{-4} m/s^2 (Bo=0.010), the equilibrium shape would have been b and the oscillations up to the limiting c shape quite understandable, but the accelerometers give nearly double value (see Fig. 3).

But the above explanation assumes a cylindrical volume, what means in this case $V/R^3=17.95$. As said before, no record of the amount of liquid volume manually injected was kept. The results of volume computation from film frames is shown in Fig. 3a, where the corresponding cylindrical value is also plotted for reference. From MET 6/3:11 to 6/3:14 this assumption seems justified (the mean value of these 90 shapes is 99.8% of the cylindrical one), but if the average is taken from MET 6/3:11 to 6/3/17 (180 shapes) a value of 98.9% of the cylindrical value is obtained, what, although close to it, make big changes to the reasoning above: now, instead of the limit Bond number being 0.015, the smaller volume would reduce the limit to Bo=0.012, which corresponds to a neck radius $Y_{neck}/R=0.85$, and the question arises, how could the necking observed at MET 6/03:10:49 (see Fig. 3b) go beyond that limit without breaking?.

Run 5: Disc rotation at 13 rpm

With a disc separation of 90 mm and (as before) cylindrical volume, the discs were spun to 13 rpm. Image analysis shows that even before the speed was reached, a necking started that finally ended in bridge disruption, also in the amphora-like mode, contrary to theoretical predictions for zero-gravity at this slenderness. The residual gravity seems to be the explanation, shifting the transition from C-mode to anphora-mode to a lower slenderness.

Unfortunately, a final trial at a length of 75 mm and 16 rpm, which would have shown C-mode instability, was not performed on SL-D1 for time constrains.

CONCLUSIONS

1. SL-D1 has provided very valuable experimental data (some of it still to be analyzed) on the mechanical behaviour of long liquid columns in a real microgravity environment.

2. Residual acceleration in SL-D1, of the order of 10^{-4} g (g = Earth gravity) is still so high that prevents experimentation with cylindrical liquid columns beyond 9/10 of the theoretical zero-gravity stability limit. Future Space Station environments are not expected to perform any better on that.

3. Platform maneuvers easily break long liquid bridges, but do not damaging short ones. This conclusion and the former came out after SL-D1, where columns lengths of 91 % of the stability limit were handled, because earlier experience in SL-1 with columns up to 54 % of the limit were little sensitive to residual accelerations (in fact, the effect of a Shuttle maneuver, a gentle push on the column, was the only noticeable event on that respect).

4. Volume computations from the liquid outer shape seem to point out a slight decrease of nearly 1% over a period of 6 minutes where it should be constant according to schedule. This teaches that redundancy in data collection during rare experimental occasions must be increased.

5. Observed natural oscillation of the liquid column (Fig. 3b) indicate a period of some 21 s for the first axial mode and nearly a third of that for the first transversal mode. These values support the thesis (Sanz, 1985) that the volume level was near cylindrical and not so close to instability as the 98.9% value (referred to above) would imply.

6. A discrepancy is found between the residual axial gravity that would theoretically cause a deformation as the mean value of oscillating shape in Fig. 3b (see Fig. 4), and the accelerometer readout.

5. Apart the latter, in all cases analyzed, the behaviour of long liquid columns in a real microgravity environment has been in agreement with theory up to the accuracy reached (~1%).

ACKNOWLEDGEMENT

This project is financed by the Spanish Space Research Commission (CONIE). We are indebted to Mr. J. López for his painstaking digitizing of the photographs.

REFERENCES

Da Riva, I. and Martínez, I. (1986). Floating liquid zones. Naturwissenschaften 73, 345-347.

Martínez, I. (1984). Liquid column stability. In Materials Sciences under Microgravity ESA SP-222, 31-36.

Martínez, I. and Meseguer, J. (1986). Floating liquid zones in microgravity. In Norderney Symposium on Results of Spacelab-D1 Mission DVFLR (FRG).

Martínez, I. and Rivas. D. (1982). Plateau Tank Facility for simulation of Spacelab experiments. Acta Astronautica 9, 339-342.

Martínez, I. and Sanz, A. (1983). Long liquid bridges aboard sounding rockets. ESA Journal 9, 323-328.

Meseguer, J., Mayo, L.A., Llorente, J.C. and Fernández, A. (1986). Experiments with liquid bridges in simulated microgravity. J. Crystal Growth (accepted).

Sanz, A. (1985). The influence of the outer bath in the dynamics of axisymmetric liquid bridges. J. Fluid Mech. 156, 101-140.

Sanz, A. and Martínez, I. (1983). Minimum volume for a liquid bridge between equal discs. J. Colloid Interf. Sci. 93, 235-240.

LIQUID BRIDGE BREAKAGES ABOARD SPACELAB-D1

José MESEGUER, Angel SANZ and Jesús LOPEZ

Laboratorio de Aerodinámica, ETSI Aeronáuticos,

Universidad Politécnica, 28040 Madrid, Spain.

The study of the stability of long liquid columns under microgravity was the purpose of one of the experiments carried out aboard Spacelab-D1. In this paper a preliminary analysis of this experiment, mainly concerning the different liquid column breakages, is presented. As shown in the paper, the behaviour, both static and dynamic, of long liquid bridges can be accurately predicted by using available theoretical models.

1. Introduction

The experiment Floating Liquid Zone (FLIZ), dealing with the behaviour of long liquid bridges under mechanical disturbances in a low gravity environment, was carried out by german payload specialist Dr. R. Furrer during the Spacelab-D1 Mission in November 1985 [1]. This experiment was performed in the Fluid Physics Module (FPM), one of the multiuser facilities provided by the European Space Agency for experimentation aboard spacecraft [2].

The configuration of the FLIZ experiment consisted in a volume of liquid held by surface tension forces between two equal diameter, coaxial solid disks, as sketched in fig. 1. The disks were made of Aluminium, with a 30^{o} sharp edge to avoid liquid spreading, the disk radius being R_o = 0.0175 m. Working liquid was a low viscosity dimethyl silicone oil (viscosity $\nu = 5 \times 10^{-6}$ $m^2.s^{-1}$, density ρ = 920 $kg.m^{-3}$ and surface tension σ = 0.02 $N.m^{-1}$) with tracers

(Eccospheres, 0.15 x 10^{-3} m in diameter and 0.1 kg.m^{-3} of concentration) to enhance inner motion visualization.

During the FLIZ experiment, the liquid bridge broke down six times, and these breakages are analyzed in this paper by comparing experimental results with available theoretical ones. As published elsewhere [3, 4, 5, 6] concerning liquid bridge breakage, the most suitable result to be experimentally checked is the partial volume (defined as the ratio of the volume of the larger drop appearing after liquid bridge breakage to the whole liquid column volume) because partial volume depends mainly on variables which can be easily controlled and experimentally measured (volume of the liquid column and the slenderness $\Lambda = L/(2R_o)$, where L stands for the distance between the disks). On the other hand, some other aspects of the liquid bridge breakage (i.e. the breaking time) are extremely difficult to check because of the strong dependence of these results on initial conditions, which are too hard to control accurately. Therefore, partial volumes obtained from the FLIZ experiment are compared with theoretical partial volumes obtained by solving a one-dimensional slice model for the dynamics of the liquid bridge. Since the ability of such slice model to predicts the dynamic behaviour of axisymmetric liquid bridges has been already tested through experiments in which microgravity was simulated by means of neutral buoyancy techniques [4, 5], one could expect similar agreement in the case of liquid bridges aboard a space station. The results presented here corroborate such assumption; experimental partial volumes obtained aboard Spacelab-D1 are in agreement with theoretical ones.

2. Breaking sequences

To analyze the different breaking sequences occurred during the FLIZ experiment, our sources of information have been a 16 mm film (shot at 0.5 frames per second) plus listings of the values of the experimental parameters

(disk positions, rotation speeds, accelerometer measurements, etc.) and voice records of the communications between the spacecraft and the Earth.

Since the breaking of liquid bridges was not the main goal in FLIZ procedures, available information on these breakages is quite different from one to another breaking sequence. In addition, since liquid injection and removal was performed manually, the only available source of information concerning liquid bridge volumes are the pictures.

The status of the several breaking sequences is summarized in table 1. Observe that Run 1, Run 3 and Run 5 are reasonably well documented. On the other hand, the breaking in Run 4 can not be analyzed because no pictures were shot after liquid column disruption. Concerning Run 2, the liquid bridge breaking happened just after vibration trials (an axial oscillatory motion.5 mm in amplitude and frequencies ranging from 0 to 1.6 Hz was imposed to the rear disk), and probably surprised the payload specialist (he stopped the film camera once vibration trials were finished, and there is a gap of about 1.5 min before the next picture). Finally, in the case of Run 6, an amount of data covering a period of about 8 min, which includes a isorotation trial and the sequent breaking process, has been unfortunately lost; so, in this case, the only sources of information are the film plus the voice records.

To measure liquid bridge volumes, the film frames have been enlarged and the contours of liquid bridge interfaces digitized. Since the reference length is the disk diameter, and in some pictures disks are not very well defined (see fig. 2), this method of calculation of liquid bridge volumes becomes very sensitive to the accuracy in disk diameter measurements; therefore, when possible, several pictures showing the same liquid bridge configuration have been measured, the values of the volumes here reported are the average values.

In the following, unless otherwise stated, volumes are made dimensionless with R_o^3. Two additional parameters are introduced: the static Bond number $B = \rho g R_o^2/\sigma$, and the Weber number $W = (\rho\Omega^2 R_o^3/\sigma)^{1/2}$, g and Ω being the axial

acceleration and the disk rotation speed, respectively.

To get an estimation of the value of Bond number during the FLIZ experiment (we consider only axial acceleration because lateral accelerations have higher order effects on stability limits [7]) the accelerometer readout supplied by DFVLR* has been used. The accelerometer gives the peak value sampled every second of acceleration in a reference system having one of the axes parallel to the liquid column axis [8]. The peak values of axial acceleration g^+ and g^-, respectively, during a period starting 3 min before breaking in Run 1, as well as the mean acceleration value g_m, are shown in fig. 3 (although accelerometer data are available at each 1 s, in this graph the interval between two sequent data is 5 s, so that high frequency perturbations do not explicitly appear in fig. 3).

In the case of a linear system (as it is well known from random process theory [9]) the mean level of a stationary random perturbation is transmitted through the system as a constant signal; that is, the superposed random perturbation does not affect the relation MLI/MLO = H(0) between the mean level input (MLI) and the mean level output (MLO), $H(\omega)$ being the transfer function which is characterized by the static response H(0) (already known for almost cylindrical liquid bridges in a reasonable number of cases [6,7,10-14]) and the resonance frequencies ω [3, 4]. This principle can be used to describe the dynamics of a liquid bridge, which can be considered as a linear system provided the interface deformations are small enough. In this case, the input is the imposed perturbation and the output would be some measurement of the interface deformation.

Unfortunately, the previous considerations are not strictly applicable to the phenomenon under study because the liquid bridge breaking is a non linear process. However, the principal statement of the linear analysis (the main contribution to the output is the mean level of the input) can be used as a

* Deutsche Forschung- und Versuchsanstalt fur Luft- und Raumfahrt e.V.

first insight in the problem, and to get an estimation of the mean level input a time averaged value, g_a, of the mean acceleration g_m can be used.

The dependence on the averaging time of the average axial acceleration g_a, defined as

$$g_a(t) = \frac{1}{t_b - t} \int_t^{t_b} g_m(\tau) d\tau \qquad (1)$$

is shown in fig. 4. In eq. (1) t stands for the time and the subscript b denotes the breaking instant (which coincides with the time origin, $t_b = 0$, in fig. 4). As it can be observed, this averaged value becomes nearly constant as the averaging time $t_b - t$ increases. Therefore, an estimation of the value of Bond number during FLIZ experiment based in this averaged value g_a could be $B = \rho g_a R_o^2/\sigma \sim 2 \times 10^{-3}$, this force being directed toward the feeding disk.

2.1. Run 1

Basically, the beginning of the different trials of the FLIZ experiment was the formation of a long liquid column. To perform this task, FLIZ procedures stated that once a short liquid bridge was formed, the payload specialist should increase disk separation (by moving the feeding disk) until the desired slenderness Λ is reached and, at the same time, inject working liquid into the liquid bridge to keep its volume nearly cylindrical ($V = 2\pi\Lambda$) at any instant. This process is represented by line **a** in the stability diagram shown in fig. 5. The first breaking occurred because the injection law followed by the payload specialist (as already stated, injection was performed manually) was not that intended; therefore, the final configuration was very close to the minimum volume stability limit [5, 10] and thus, taking into account the value of the Bond number estimated in § 2, breaking in Run 1 happened because the liquid bridge became smaller than that of the minimum volume stability limit for the corresponding value of B.

The liquid bridge volume at the breaking configuration and the partial

volume, both theoretical and as measured from photographs, are shown in table 2 (in all the cases the larger drop was the one anchored to the feeding disk, which is in agreement with the above mentioned sense of axial acceleration).

Theoretical partial volumes corresponding to experimental configurations have been obtained from fig. 6, which has been plotted from previous results already published in [5, 6]. Fig. 6 gives, for each value of the liquid bridge volume V and the slenderness Λ, the partial volume v_p, calculated by using a one-dimensional slice model for the dynamics of the liquid column [3 - 6]. Although v_p depends mainly on V and Λ, in fig. 6 the dependence on the Bond number of the minimum volume stability limit is also represented (for each B =constant curve the stable region is that placed above the curve).

Then, selecting the appropriated Λ = constant curve and the liquid bridge volume V, obtained from measurements of pictures, the theoretical value of v_p results*. Observe that, since the slope of the Λ curves increases as the liquid bridge volume decreases, the error in theoretical v_p values increases as V decreases. In the first breaking (see table 2) measured values of v_p are about 3.5 % smaller than theoretical values (Run 1 gives the highest difference between experimental and theoretical values). The reason for this comparatively large difference could be that breaking in Run 1 happened after a liquid injection process (which tends to push the liquid towards the rear disk) combined with feeding disk separation (which has a similar effect) whereas theoretical results were obtained by assuming a liquid bridge at rest to which a perturbation (Bond number) is imposed at the initial time.

---

* Note that, except in the case of Run 1, according to the mean value of Bond number estimated in § 2, all static configurations at breaking were stable. This indicates that axial mean acceleration was not the cause of these liquid bridge breakages, as will be explained later.

2.2. Run 2

As shown in table 1, Run 2 breaking is not very well documented. This breaking happened after oscillation trials, the resulting static liquid bridge configuration being stable (fig. 5). Liquid column breaking probably occurred because of an extremely high peak of axial acceleration. In any case, the main problem in the study of this breakage is that the breaking process was not filmed, so that it is not possible to correlate liquid bridge evolution with available acceleration recording. The values of axial mean acceleration, g_m, and time averaged acceleration, g_a, covering a period which roughly coincides with the not-filmed breaking process, are shown in fig 4; in this plot the time origin has been fixed arbitrarily, coinciding with the first picture in which the liquid bridge appears broken in two drops.

Concerning partial volume, as shown in table 2, the experimental value is about 1.4 % higher than the theoretical value obtained from fig 6.

2.3. Runs 3, 5 and 6

Each of these three liquid bridge breakages took place after a isorotation trial. In these three cases, the static liquid bridge configurations were stable (figs. 5 and 6) but they become unstable when the prefixed rotation speeds were imposed (see fig. 7). Rotation speeds and slendernesses were selected in FLIZ procedures aiming to check the dependence on rotation speed of instability modes (axisymmetric mode or C mode [10, 11, 12]). Rotation speeds and slendernesses were Ω = 10 rpm, Λ = 2.875 (Run 5), Ω = 13 rpm, Λ = 2.571 (Run 6) and Ω = 12 rpm, Λ = 2.714 (Run 3) which correspond to axisymmetric modes, to C modes and to the border between these two types of instability, respectively. A fourth isorotation trial, represented by a square in fig. 7 (Ω = 16 rpm, Λ = 2.143) was foreseen in FLIZ procedures, but there was no time to carry it out during Spacelab-D1 Mission.

In these three breakages the breaking process was axisymmetric. This

behaviour is obvious in the Run 3 case and even in the Run 5 case (fig. 7), but it is not so clear in the Run 6 breaking, where one could expect a C mode breaking. To explain this last case, additional perturbations, other than disk rotation, must be considered in the stability analysis. Fig. 8, which has been drawn after theoretical results reported in [12], shows the maximum amplitude of the interface deformation ε of stable equilibrium shapes in the Λ-W stability diagram. As it can be observed, except in the region bounded by lines BE and BC, the perturbation level needed to excite C mode instabilities is higher than that needed in the axisymmetric case. The main conclusion which can be obtained from fig. 8 is that any white noise, such as that existing during Spacelab-D1, acting on the liquid bridge ($\varepsilon > 0$) moves point B effectively towards higher values of W, increasing the axisymmetric instability region and decreasing the C mode instability one. Therefore, the axisymmetric behaviour in Run 6 breaking may be explained independently of the value of the axial acceleration during Run 6, which would be assumed to be similar to that measured during the remaining liquid bridge breakages ($B \sim 2 \times 10^{-3}$).

The evolution of the liquid bridge neck during the breaking processes under consideration is shown in fig. 9. Observe that in the case of Run 3 there is an oscillatory motion superposed to the breaking evolution. Concerning partial volumes (table 2) there is a surprising agreement between theoretical and experimental values (the maximum difference being 1.2 % in the Run 5 case) in spite of the fact that in these three trials the liquid bridge was rotating whereas theoretical results were obtained by using a mathematical model which does not includes liquid column rotation. The reason for this agreement is that, once axisymmetric instabilities are excited, they govern the sequent liquid bridge evolution.

3. Conclusions

Five liquid bridge breaking sequences that occurred aboard Spacelab-D1 have been analyzed and compared with theoretical predictions. Although our attention has been focused mainly on breaking processes, the results obtained allow us to establish two main conclusions. First, theoretical stability studies predict accurately all of these liquid bridge breakages. Second, there is agreement between experimental and theoretical partial volumes, which seems to indicate that the breaking of a liquid bridge is a phenomenon mainly driven by surface tension (at least for the level of perturbations reached aboard Spacelab-D1), the different perturbations imposed to the liquid column, either accidental or intentionally, acting as a trigger that causes capillary instabilities to develop.

Acknowledgement

This work has been supported by the Spanish National Commission for Space Research. The authors acknowledge the collaboration of Dr. I. Martínez.

REFERENCES

[1] Scientific Goals of the German Spacelab Mission D1, P.R. Sahn and R. Jansen, eds., (DFVLR, Koln, 1985).

[2] A. Gonfalone, in: ESA SP-222, Paris, ESA (1984), 3.

[3] J. Meseguer, J. Fluid Mech. 130 (1983) 123.

[4] A. Sanz, J. Fluid Mech. 156 (1985) 101.

[5] J. Meseguer and A. Sanz, J. Fluid Mech. 153 (1985) 83.

[6] J. Meseguer, J. Crystal Growth. 73 (1985) 599.

[7] S. R. Coriell, S. C. Hardy and M. R. Cordes, J. Colloid Interface Sci. 60 (1977) 126.

[8] P. Zimmermann, The German Microgravity Laboratory for Material Science and Space Processing Experiments. Growth of Protein Crystals by Diffusion into Sodium Solution. A Material Science Experiment in Spacelab,,(MBB Space Division, Ottobrunn, Germany, Sep. 1979).

[9] J. S. Bendat and A. G. Piersol, Random Data: Analysis and Measurement Procedures, (Wiley Interscience, New York, 1971).

[10] I. Da Riva and I. Martínez, in: ESA SP-142, Paris, ESA (1979), 67.

[11] I. Martínez, in: COSPAR Space Research XVIII, Pergamon (1978), 519.

[12] J. M. Vega and J. M. Perales, in: ESA SP-191, Paris, ESA (1983), 247.

[13] J. Meseguer, in: ESA SP-222, Paris, ESA (1984), 297.

[14] J. Meseguer, L. A. Mayo, J. C. Llorente and A. Fernández, J. Crystal Growth. 73 (1985) 609.

Table 1

Availability of information concerning liquid bridge breakages during FLIZ experiment (Spacelab-D1)

Run*	Pictures prior to breaking available?	Number of pictures shot after breaking	Parameter listing available?
1	YES	10	YES
2	NO	2	YES
3	YES	15	YES
4	YES	0	YES
5	YES	22	YES
6	YES	21	NO

* Breaking sequences are numbered chronologically

Table 2

Liquid bridge breakages during FLIZ experiment aboard Spacelab-D1. Λ: slenderness, V: dimensionless liquid bridge volume, v_{pe}: experimental partial volume, v_{pt}: theoretical partial volume.

RUN	Λ	V $\pm$ 0.3	v_{pe} $\pm$ 0.004	v_{pt}
1	2.714	13.5	0.739	0.765 $\pm$ 0.018
2	2.714	16.8	0.879	0.867 $\pm$ 0.006
3	2.714	16.8	0.871	0.867 $\pm$ 0.006
5	2.857	17.4	0.846	0.856 $\pm$ 0.006
6	2.571	16.5	0.884	0.881 $\pm$ 0.006

FIGURE CAPTIONS

Fig. 1. Sketch of the liquid bridge (FLIZ experiment, Spacelab-D1). FD: feeding disk, RD: rear disk.

Fig. 2. Breaking sequences of long liquid bridges aboard Spacelab-D1. In each picture series times are, relative to the bottom picture, -10 s, -4 s, -2 s and 0 s.

Fig. 3. Accelerometer data in the liquid bridge axial direction prior to the first liquid column breaking (Run 1). Black circles correspond to readout of accelerometer (peak values of acceleration sampled at 1 s interval, g^+ and g^-, respectively) whereas white circles indicate mean acceleration g_m.

Fig. 4. Axial mean acceleration g_m (white circles) and averaged acceleration, g_a (black circles) prior to breakage for several liquid bridge sequences. In each plot the time origin corresponds to the breaking time with an error of ± 1 s, except in the Run 2 case (see § 2.2).

Fig. 5. Variation with Bond number B of the minimum volume stability limit V. Line **a** corresponds to cylindrical volume liquid bridges, $V = 2\pi\Lambda$. Black circles indicate where the liquid column breaking occurred, whereas white circles indicate the filling law manually followed in the first trial (Run 1).

Fig. 6. Partial volume v_p versus minimum volume stability limit V. Numbers on the curves indicate the values of the slenderness Λ (continuous lines) and the Bond number B (dashed lines). Line **a** corresponds to cylindrical volume liquid bridges, $V = 2\pi\Lambda$. Black circles indicate experimental liquid bridge configurations at breaking during the FLIZ experiment and the heavy lines indicate the accuracy in measurements of the liquid bridge volume.

Fig. 7. Variation with Weber number W of the maximum stable slenderness Λ of cylindrical volume liquid bridges ($V = 2\pi\Lambda$) in gravitationless conditions ($B = 0$); line ABC corresponds to axisymmetric stability limit, $\Lambda(1+W^2)^{1/2}=\pi$, whereas line DBE corresponds to non-axisymmetric (C mode) stability limit, $2\Lambda W=\pi$ [12]. Therefore, there are four different regions in this stability diagram: the region below line ABE is stable, but the region associated with the acute angle ABD is a region in which there is instability to axisymmetric modes but stability with respect to C modes (the contrary occurs in the region EBC); finally, in the region above line DBC both kind of instabilities take place. Black circles indicate experimental liquid bridge configurations during the FLIZ experiment. The square corresponds to a fourth isorotation trial foreseen in FLIZ procedures which was not performed because of time constraints.

Fig. 8. Variation with the slenderness Λ and the Weber number W of the maximum interface deformation ϵ (defined as sketched in the insert) of stable equilibrium liquid bridges.

Fig. 9. Variation with time t of the neck radius of the liquid bridge r and the Weber number W during isorotation trials performed aboard Spacelab-D1. Neck radii have been measured from pictures whereas W curves have been plotted after parameter listing; line type indicates when data was available (continuous line) or not (dashed line).

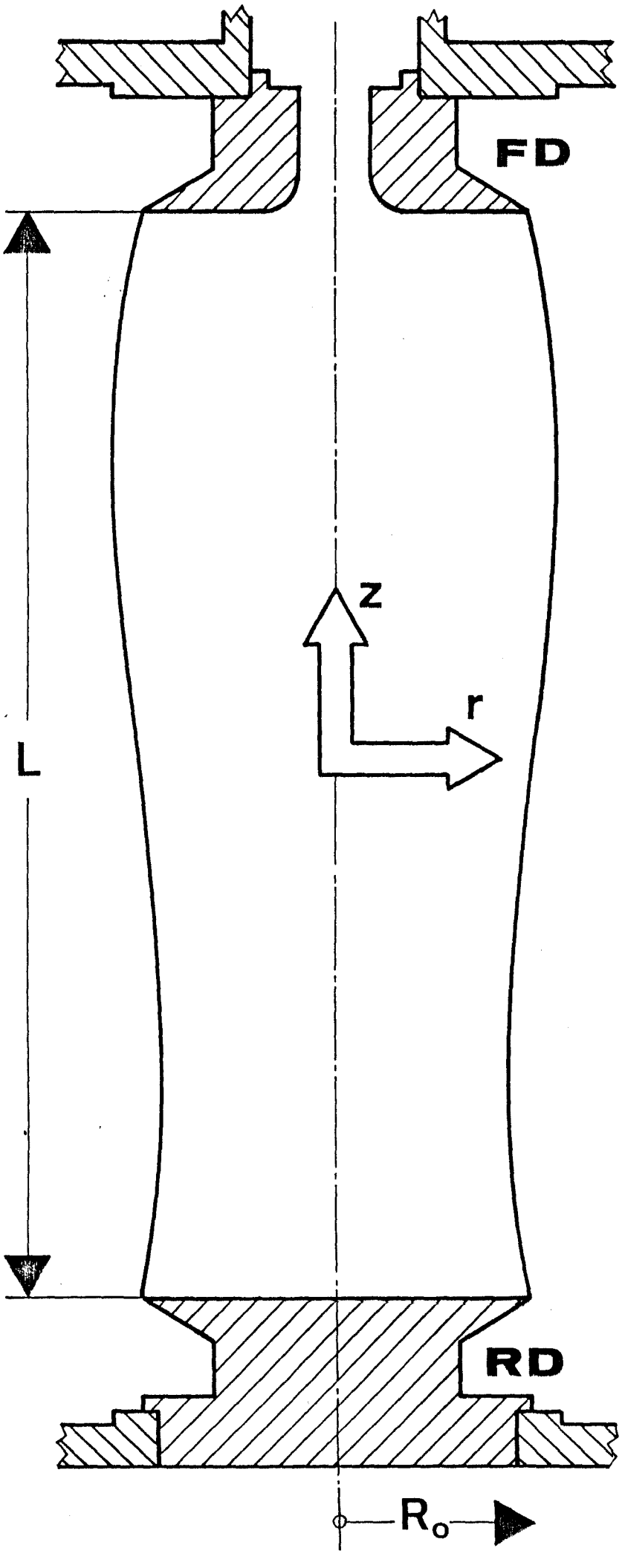

Fig. 1

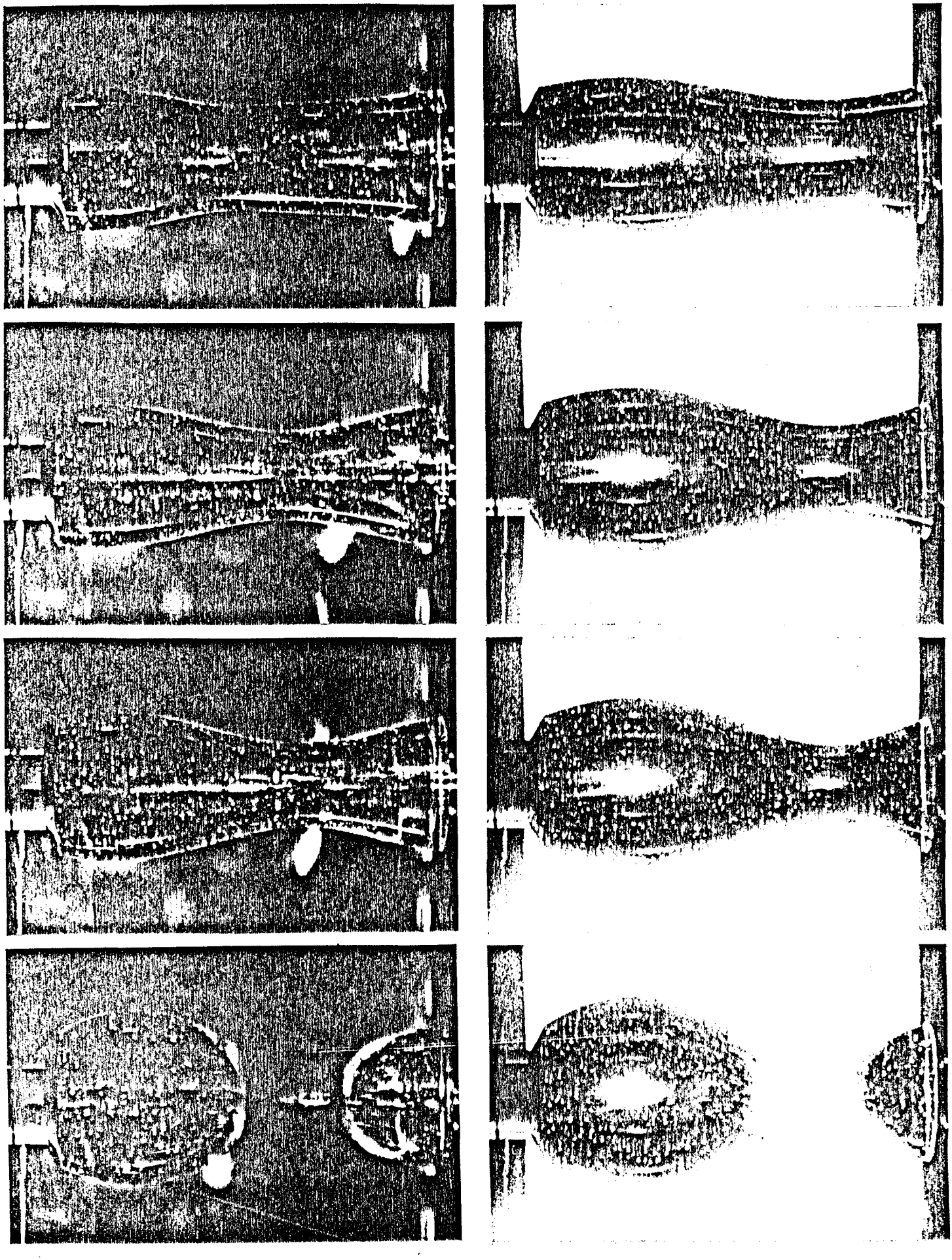

Fig. 2a

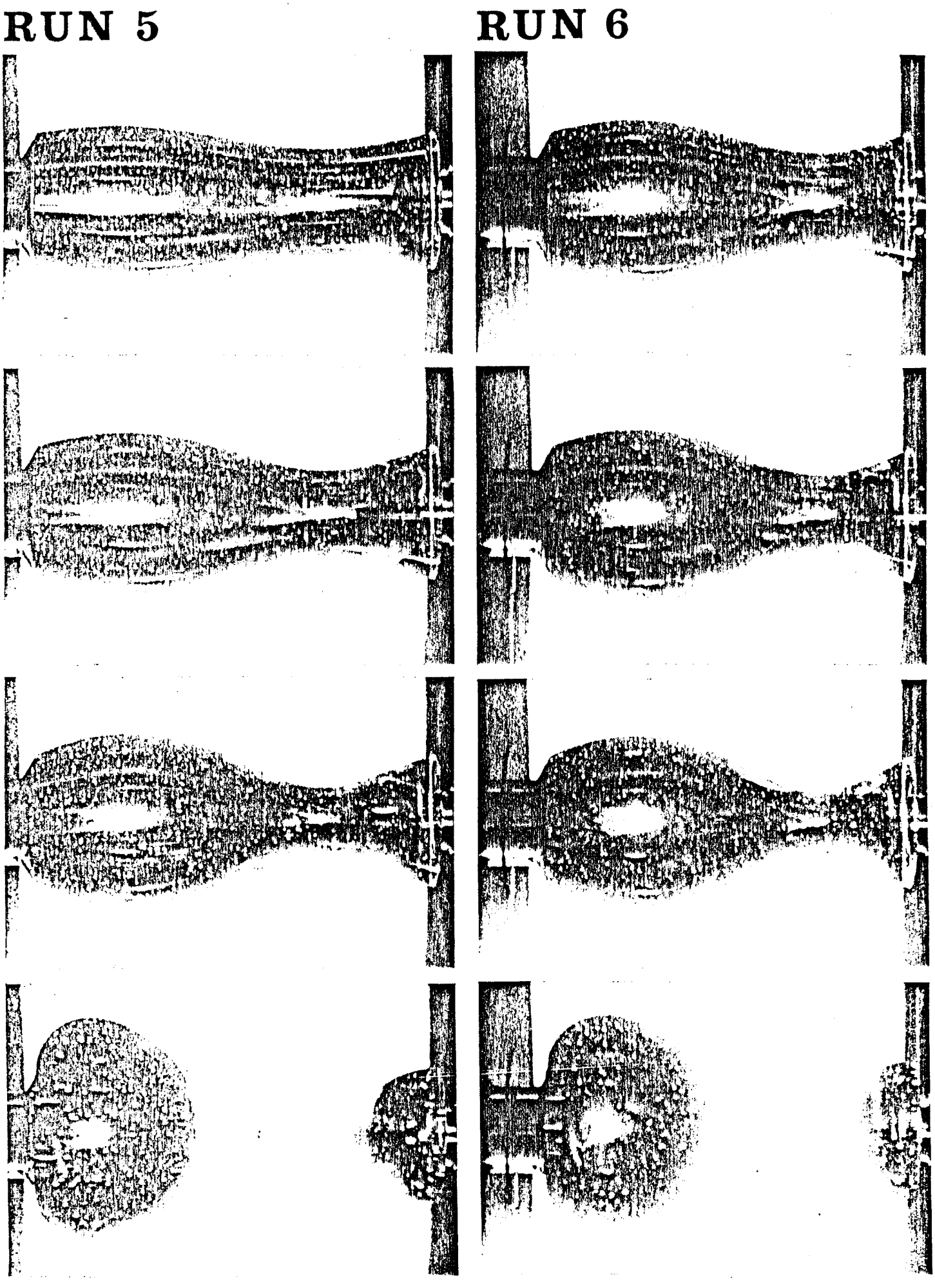

Fig. 2b

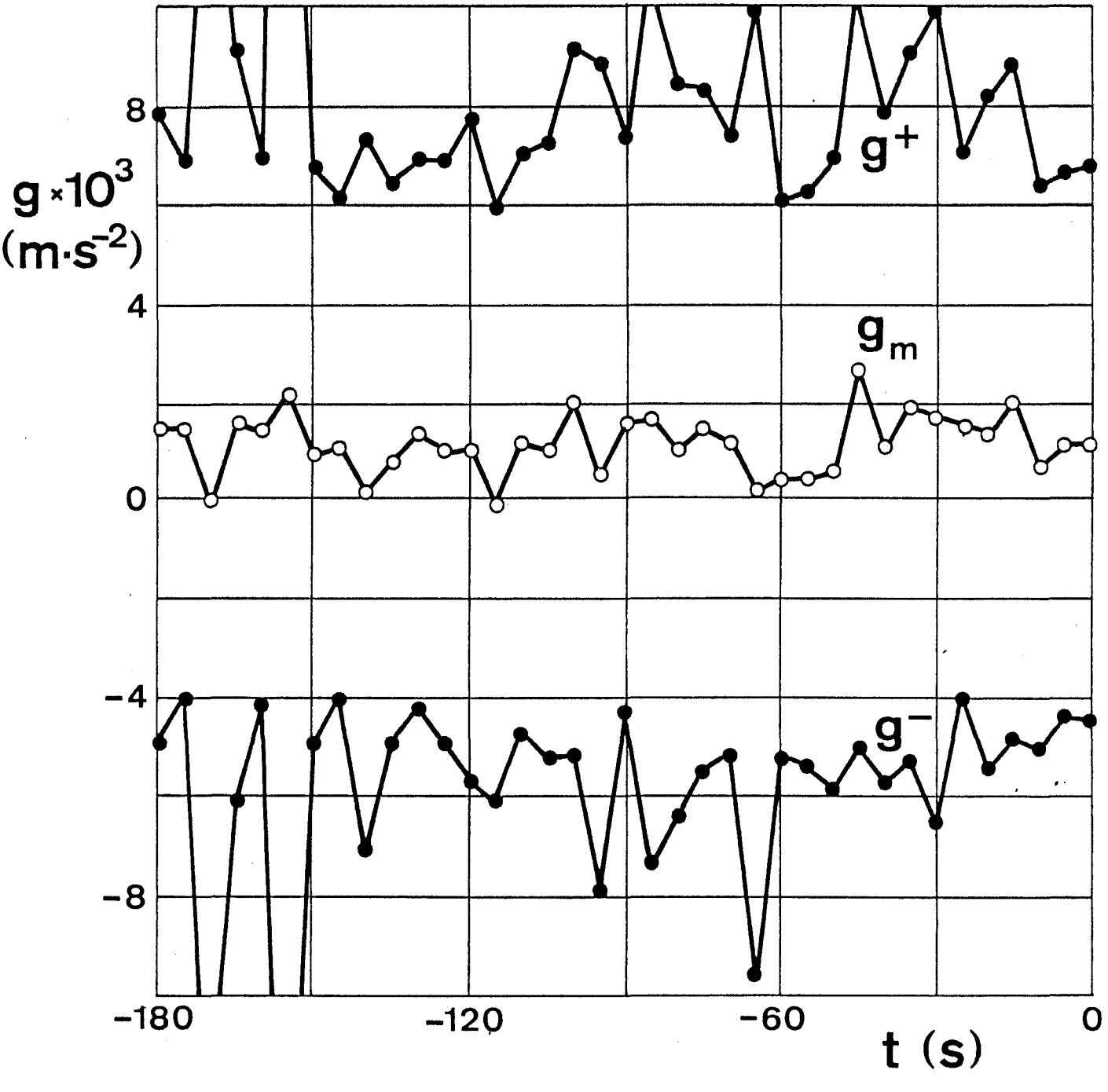

Fig. 3

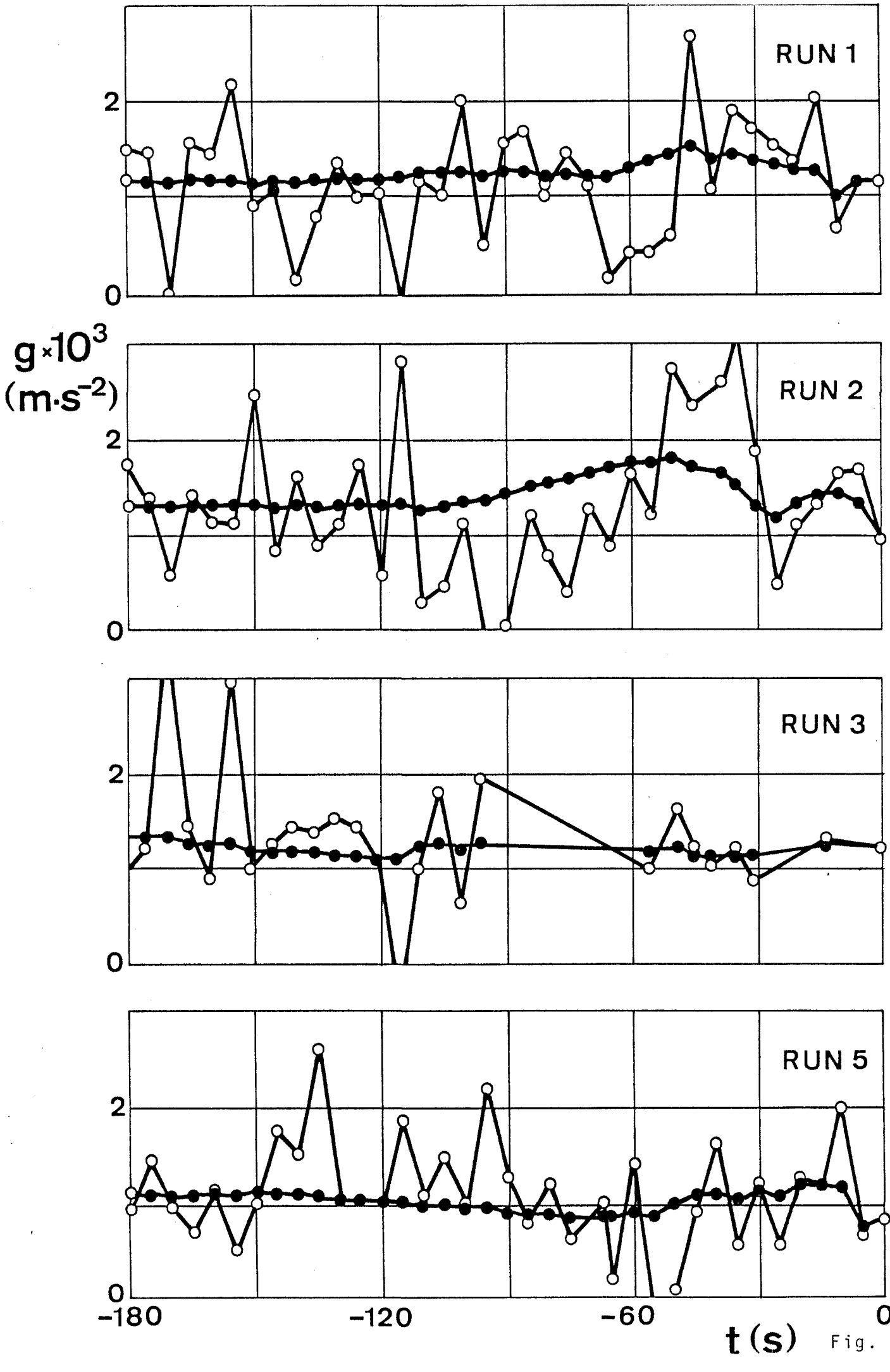

Fig. 4

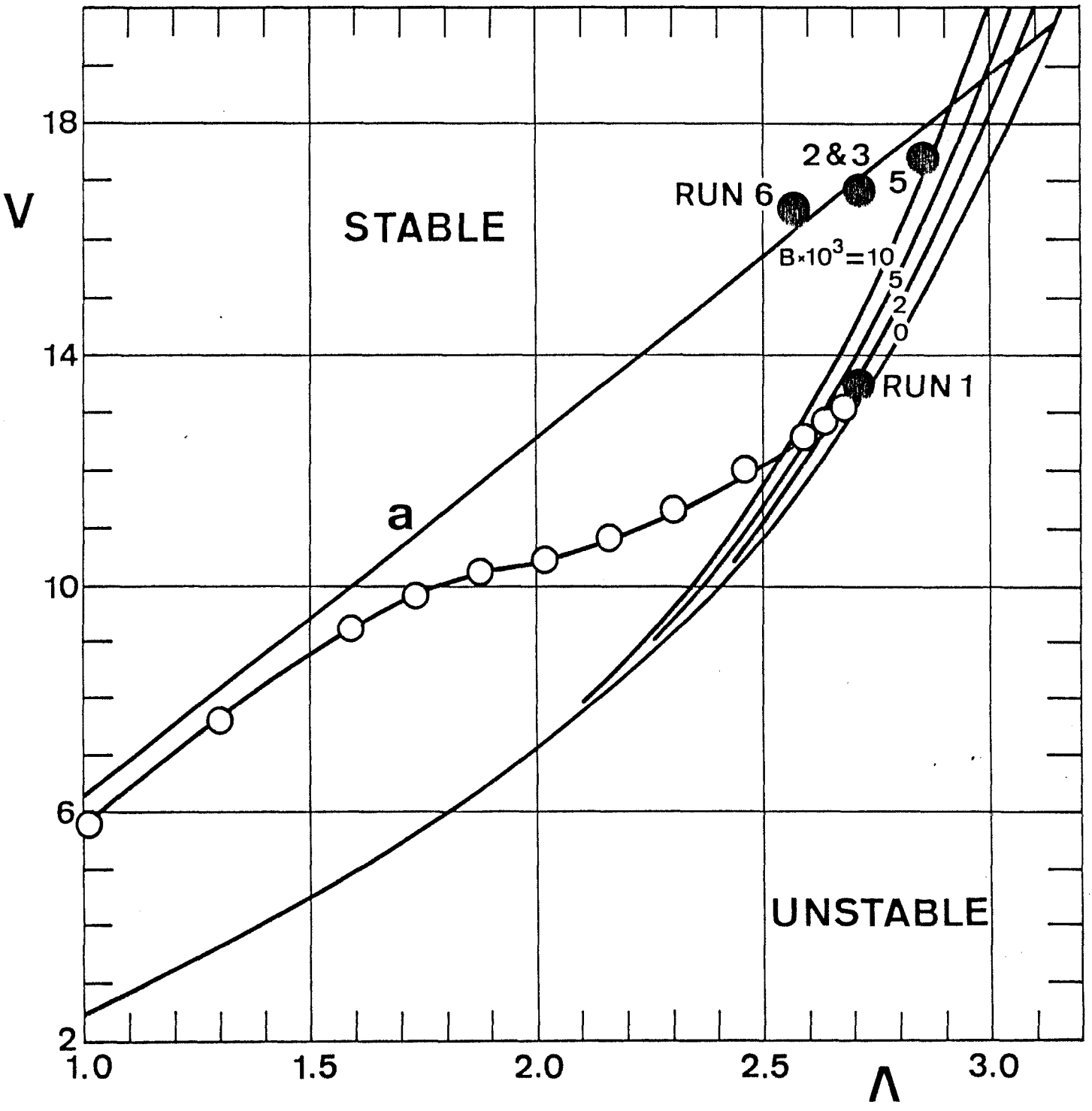
V
18
14
10
6
2
1.0
1.5
2.0
2.5
3.0
Λ
STABLE
UNSTABLE
RUN 6
2&3
5
RUN 1
B×10³=10
5
2
0
a

Fig. 5

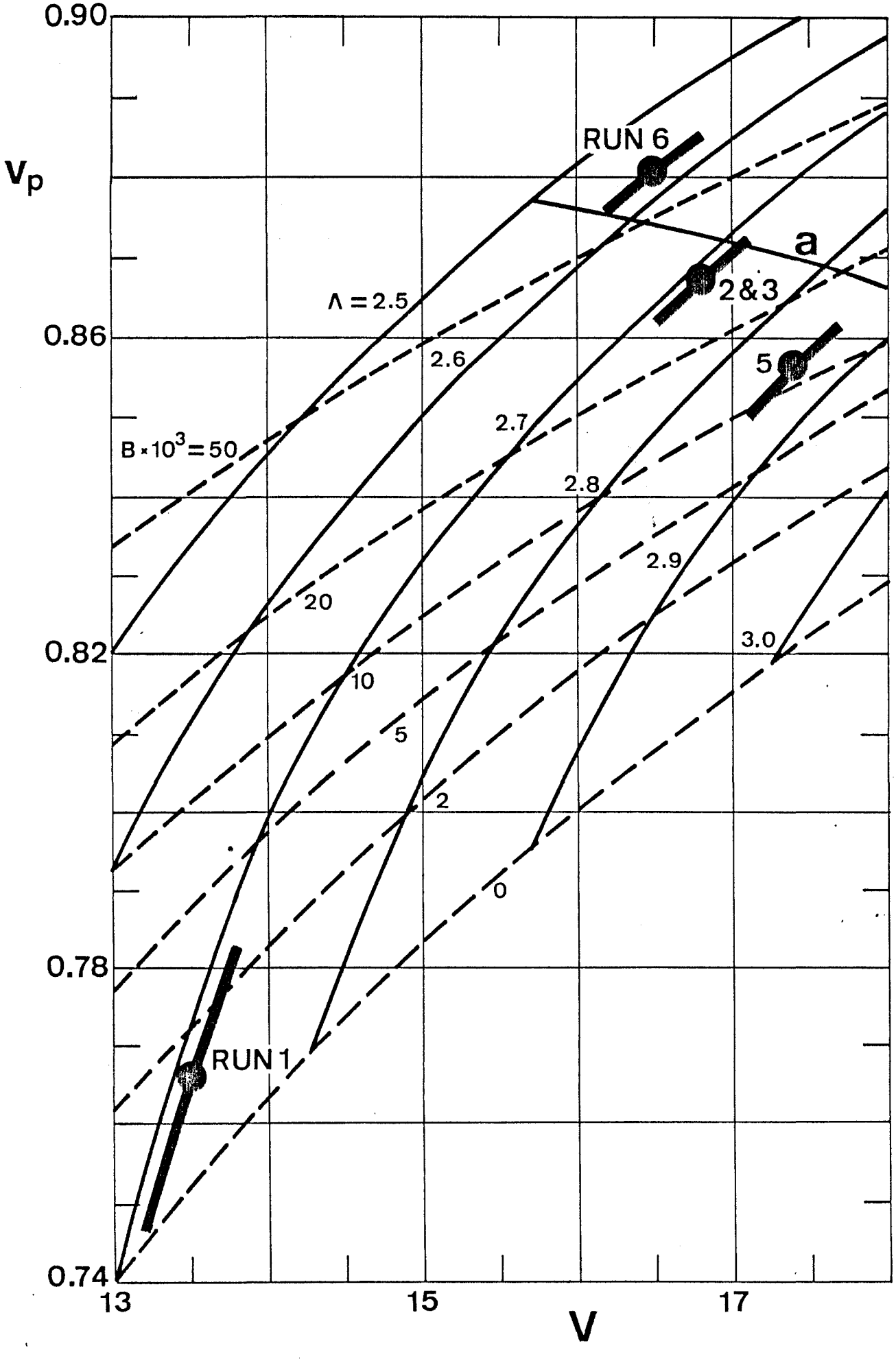
0.90
0.86
0.82
0.78
0.74
V_p
13
15
17
V
RUN 6
a
2&3
5
RUN 1
Λ = 2.5
2.6
2.7
2.8
2.9
3.0
$B \times 10^3 = 50$
20
10
5
2
0

Fig. 6

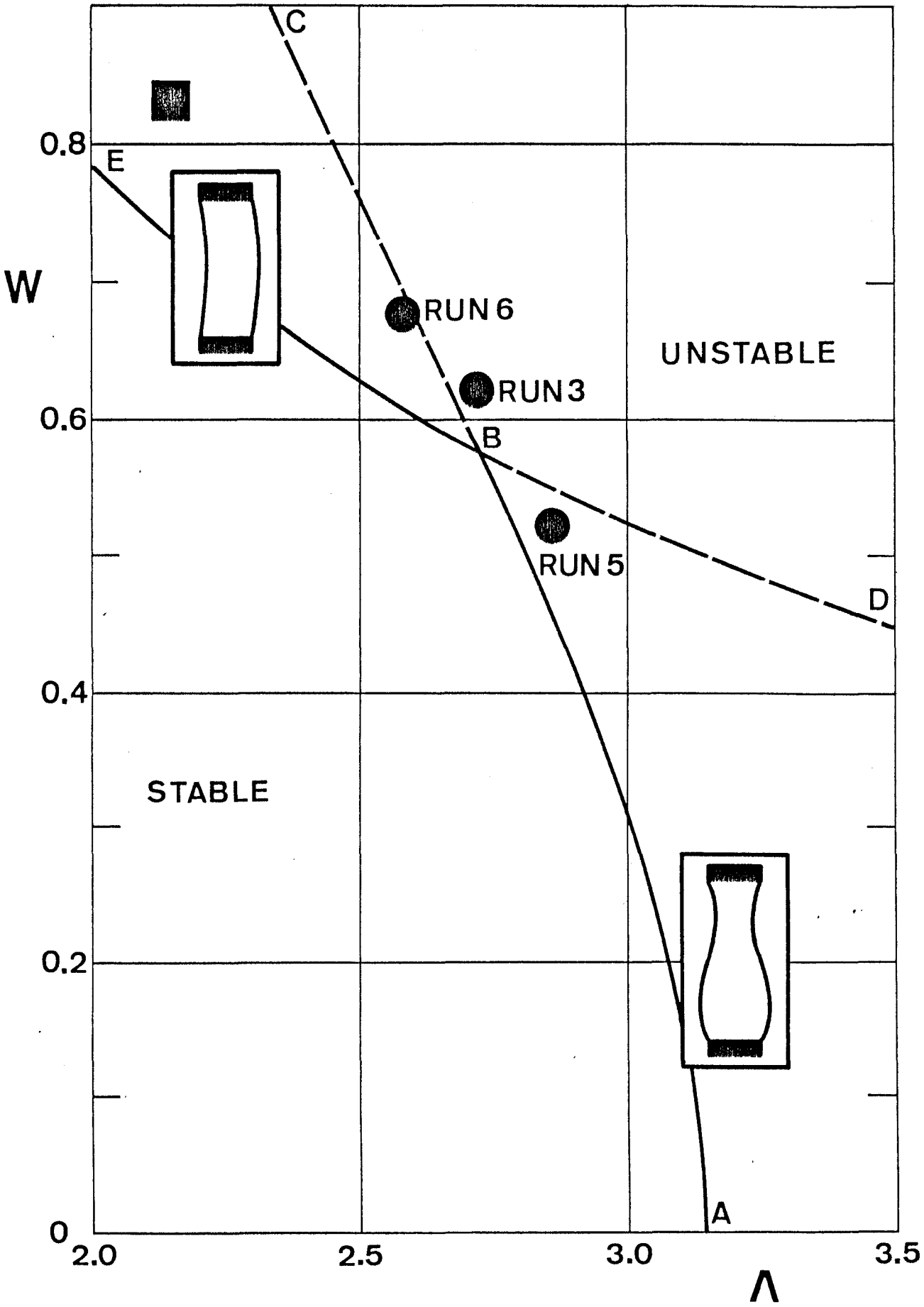
C
E
RUN 6
RUN 3
RUN 5
B
D
A
UNSTABLE
STABLE
W
Λ
0.8
0.6
0.4
0.2
0
2.0
2.5
3.0
3.5

Fig. 7

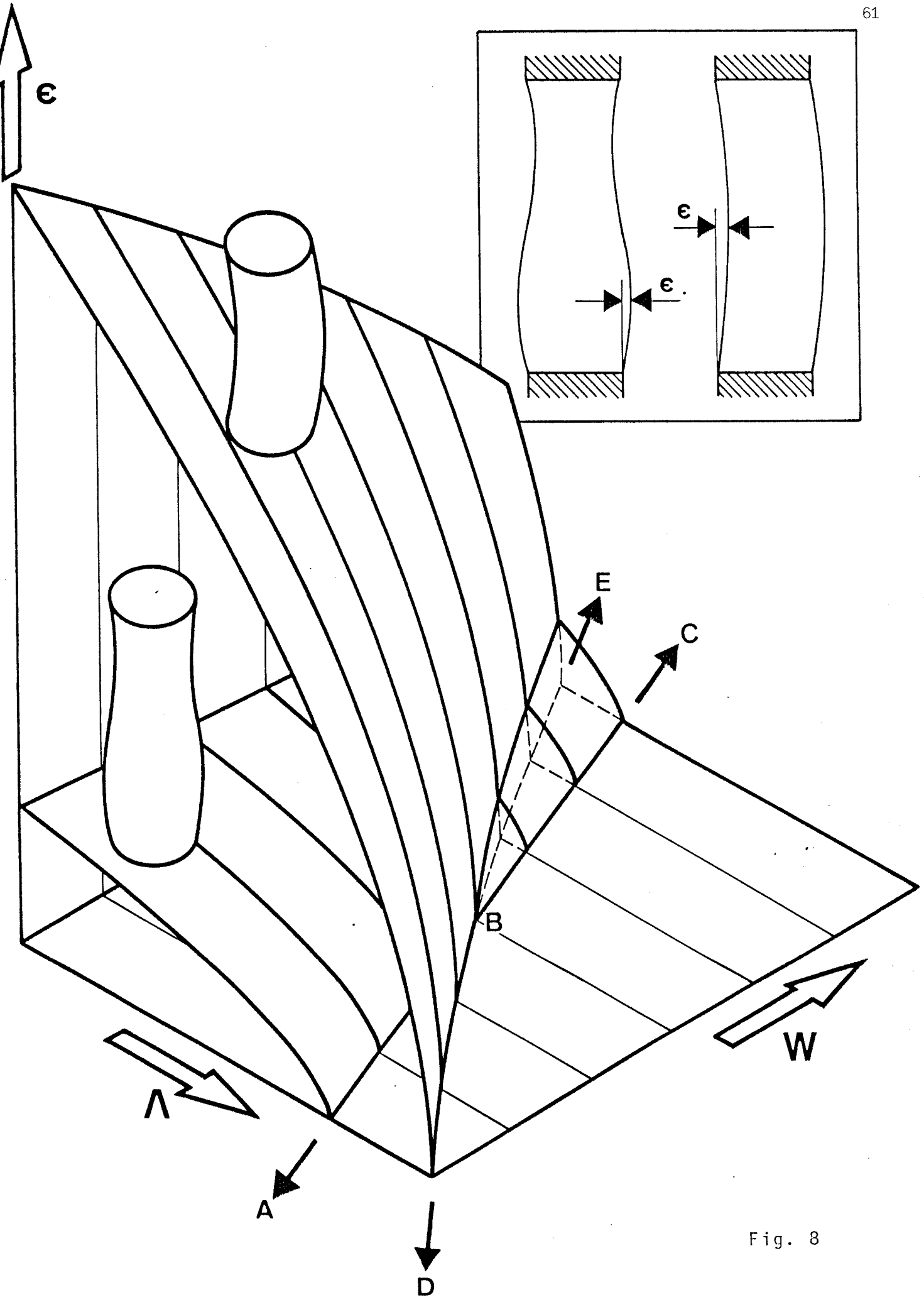

Fig. 8

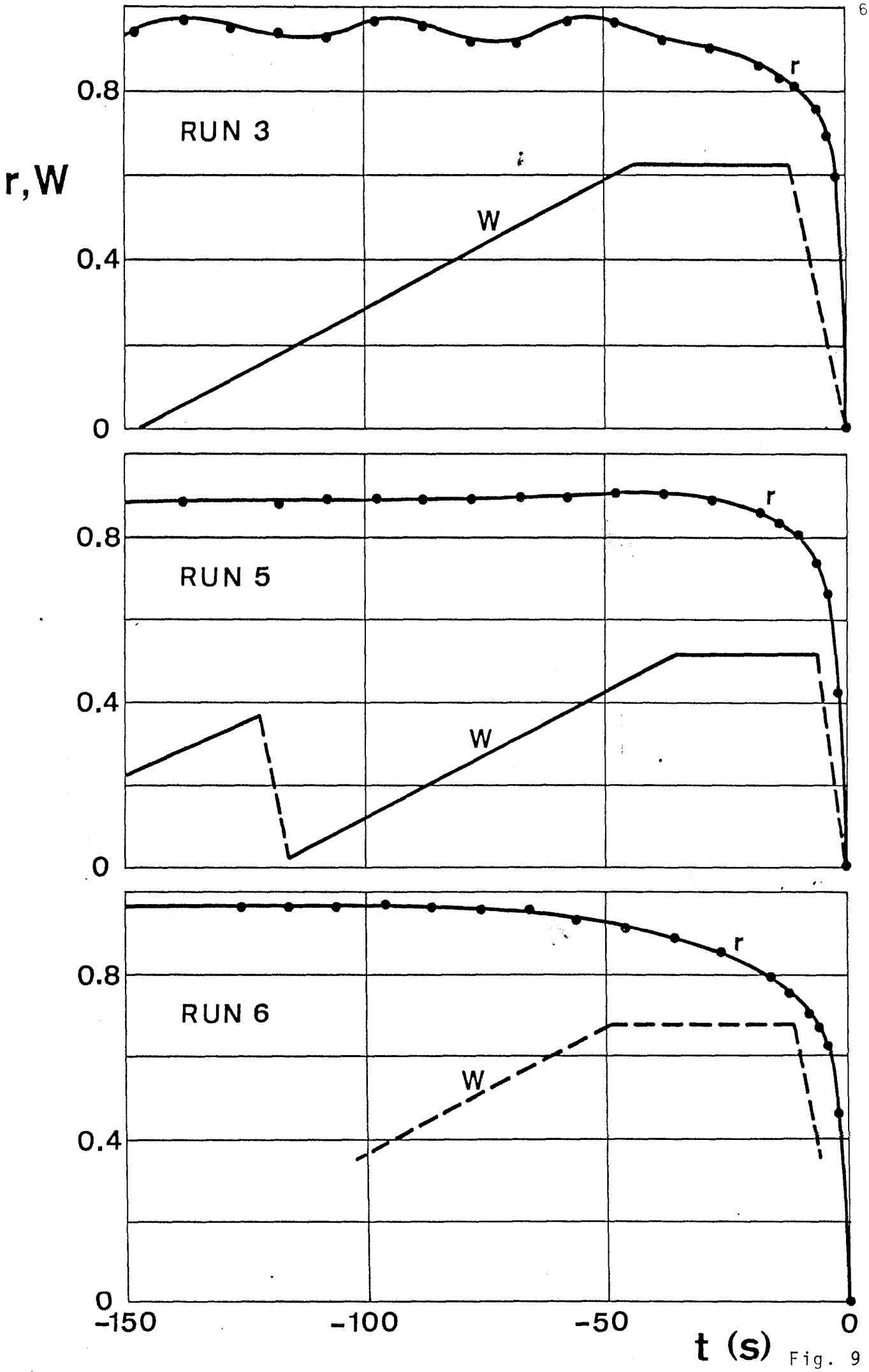

Fig. 9

STABILITY OF LONG LIQUID COLUMNS IN SPACELAB-D1

by I. Martinez

Universidad Politécnica de Madrid, E.T.S.I.Aeronáuticos, 28040-Madrid, Spain

ABSTRACT

An updated analysis of Experiment FPM-04-FLIZ, carried out aboard Spacelab-D1 mission in November 1985, is given. An account of the activities performed, problems found, raw data obtained, method of analysis and results achieved, is presented.

Keywords: microgravity, capillarity, stability, experiment, liquid bridge, floating zone, space operations, telescience.

1. INTRODUCTION

The configuration of experiment WL-FPM-04,"FLIZ" (Floating Liquid Zones) consisted of a near cylindrical volume of liquid held by surface tension forces between two equal in diameter coaxial solid discs at whose borders the liquid is attached. Discs were made of aluminium, with a 30° receding sharp edge to avoid liquid spreading, the discs radius being R = 0.0175 m (D=0.035). Working liquid was a low viscosity dimethyl silicone oil (viscosity $\nu = 5 \times 10^{-6}$ m^2/s^1, density $\rho = 920$ kg/m^3 and surface tension $\sigma = 0.02$ N/m) with tracers (Eccospheres of 0.15 mm in diameter and concentration of 0.1 kg/m^3) to enhance inner motion visualization.

The nominal experiment sequence envisaged [1] basically consists of: liquid injection, disc vibration and rotation of both discs, and was similar (slightly reduced) to the one tried on Spacelab-1 (SL-1) in 1983 where wetting and spreading problems with the nominal configuration allowed only partial success [2]. There, although the much wanted C-mode deformation of the liquid column was indeed finally excited by rotating a large liquid bridges with a length to mean diameter ratio of 1.7, most of the time the liquid went out of control beyond the small mechanical and chemical (anti-spread coating) barriers. As on that occasion, the interest here was to check the liquid bridge response against available theories, mainly concerning its stability limit, a problem of practical importance in crystal growth by the floating zone technique [3].

The preparation, performance and early results of this experiment has been described in earlier papaers [4-6]. The same Fluid Physics Module (FPM), but with corrected end-discs (more protruding and cut back) and a manually operated syringe for liquid injection was used. A small video-camera and a 16 mm cine-camera, the later shooting a frame every 2 seconds for "hot" phases of the experiment and every 92 seconds for the rest of time, were the main source of data for later analysis (this odd figure was chosen to simplify manual settings).

After SL-1 and before SL-D1, some other trials were performed on the sounding rocket TEXUS-12 (May 1985) with big success [7]. Long (80 mm) cylindrical liquid bridges were established in less than a minute, demonstrating that sounding rocket flights (lasting 6 minutes) can be used to perform experiments in microgravity with large liquid masses.

The overalll performance of FLIZ experiment was excellent: in particular, a large liquid mass was accurately positioned in the test chamber, well anchored to the sharp edges of coaxial discs. Long cylindrical liquid columns of slenderness (length/diameter) 2.86 were easily established several times (the limit for no gravity being π). A long cylindrical liquid column subjected to specified axial vibrations showed deformations with as many nodes (1, 2, 3, 4 and 5) as predicted by theory for each case. Several (four) long cylindrical liquid columns were made to rotate at increasing rates and all them destabilized near the theoretical limit. The breaking of long cylindrical liquid bridges when subjected to perturbations beyond the stability limit gave way to two separate drops with relative volumes as predicted by theory [8].

It is a pity that the big time-constraint in SL-D1 did not allow to finish the sequence of rotation trials and the much wanted C-mode instability could not be realized this time.

2. EXPERIMENT EXECUTION

For this research, Payload Specialist (PS) Dr. Furrer was in charge of the in-flight experimentation. The nominal time allocation was from Mission Elapsed Time (MET) 5/22:48:00 to 6/00:49:00 (two hours). Actual start time was 5/23:21:00 (FPM

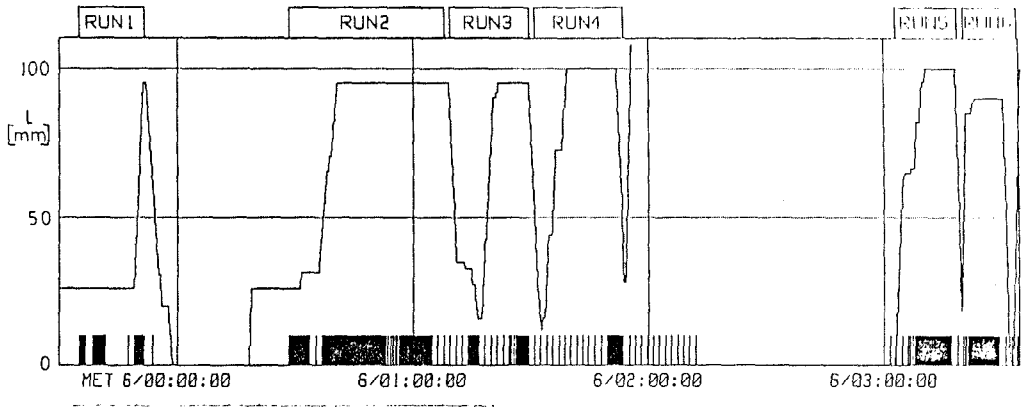

Fig. 1. Actual disc separation L versus time during the SL-D1 experiment FLIZ. Vertical lines at the bottom indicate when photos were taken (sparse lines have 92 s interval, whereas filled areas correspond to packed lines at 2 s interval).

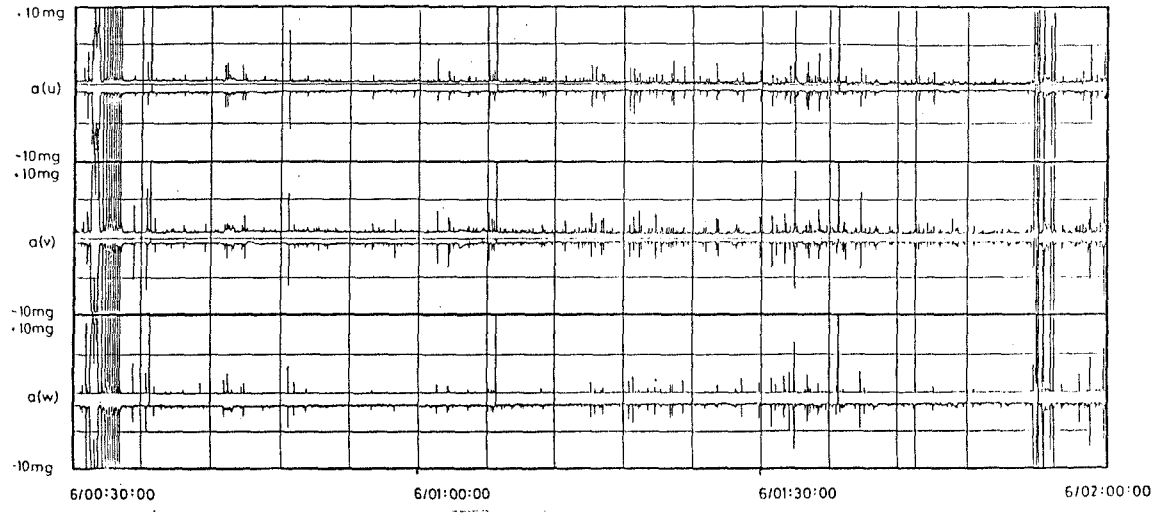

Fig. 2. Signal from accelerometers near the Fluid Physics Module in Spacelab-D1. The maximum value inside a 1 s interval, for each of the six directions, is recorded. The unit mg stands for 10^{-3} times Earth gravity.

power up), and the first good picture (it was frame number 45, but the previous were over-exposed) was taking 14 minutes later, already showing a liquid drop formed on the feeding disc (FD). There was no air/ground link at the time.

After all the problems of handling the working liquid in SL-1, there was no foreseen breakage of the liquid column until late in the experiment sequence. However, it turned out that the intended overpassing of the rotational stability limits always ended in bridge disruption. Fortunately, the PS had great dexterity in recovering back and start anew, what has served to divide the experiment in "Runs", as shown in Fig. 1, that group all trials ended in disruption of the liquid bridge; a total of 6 such Runs have been recorded, a detailed description of which can be found in Table 1 of Ref. [5].

The most peculiar finding during SL-D1 was the effect of g-jitter, much higher than in SL-1 and TEXUS-12. The accelerometer data from SL-1 and SL-D1 show similar levels of g-jitter, namely 10^{-3}g (10^{-2}m/s^2) high frequency peaks, with a 100 μg averaged mean (Fig. 2), but the liquid column behaves widely differently (in SL-1 interfacial deformations caused by noise were unnoticeable). The explanation found is due to the increased stability of low slender columns (1.7 in SL-1 against 2.86 for SL-D1, the stable limit (for zero gravity) being π; a steady linear theory predicts 20 to 30 times larger deformations for the same stimuli).

In spite of the fact that the PS asked the other crew-members to keep quiet and was granted from the Shuttle pilot a no-maneuvers period, the long columns achieved in SL-D1 were trembling (slowly)

and this noisy ambient may have contributed to premature breaking of the column. Although these breakings demanded extra crew-time for liquid recovery, they have provided additional source of information to check theoretical results on breaking dynamics [8].

3. RESULTS AND ANALYSIS

RUN 1: The aim was to establish a long cylindrical column by manual liquid injection (turning a syringe handle) while the disc separation was being automatically increased. First, a short liquid bridge was obtained by slow injection of liquid through a 6 mm filling hole in the FD (35 mm in diameter) which remained anchored at the disc edge, growing until it came in contact with the rear disc (RD) that was 26 mm apart. At that time, some major Shuttle maneuvers happened to take place, widely deforming the bridge (which would have certainly brake, had it occurred at larger slendernesses).

During the cylindrical stretching, the PS did not manage to fill liquid at the pace the discs were separating, to achieve a cylindrical evolution, following instead the path shown in Fig. 3, that eventually became unstable and the column broke in two spherical drops. This unforeseen circumstance has furnished an unexpected verification of the validity of the stability analysis of non-cylindrical liquid bridges in a real microgravity environment (this limit had been tested earlier using neutral buoyancy simulation [9]).

At that time, direct video link was available and thus, instead of some experiment sequence, a close view of the operator's hand thoroughly cleaning the rear disc to start a new trial was seen. This, in fact, was a good demonstration for the safety team, who had cast doubts (and establish some hard rules) on the possibility of cleaning the FPM test chamber in flight.

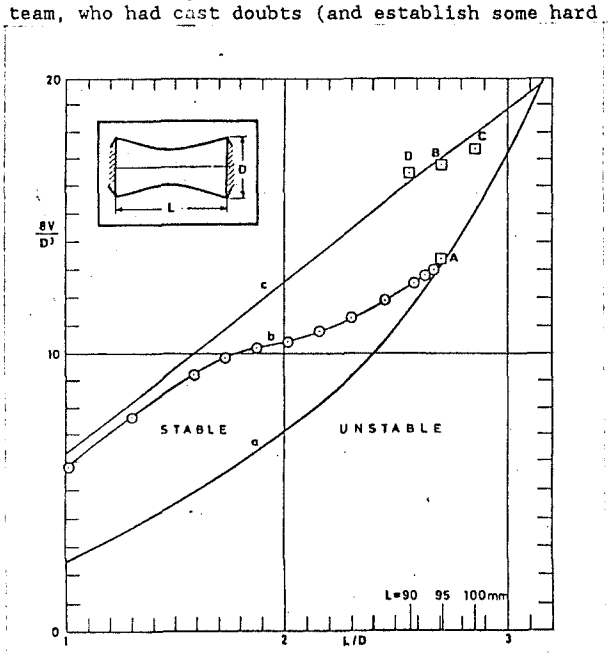

Fig. 3. Actual path in the stability diagram followed by liquid column in the Run-1. It is seen how it deviates from the cylindrical evolution and gets unstable.

RUN 2: After cleaning, injecting liquid to form a 26 mm bridge as above and sligthly stretching to 31 mm, the Payload Specialist started a long talk (with video coverage) with the investigator on ground, concerning liquid visualization and ambient noise. This remote interactive research is a good example of the novel telescience approach.

After a carefull column stretching (with some safety pauses) the 95 mm length was achieved and the oscillation trials performed. The RD was set to a sinusoidal axial oscillation of 0.93 mm pick to pick at selected frequencies of 0.1, 0.3, 0.7, 1.1 and 1.6 Hz, roughly corresponding to the first natural frequencies predicted by theory for a cylindrical liquid column of such a slenderness. During the 3 minutes at 0.1 Hz, the PS could not distinguish any privileged movement of the liquid (neither it is apparent on the photographs), but for the rest, standing waves with 2, 3, 4 and five inner nodes, respectively, were found, as expected.

The oscillation stopped at 6/01:03:46, but then the liquid column unexpectedly broke. The PS was not looking at it and only the "safety" recording of 1 frame every 92 seconds was on. The accelerometers clearly show a big Shuttle manouver at MET 6/01:06:44 that surely caused the brakage.

RUN 3: The breaking in Run 2 left two drops well attached to the edges of the discs and thus the PS tried to approach the disc and merge the drops to re-establish the bridge. One of the most intriguing findings of this experimentation has been the fact that the two drops could not be merged, no matter how much the PS pressed one against the other by squeezing the supporting discs (rotation of the discs did not help). The only way out he could find was to remove the liquid on the FD back to the syringe and then get the FD in contact with the drop at RD (the spreading over the wet solid FD was easy and a bridge established).

In this Run the first rotation of the column beyond the theoretical stability limit was performed and, even when the PS stopped rotation after some 30 seconds, the liquid shape deformation inevitably grew until bridge disruption. Figure 4 shows hte points tried in the stability diagram, whereas Fig. 5 presents the response of the liquid column.

RUN 4: The same process of drop merging of Run 3 was followed here to re-establish a bridge after the former rupture. The PS started rotation of a 100 mm column at 10 rpm, but the announcement of coming Shuttle manouvers forced him to recover back and abort the trial. The time allocation for FLIZ was by now exhausted, but the highly motivated PS managed to continue it during his spare time.

RUN 5: The start was one hour later with a dry test-chamber and the objective was to try again Run 4. The random oscillation in this column (100 mm long) were so pronounced, even when the PS managed from the Shuttle crew to have a free drift period, that at some instances it seems the column is going to break (although it stood like that for

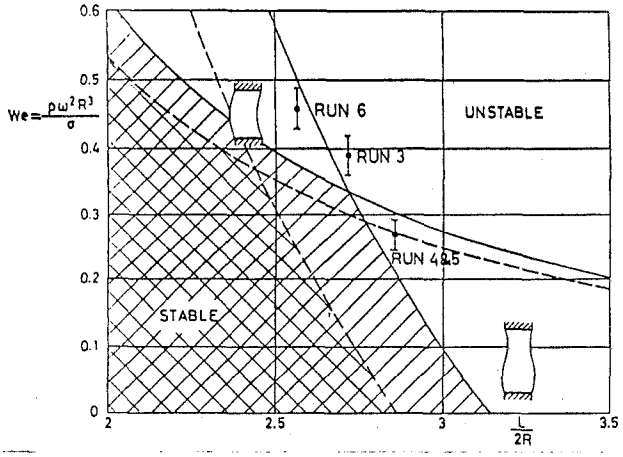

Fig. 4. Points in the rotation-slenderness stability diagram for cylindrical liquid columns, exercised during SL-D1. Dashed line indicates the effect of an axial residual gravity on the rotational stability limit.

5 minutes). When subjected to 10 rpm of rotation, the column broke (Fig. 6) in an amphora-shape mode, as expected.

An important point to note is that the mean residual acceleration computed after the mean shape-deformation from the film is [6] around 70 μg, whereas the mean value from the accelerometers is 120 μg. This discrepancy is atributed to the zero-point uncertainty of the sensors (they were six, one measuring in each direction, with a range from 10^{-2}g to 10^{-5}g and a resolution of 10^{-6}g (1 μg).

RUN 6: The goal of this Run was to excite a C-mode deformation in a liquid column 90 mm long. When the stability limit was surpassed at 13 rpm, the column deformed in an amphora-like mode instead of in C-mode. The explanation now given is as follows. As above mentioned, the accelerometer data indicate a residual axial acceleration of some 100 μg which tends to promote the amphora-like instability above the C-mode one by shifting the rotational stability limit to lower slendernesses, as sketched in Fig. 4.

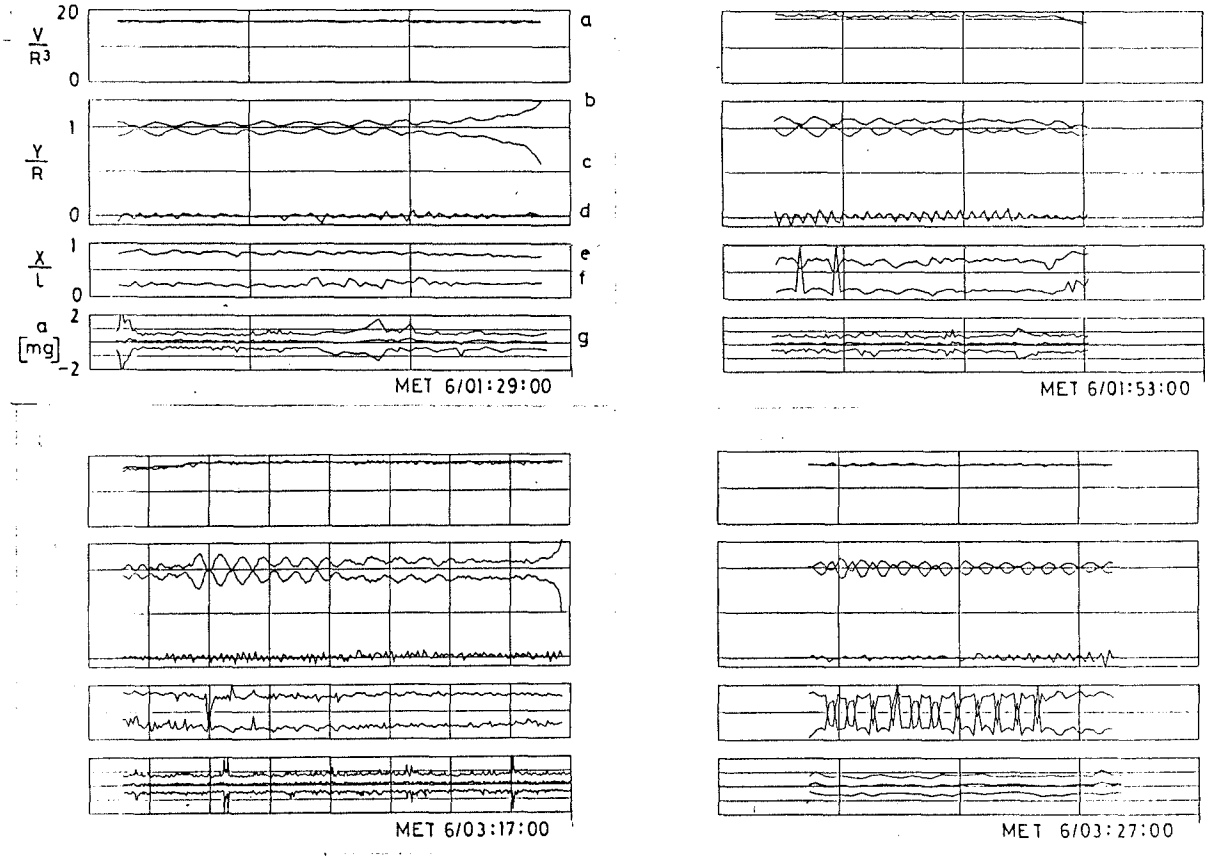

Fig. 5. Some results on time evolution of long nearly-cylindrical liquid columns (for the 4 cases with rotation). Time origin is marked in each case, and grid spacing is always 60 seconds. **a)** Liquid volume computed from the pictures compared with the scheduled one. **b)** and **c)** Radius at 3/4 and 1/4 of the column length, respectively (they nearly correspond to the maximum bulge and neck). **d)** Deformation of the column center-line at mid length (natural frequency is about three times that of b). **e)** and **f)** Position of maximum bulge and neck along the column, respectively. **g)** Accelerometer data in the axial direction, mean value and averaged mean.

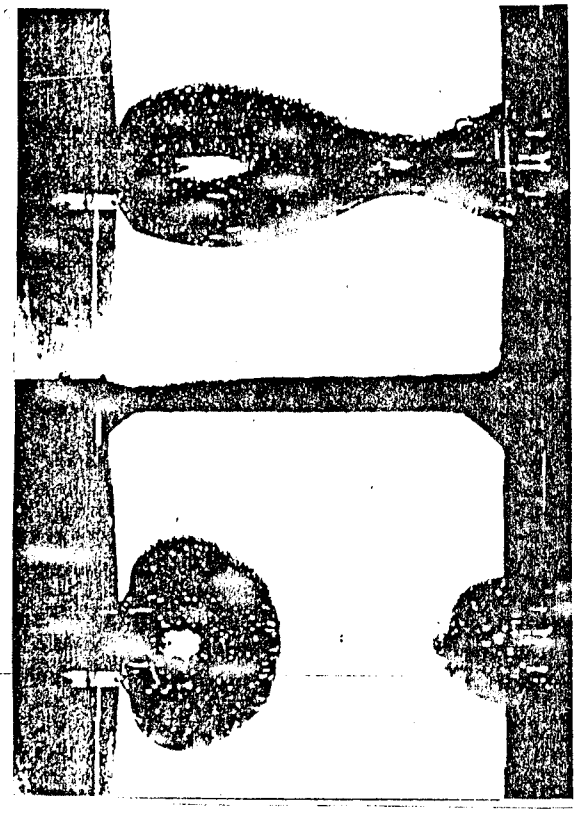

Fig. 6. Two consecutive film frames (at 2 s interval) showing the breaking of a 100-mm-long cylindrical liquid column.

By that time, experiment FLIZ had used resources (mostly crew-time) over and above initial allocation and was concluded. Unfortunately, the only Run remaining in the nominal procedures was a last rotation trial at 16 rpm with a column of 75 mm which would have clearly shown a C-shape disruption mode.

4. LESSONS LEARNT

The details compiled here concern marginal problems ocuured during Spacelab flight and are irrelevant to the results of the investigations, but their inclusion will help future users and managers of research facilities in space to better plan their task.

A first logistic problem arose during the setup: a background mask-sheet, intended to enhance visualization and ulterior data analysis from the images, was not found by the PS. It was properly labeled, but, in order to avoid profusion of small containers, was decided to be included in an already available envelop which belonged to another FPM user. The ESA support team and the investigators knew these details (it seems they escaped the PS attention), but during the flight, when the PS asked for assistance to find it, the investigator (who had to talk to the PS through two or three intermediate relay personnel) realized that the short allocated time was running out and instructed the PS to forget about the plastic sheet. This multi-relay voice link caused more waste of time than the already said above. Sometimes the PS sent a message to the investigator on ground, who correctly received it and was prompt to answer, but another member in the link did not catch it and asked the PS to repeat the message or clarify some point on it. Besides, the PS was constantly requested from ground during the scarce voice-link periods to take messages for other business, what distracted him and prevented a more interactive operation.

Another weak point was connected with liquid volume recording. The FPM reservoir used in SL-1 was awkward to control, but its settings were automatically recorded every second. The small manual syringe specially designed for SL-D1 was much more handy, and helped a lot the PS to control the liquid supply and removal, but it was not connected to the data acquisition system. Training on ground was unrealisticaly optimist; once up there, the PS was so busy coping with a highly sensitive liquid column, that he had no time to keep on top a detailed logbook of the syringe counter. Besides, when at some point the PS measured the syringe counter it was for instance 25.2 handle turns, instead of the 26.1 expected for a cylindrical column of that length, an error beyond normal experience on ground trials. Thus, all volumes had to be estimated from the shape on the images.

Concerning data retrieval, D1 mission was much better than SL-1, but still an entangled job far from being satisfactory. The problem is that the investigator does not know before hand how much data will be needed because it all depends on the actual development of the experiment. Besides, a major impact on data requirement in these pioneering space research is the relaibility of the data sources (problems with FPM cine-camera, malfunction of on board video-tape recording, possible errors in data acquisition, etc). For example, when the PS selected (according to the procedures) 12 rpm synchronously for both discs, the printout shows unrelated scatter from 11.2 to 12.7 in disc rotation rates (in contrast to an FPM resolution of 0.1 rpm). Even when reliable data is available, it is difficult to handle; for instance, the bulky printout of FPM housekeeping and accelerometer data. Major steps will be needed if an automated data acquisition (and image processing) capability is wanted in future (presently, the outline of some 500 enlarged pictures have been manualy digitized).

Contrary to the above drawbacks, the incorporation of a frame counter to the FPM housekeeping data for SL-D1 has represented a great improvement with respect to SL-1 (the FPM camera does not yet record time on film).

5. CONCLUSIONS

The purpose of this experiment was to study the mechanical stability of long liquid columns under real microgravity conditions and the aim has been achieved with success.

Apart of minor details as those described on the last section, everything worked as expected: the liquid column was vibrated at the frequencies foreseen in the procedures, and the influence of rotation on the maximum stable length of the liquid bridge was checked through three different rotation tests (another rotation trial was not performed due to lack of time, in spite of the

generous time extensions granted to this experiment). In particular:

1. A large liquid mass was accurately positioned in the test chamber, well anchored to the sharp edges of coaxial discs 35 mm in diameter and up to 100 mm apart.
2. Long cylindrical liquid columns of slenderness (length/diameter) 2.86 were easily established several times.
3. Present values of residual acceleration for the Shuttle in free-shift (some 70 μg, measured from the liquid bridge response) prevent any further increase in column slenderness.
4. Volume computations from the liquid outer shape seem to point out a slight decrease of nearly 1% over a period of 6 minutes where it should be constant according to schedule (this teaches that redundancy in data collection during rare experimental occasions must be increased).
5. The breaking of long cylindrical liquid bridges when subjected to perturbations beyond the stability limit gave way to two separate drops with relative volumes as predicted by theory.
6. Observed natural oscillation of the liquid column (Fig. 5) indicate a period of some 21 s for the first axial mode and nearly a third of that for the first transversal mode. These values are in good agreement with theoretical predictions for cylindrical bridges [10].

ACKNOWLEDGEMENT
This research is being supported by founds from the Spanish Commission on Space Research (CONIE).

REFERENCES

1. Martinez, I., "Floating zone hydrodynamics", Wissenschaftliche ziele der Deutschen Spacelab mission D1, 40-41, 1985.
2. Martinez, I., "Liquid column stability", ESA SP-222, 31-36, 1984.
3. Martinez, I. & Eyer, A., "Liquid bridge analysis of silicon crystal growth experiments under microgravity", J. Crystal Growth 75, 535-544, 1986.
4. Da Riva, I. & Martinez, I., "Floating liquid zones", Naturwassenschaften, Springer-Verlag, 1986.
5. Martinez, I. and Meseguer, J., "Floating liquid zones in microgravity". In Norderney Symposium on Results of Spacelab-D1 Mission, DVFLR (FRG), 1986 .
6. Martinez, I., "Stability of liquid bridges: results of SL-D1 experiment", IAF-86-272, 1986.
7. Martinez, I. & Sanz, A., "Long liquid bridges aboard sounding rockets", ESA Journal 9, 323-328, 1985.
8. Meseguer, J., Sanz, A. & López, J., "Liquid bridges breakages aboard Spacelab-D1", (to be published in J. Crystal Growth), 1986.
9. Sanz, A. & Martinez, I., "Minimum volume for a liquid bridge between equal disks", J. Colloid Interf. Sci. 93, 235-240, 1983.
10. Sanz, A., "The influence of the outer bath in the dynamics of axisymmetric liquid bridges". J. Fluid Mech. 156, 101-140, (1985).

OSCILACIONES LIBRES DE PUENTES LIQUIDOS EN EL SPACELAB-D1

A. Sanz, J. Meseguer

1. INTRODUCCION

El objeto de realizar experimentos en el espacio es el de reducir la influencia de la gravedad para así poner de manifiesto aspectos que en un laboratorio terrestre quedarían enmascarados o serían indetectables.

El nivel medio de la aceleración existente en una plataforma espacial del tipo del Spacelab es del orden de 10^{-2} m.s^{-2} (10^{-3} g). Este valor es suficiente para la realización de una amplia gama de experimentos en los que tal nivel supone, prácticamente, condiciones de ingravidez completa. Sin embargo, existe otro tipo de experimentos muy sensibles a la microgravedad residual (un buen ejemplo es el de las columnas líquidas largas) en los que no es posible despreciar los efectos asociados a esta perturbación de fondo. Por supuesto el nivel tolerable de perturbación depende de la configuración experimental, reduciéndose drásticamente conforme la configuración en estudio se acerca a un límite de estabilidad sensible a este tipo de perturbación.

Refiriéndonos al experimento "FLIZ" (Floating Liquid Zones, Spacelab-D1, Noviembre de 1985) relacionado con el comportamiento de

puentes líquidos entre discos iguales* y coaxiales frente a perturbaciones mecánicas (Da Riva y Martínez, 1986, Martínez y Meseguer, 1986), durante la secuencia experimental se produjeron varias roturas del puente líquido, no previstas en los procedimientos, casi todas debidas a la acción de la gravedad residual (Meseguer, Sanz y López, 1986). Así pues, resulta del mayor interés el estudio de la respuesta del puente líquido a una perturbación de fondo como es la microgravedad residual, aunque ésta sea muy reducida y el fin último del análisis sea el caso de total ingravidez. Estudios de esta naturaleza han sido realizados para campos tales como biología y mecánica de fluidos (Langbein, 1986) aunque tan sólo de forma cualitativa.

En las páginas siguientes se presenta un análisis teórico y experimental de la respuesta de un puente líquido largo sometido únicamente a una aceleración axial aleatoria. Para el estudio teórico se han considerado dos modelos, basados en los modelos unidimensionales presentados en Meseguer (1983a) y Rivas y Meseguer (1984). El primero es un modelo lineal, no viscoso, de la dinámica de puentes líquidos de volumen cilíndrico, que permite determinar la función de transferencia (o respuesta en frecuencia) para cualquier valor de la esbeltez del puente (la esbeltez, Λ, se define como $\Lambda = L/(2R_o)$, donde L es la separación entre discos (Fig. 1)). La validez de este primer modelo parece limitada,

---

* El radio de los discos era $R_o = 0.0175$ m y las propiedades del líquido (dimetil silicona) densidad, $\rho = 920$ kg.m^{-3}, tensión superficial $\sigma = 0.02$ N.m^{-1} y viscosidad $\nu = 5 \times 10^{-6}$ m^2.s^{-1}.

por comparación con los resultados del modelo tridimensional desarrollado en Sanz (1985), al rango $\Lambda > 2$ y al primer modo de oscilación. Obviamente, se podría haber conseguido una mayor aproximación desarrollando un modelo tridimensional análogo al de Sanz (1985) pero esto habría representado, habida cuenta de la complejidad de las expresiones que aparecen en el modelo tridimensional, un esfuerzo que parece innecesario para analizar las configuraciones experimentales, en las que $\Lambda > 2.5$.

El segundo modelo se deriva de la formulación presentada en Rivas y Meseguer (1984) para el análisis, en variables de semejanza, de la dinámica de puentes líquidos casi cilíndricos cerca del límite de estabilidad, $\Lambda = \pi$. Con este segundo método se puede estudiar la influencia de la viscosidad en la función de transferencia así como el cambio de la primera frecuencia de resonancia debido a un nivel medio de microgravedad.

En el apartado experimental se ha analizado la respuesta del puente en cuatro períodos distintos del experimento FLIZ. La elección de los períodos estudiados, como se explica con más detalle posteriormente, ha dependido en primer lugar de la disponibilidad de registro gráfico (partes de la secuencia experimental no fueron filmadas o fueron filmadas con intervalos demasiado grandes entre fotografías consecutivas) y en segundo lugar de la inexistencia en esos períodos de perturbaciones intencionadamente impuestas (aunque este segundo condicionamiento no se cumple en algunos casos y parte del período estudiado coincide con el inicio del algún ensayo de rotación). Previo al estudio de la respuesta del puente se presenta un análisis de la aleatoriedad de la perturbación,

lo que permite deducir que, en los períodos analizados, la componente axial de la microgravedad residual puede ser considerada como un ruido blanco superpuesto a un nivel medio.

Aunque las conclusiones que se deducen del análisis experimental de la función de transferencia están fuertemente condicionadas por la estructura de los datos disponibles (salvo los concernientes a la respuesta estática y a las frecuencias de resonancia) el método seguido ilustra la forma en que se podrían emplear las técnicas del análisis modal y análisis digital de señales para determinar la función de transferencia, y diseñar, para futuros experimentos, la arquitectura de la toma de datos a fin de satisfacer los requisitos de precisión y resolución que se establezcan de antemano.

2. MODELOS MATEMATICOS

2.1. Modelo lineal

Sea un puente líquido esbelto (Fig. 1) sometido a una perturbación axial dependiente del tiempo. Con las hipótesis simplificativas presentadas en Meseguer (1983a) para el modelo unidimensional, la formulación del problema, en variables adimensionales, resulta

$$(R^2)_t + (WR^2)_z = 0 \ , \tag{2.1}$$

$$W_t + (W^2)_z = -P_z \ , \tag{2.2}$$

$$P = \frac{1}{(1+R_z^2)^{3/2}} \left[\frac{1+R_z^2}{R} - R_{zz} \right] + B(t)z \tag{2.3}$$

$$R(\pm\Lambda,t) = 1 \quad , \quad W(\pm\Lambda,t) = 0 \quad , \tag{2.4}$$

$$\int_{-\Lambda}^{\Lambda} R^2 dz = 2\Lambda \quad . \tag{2.5}$$

En estas expresiones y en las que sigue, a menos que se indique lo contrario, las longitudes están adimensionalizadas con el radio de los discos, R_o, el tiempo con $(\rho R_o^3/\sigma)^{1/2}$, la velocidad axial con $(\sigma/\rho R_o)^{1/2}$ y la presión reducida con $\sigma/\rho R_o$, donde ρ y σ son, respectivamente, la densidad y la tensión superficial del líquido. B(t) es un parámetro que mide la relación entre las fuerzas inerciales y las capilares (número de Bond), $B(t) = \rho a(t) R_o^2/\sigma$, siendo a(t) la aceleración axial, y Λ es la esbeltez definida anteriormente ($\Lambda = L/(2R_o)$).

Suponiendo que la perturbación axial es suficientemente pequeña se podrá escribir como

$$B(t) = \varepsilon b(t) = \varepsilon \sum_n (\mu_{sn} \operatorname{sen}\omega_n t - \mu_{cn} \cos\omega_n t) \quad , \tag{2.6}$$

con $\varepsilon << 1$. Introduciendo los desarrollos asintóticos de las variables del problema

$$R = 1 + \varepsilon r + \ldots \quad , \quad W = \varepsilon w + \ldots \quad , \quad P = 1 + \varepsilon p + \ldots \tag{2.7}$$

en las expresiones (2.1) a (2.5) y despreciando términos de orden ε^2 resulta el siguiente problema linealizado

$$2r_t + w_z = 0 \quad , \tag{2.8}$$

$$w_t + p_z = 0 \quad , \tag{2.9}$$

$$p = - r - r_{zz} + b(t)z \quad , \tag{2.10}$$

$$r(\pm\Lambda,t) = 0 \quad , \quad w(\pm\Lambda,z) = 0 \quad , \tag{2.11}$$

$$\int_{-\Lambda}^{\Lambda} r\,dz = 0 \tag{2.12}$$

Procediendo ahora como en Meseguer (1983a) se obtiene, por último, al eliminar r y sus derivadas de la formulación,

$$w_{zzzz} + w_{zz} + 2w_{tt} + 2b_t = 0 \quad , \tag{2.13}$$

$$w(\pm\Lambda,t) = 0 \quad , \quad w_z(\pm\Lambda,t) = 0 \quad . \tag{2.14}$$

Para resolver la ecuación (2.13), habida cuenta de la expresión (2.6), pondremos

$$w(z,t) = \sum_n (u_{sn}\text{sen}\omega_n t + u_{cn}\cos\omega_n t) \tag{2.15}$$

con lo que la ecuación (2.13) resulta

$$\sum_n (u_{cn_{zzzz}} + u_{cn_{zz}} - 2\omega_n^2 u_{cn} + 2\mu_{sn}\omega_n)\cos\omega_n t + \sum_n (u_{sn_{zzzz}} + u_{sn_{zz}} - 2\omega_n^2 u_{sn} + 2\mu_{cn}\omega_n)\text{sen}\omega_n t = 0 \quad . \tag{2.16}$$

Puesto que esta ecuación ha de ser válida para cualquier valor de t, los términos entre paréntesis habrán de ser nulos, quedando, para un término genérico

$$u_{zzzz} + u_{zz} - 2\omega^2 u + 2\mu\omega = 0 \quad , \tag{2.17}$$

$$u(\pm\Lambda) = u_z(\pm\Lambda) = 0 \quad . \tag{2.18}$$

La solución de (2.17) es

$$u = \frac{\mu}{\omega} + C_1 e^{az} + C_2 e^{-az} + C_3 \cos bz + C_4 \operatorname{sen} bz \tag{2.19}$$

donde a y b son la parte real de las raices ξ_i de la ecuación característica

$$\xi^4 + \xi^2 - 2\omega^2 = 0 \quad , \tag{2.20}$$

es decir,

$$\xi_1 = a = \pm\left[\frac{1}{2}(1+8\omega^2)^{1/2}-1\right]^{1/2}, \quad \xi_2 = ib = \pm i\left[\frac{1}{2}(1+8\omega^2)^{1/2}+1\right]^{1/2} \tag{2.21}$$

Dado que la función u(z) ha de cumplir las condiciones de contorno (2.18), de la aplicación de éstas se obtiene un sistema de 4 ecuaciones para determinar las constantes C_i

$$\begin{bmatrix} e^{a\Lambda} & e^{-a\Lambda} & \cos b\Lambda & \operatorname{sen} b\Lambda \\ e^{-a\Lambda} & e^{a\Lambda} & \cos b\Lambda & -\operatorname{sen} b\Lambda \\ ae^{a\Lambda} & -ae^{-a\Lambda} & -b\operatorname{sen} b\Lambda & b\cos b\Lambda \\ ae^{-a\Lambda} & -ae^{a\Lambda} & b\operatorname{sen} b\Lambda & b\cos b\Lambda \end{bmatrix} \begin{bmatrix} C_1 \\ C_2 \\ C_3 \\ C_4 \end{bmatrix} = -\frac{\mu}{\omega} \begin{bmatrix} 1 \\ 1 \\ 0 \\ 0 \end{bmatrix} \tag{2.22}$$

del que se obtiene

$$C_i = -\frac{\mu}{\omega}\frac{D_i}{D} \quad , \quad i = 1,2,3 \; ; \quad C_4 = 0 \tag{2.23}$$

donde

$$D = 8\, D_m D_p \quad , \quad D_1 = D_2 = 4bD_m \text{senb}\Lambda \; , \; D_3 = 8aD_m \text{cosha}\Lambda \; , \tag{2.24}$$

siendo

$$\left.\begin{aligned} D_m &= a\text{cosha}\Lambda\text{senb}\Lambda - b\text{senha}\Lambda\text{cosb}\Lambda \\ D_p &= b\text{cosha}\Lambda\text{senb}\Lambda + a\text{senha}\Lambda\text{cosb}\Lambda \end{aligned}\right\} . \tag{2.25}$$

Introduciendo estas expresiones en (2.19) resulta, finalmente

$$u = \frac{\mu}{\omega}\left(1 - \frac{b\text{coshaz}\,\text{senb}\Lambda + a\text{senha}\Lambda\text{cosbz}}{b\text{cosha}\Lambda\text{senb}\Lambda + a\text{senha}\Lambda\text{cosb}\Lambda}\right) \quad . \tag{2.26}$$

Conocidas u_{cn} y u_{sn} la forma de la entrefase se obtiene de la ecuación de continuidad (2.8)

$$r(z,t) = \sum_n \left(f_{sn}\text{sen}\omega_n t - f_{cn}\cos\omega_n t\right) =$$

$$= \frac{1}{2}\sum_n \frac{1}{\omega_n}\left(u_{sn_z}\cos\omega_n t - u_{cn_z}\text{sen}\omega_n t\right) \quad , \tag{2.27}$$

resultando, para cualquier término genérico f_{sn} ó f_{cn} (teniendo en cuenta que $ab = \sqrt{2}\omega$)

$$f = \frac{u_z}{2\omega} = \frac{\sqrt{2}\mu}{2\omega}\,\frac{\text{senhaz}\,\text{senb}\Lambda - \text{senha}\Lambda\text{senbz}}{b\text{cosha}\Lambda\text{senb}\Lambda + a\text{senha}\Lambda\text{cosb}\Lambda} \quad , \tag{2.28}$$

Es interesante ver que cuando $\omega \to 0$ el resultado obtenido recupera el problema estático. En efecto, teniendo en cuenta que $\omega \to 0$ implica $a \to \sqrt{2}\omega$ y $b \to 1$, resulta

$$f = \mu(z - \frac{\Lambda}{\text{sen}\Lambda} \text{ senz}) + O(\omega) \qquad (2.29)$$

resultado que coincide con el obtenido en Meseguer (1983b).

Otra característica a destacar de la solución obtenida es que la forma de la entrefase es antisimétrica respecto a $z = 0$, es decir, $f(z) = -f(-z)$. Según esto, una perturbación axial tan sólo puede excitar los modos de oscilación impares (con un número impar de nodos).

En la figura 2 se muestra la respuesta en frecuencia de puentes líquidos de diversas esbelteces según resulta de este modelo. La respuesta en frecuencia se ha definido como el cociente entre la máxima deformación de la entrefase y la amplitud de la perturbación, $H(\omega) = f_{max}/\mu$. Fijado Λ, las frecuencias de resonancia vienen dadas por los valores de ω que anulan el determinante D. Estas frecuencias de resonancia coinciden con las obtenidas en Meseguer (1983a) para los modos impares.

2.2. Modelo autosemejante

El estudio de la dinámica de puentes líquidos casi cilíndricos de esbelteces próximas al límite de estabilidad, $\Lambda = \pi$, ha sido realizado por Rivas y Meseguer (1984) utilizando un modelo unidimensional basado en la teoría de los medios continuos de Cosserat. En el citado artículo se

demuestra que la evolución del puente líquido puede ser analizada en términos de las variables de semejanza α,θ y de los parámetros γ,β definidos mediante las expresiones

$$\alpha = \frac{1}{4} S(\frac{1}{3}\delta)^{-1/2}, \theta = \frac{2}{5} t(2\delta)^{1/2}, \gamma = \frac{5}{2} C(2\delta)^{-1/2}, \beta = \frac{1}{2} B\delta^{-1}(\frac{1}{3}\delta)^{-1/2} \qquad (2.30)$$

En estas expresiones S indica la amplitud de una perturbación sinusoidal en el área de la sección recta ($R^2(z,t) = 1 + S(t)\text{sen}\frac{\pi z}{\Lambda}$); δ es la esbeltez equivalente del puente, $\delta = 1 - \frac{\Lambda}{\pi} + \frac{1}{2}(\frac{V}{2\pi\Lambda} - 1)$, donde V es el volumen de líquido; t es el tiempo adimensional ya definido con anterioridad, C es el parámetro de viscosidad, $C = \nu(\rho/\sigma R_o)^{1/2}$, siendo ν la viscosidad cinemática del líquido; por último, B representa el número de Bond, también definido anteriormente. Con estas variables el movimiento en el puente líquido está descrito por la ecuación (3.27) del mencionado artículo de Rivas y Meseguer (1984):

$$\alpha_{\theta\theta} + \gamma\alpha_{\theta} + \alpha - \alpha^3 + \beta = 0 \qquad (2.31)$$

ecuación no lineal que retiene la influencia en las oscilaciones tanto de la viscosidad, γ, y la gravedad, β, como de la amplitud de la deformación inicial, α_o (en lo que sigue denotaremos las variables y parámetros de semejanza con nombres que identifiquen su sentido físico). La ecuación (2.31) permite pues determinar las características del movimiento oscilatorio en función de γ, β y α_o. Por ejemplo, en la figura 3 se muestra, para el caso $\gamma = 0$, la variación con α_o y β del período de oscilación, Θ_T, obtenido mediante integración numérica de la ecuación (2.31). La variación con β de la forma de la entrefase en el equilibrio,

α_{oe}, y el período, Θ_{Te}, de las oscilaciones de amplitud infinitesimal alrededor de la posición de equilibrio correspondiente se muestra en la figura 4; así pues, la figura 4 permite determinar la frecuencia de resonancia del puente líquido en el caso no viscoso.

Existe un par de casos en los que se puede obtener expresiones analíticas sencillas introduciendo hipótesis simplificativas adicionales en la ecuación (2.31): la primera de las aproximaciones proporciona la función de transferencia del puente líquido para el caso de oscilaciones de pequeña amplitud alrededor del cilindro (que es la forma de equilibrio para $\beta = 0$) mientras que con la otra se obtiene la influencia del número de Bond en la frecuencia de resonancia.

Refiriéndonos al primer caso, supongamos $\alpha << 1$ (oscilaciones de pequeña amplitud). La ecuación lineal que resulta al despreciar el término en α^3 y considerar β como una excitación variable en el tiempo, $\beta = \beta_o e^{i\Omega\Theta}$, donde $\Omega = 2\pi/\Theta_T$, es la típica de un sistema con un grado de libertad, cuya función de transferencia, relativa a las variables de semejanza, es

$$H(\Omega) = \frac{1}{\Omega^2 - 1 - i\gamma\Omega} \quad . \tag{2.32}$$

En la figura 2 se compara la función de transferencia según la expresión (2.32) con la obtenida en el apartado anterior.

Para amortiguamientos pequeños ($\gamma << 1$) la frecuencia de resonancia es $\Omega_r = 1$ ($\Theta_T = 2\pi$) y la relación de amplificación máxima $|H(\Omega)| = 1/\gamma$.

La expresión (2.32) permite caracterizar la influencia de la viscosidad en la función de transferencia del sistema y aplicar la gran cantidad de resultados obtenidos en la teoría del análisis modal (Bendat y Piersol, 1971, Newland, 1975, Kay y Marple, 1981, Ewins, 1984) para relacionar las características estadísticas de la excitación (generalmente aleatoria) con la deformación de la columna líquida.

En la otra aproximación, cuando $\beta \neq 0$ las oscilaciones de pequeña amplitud no se producen alrededor de $\alpha = 0$ sino alrededor de una cierta deformación de equilirio, $\alpha_o << 1$. Introduciendo los desarrollos $\alpha(\theta) = \alpha_o + \varepsilon\tilde{\alpha}(\theta)$, $\beta(\theta) = \beta_o + \varepsilon\tilde{\beta}(\theta)$, con $\varepsilon << 1$, en la ecuación (2.31) se obtiene

$$\alpha_o - \alpha_o^3 + \beta_o = 0 \quad , \tag{2.33}$$

$$\tilde{\alpha}_{\theta\theta} + \gamma\tilde{\alpha}_{\theta} + (1-3\alpha_o^2)\tilde{\alpha} + \tilde{\beta} = 0 \quad , \tag{2.34}$$

la frecuencia de resonancia, según la ecuación (2.34), resulta

$$\Omega_r = (1-3\alpha_o^2)^{1/2} \quad , \tag{2.35}$$

y para valores pequeños de α_o (la ecuación (2.33) sería $\alpha_o \simeq -\beta_o$) queda

$$\Omega_r \simeq 1 - \frac{3}{2}\beta_o^2 \quad . \tag{2.36}$$

En la figura 4 se han representado estas dos últimas expresiones. Los valores de Θ_{Te} obtenidos mediante la ecuación (2.35) coinciden prácticamente con los resultantes de integrar numéricamente la ecuación

(2.31), mientras que la aproximación (2.36) es válida para $\beta_o < 0.2$.

3. MEDIDA EXPERIMENTAL DE LA FUNCION DE TRANSFERENCIA

Consideraremos que el puente líquido se comporta como un sistema lineal continuo con infinitos grados de libertad que, en consecuencia, presenta infinitas frecuencias de resonancia, como ya se ha visto en § 2. Aún más, en un medio continuo la función de transferencia H no es sólo función de la pulsación ω sino también de la variable espacial $\vec{x}$, $H = H(\omega,\vec{x})$.

En nuestro caso consideraremos solamente deformaciones axilsimétricas (que en el caso lineal están desacopladas del resto) lo cual introduce una primera simplificación en el análisis de los datos experimentales: la función de transferencia sólo depende de la coordenada z (figura 1) y de la pulsación ω.

En cuanto al rango de frecuencias a considerar, existen varias razones para limitar el análisis de los datos experimentales a las proximidades del primer modo:

1. Los registros gráficos del experimento FLIZ muestran que en los períodos estudiados (oscilaciones no forzadas) la componente axilsimétrica de la deformación de la entrefase corresponde muy aproximadamente a este primer modo.
2. La forma de la excitación permite deducir, como ya se vio en § 2.1, que sólo deben de aparecer modos impares. Si se considera

la deformación como superposición de modos ortogonales entre sí (oscilando cada uno a su frecuencia de resonancia) la contribución siguiente al primer modo propio sería la del tercero, cuya frecuencia de resonancia permanece, en el intervalo de valores de Λ considerados, por encima de la que el intervalo de muestreo permite resolver (el intervalo entre dos fotogramas consecutivos es de 2 s, que corresponde a una pulsación adimensional $\omega \sim \pi/2$).

3. La amortiguación viscosa de los modos de deformación aumenta con la frecuencia propia asociada y, por tanto, la presencia de modos superiores al primero estará muy amortiguada, lo que se corresponde con las observaciones.

A estas razones debería añadirse además el que los modelos teóricos disponibles (presentados en § 2) sólo proporcionan valores fiables para el primer modo de oscilación y esbelteces mayores que 2 (modelo lineal) ó 2.8 (modelo autosemejante). No hay, pues, por el momento un modelo teórico válido para cualquier modo y esbeltez, y aunque un análisis similar al realizado en § 2.1 pero basado en el modelo tridimensional desarrollado en Sanz (1985) permitiría obtener la función de transferencia en el caso más general, tal análisis presenta complejidades matemáticas importantes, por lo que aún no está disponible.

3.1. Estimación de la función de transferencia

Con el objeto de estimar la respuesta en frecuencia $H(\omega,z)$ del puente líquido y considerando que el estudio se restringe al primer modo de oscilación, se ha elegido, como variable que caracteriza la forma de la

entrefase, la función

$$A(t) = \frac{1}{2} \left(R(\frac{1}{2} \Lambda, t) - R(-\frac{1}{2} \Lambda, t)\right) , \qquad (3.1)$$

que presenta las siguientes ventajas:

1. Al ser una medida antisimétrica de la deformación de la entrefase elimina la contribución de las oscilaciones en modos pares o simétricos.
2. Al coincidir los puntos $z = \pm \Lambda/2$ aproximadamente con los nodos de la deformación correspondiente al tercer modo, la posible contribución de este modo queda reducida al mínimo.
3. La función A(t) refleja con gran aproximación la medida de la máxima deformación del primer modo, ya que para valores grandes de la esbeltez los máximos y mínimos de la entrefase, según los modelos lineales tanto unidimensional como tridimensional, ocurren en $z = \pm \Lambda/2$.

De este modo, el problema de determinar una función de transferencia de dos variables (la pulsación ω y la coordenada axial z) se reduce al de una variable $H = H(\omega)$. Para determinar $H(\omega)$ existe en la literatura una amplia variedad de métodos (Kay y Marple, 1981), dependiendo la elección de un método u otro en gran parte del tipo de señales a analizar y, de forma más concreta, de si la señal de entrada (la microgravedad residual) es determinística o no. En nuestro caso, como se demuestra en § 3.1, la señal de entrada reúne las características de una señal aleatoria con contenido de frecuencias aproximadamente uniforme (densidad espectral

uniforme, es decir, ruido blanco) que, siguiendo las hipótesis usuales en la literatura, se considerará ergódica (las magnitudes estadísticas promediadas en el tiempo de una cierta evolución coinciden con las promediadas sobre un conjunto de evoluciones).

Respecto a la señal de salida (la deformación de la entrefase, medida por la variable A(t)) al ser la respuesta de un sistema lineal (dentro de las hipótesis enunciadas) también será una señal aleatoria aunque, debido al filtrado introducido por la función de transferencia del sistema, la respuesta aparezca como una señal cuyo espectro está limitado a una pequeñas bandas de frecuencias próximas a las de resonancia (Newland, 1975).

Para determinar $|H(\omega)|$ se ha utilizado la expresión

$$|H(\omega)|^2 = S_{AA}(\omega)/S_{BB}(\omega) \quad , \tag{3.2}$$

donde $S_{XX}(\omega)$ representa la transformada de Fourier de la función de autocorrelación de la señal X, es decir, la densidad espectral de la señal X. Como es sabido, para una señal aleatoria, la estimación de la densidad espectral a partir de los datos de una serie temporal requiere realizar un promedio, estimación suavizada $\hat{S}_{XX}$, de las estimaciones aisladas $\tilde{S}_{XX}$ realizadas bien sobre registros adyacentes o bien sobre frecuencias contiguas, con el fin de disminuir el error en la estimación (Bendat y Piersol, 1971). Este promedio ha sido posible hacerlo en el caso de la señal de entrada, pero no en el de la de salida, pues la longitud de los registros no lo permite. En este caso, para las estimaciones aisladas de

las densidades espectrales $\tilde{S}_{XX}$ se ha utilizado el método directo ("Cooley-Tukey", Bendat y Piersol, 1971), calculando la transformada de Fourier de las señales: $\tilde{S}_{XX}(\omega) = |\mathbf{X}(\omega)|^2$, donde **X** indica la transformada de Fourier de la señal X.

3.2. Análisis de la señal de entrada

La señal que constituye la excitación del sistema (puente líquido) es el número de Bond residual B(t) calculado a partir de los registros de los acelerómetros del banco de trabajo (MSDR, Material Science Double Rack) donde estaba instalado el Módulo de Física de Fluidos (FPM, Fluid Physics Module) durante la misión Spacelab-D1. Las características del sistema de acelerómetros del MSDR eran (Zimmermann (1979), Hamacher, Merbold y Jilg (1986), Hamacher, Jilg y Merbold (1986)):

Velocidad de muestreo: 1 Hz

Ancho de banda: de 0 Hz a 10 Hz

Escala: de 10^{-4} m.s^{-2} a 10^{-1} m.s^{-2}, lo que equivale, para el puente líquido, a números de Bond entre 1.4×10^{-3} y 1.4

Resolución: 10^{-5} m.s^{-2}, al que corresponde un valor $B = 1.4 \times 10^{-4}$

El sistema de acelerómetros del MSDR funcionaba de modo que registraba, en cada segundo, los máximos y los mínimos de las señales analógicas de las aceleraciones según los ejes de un cierto triedro de referencia (en la figura 5 se indica este triedro y su orientación respecto al puente líquido). El valor más pequeño de la aceleración registrable por este sistema de elección de picos está condicionado por la

existencia de vibraciones periódicas de frecuencias superiores a las de muestreo, por aceleraciones uniformes y por los errores de tarado del sistema (posición del cero). En la figura 6 se muestra un registro de estas señales para un cierto período típico de ejecución de alguno de los ensayos del experimento FLIZ.

La validez, ya cuestionable, de los datos proporcionados por el sistema de acelerómetros del MSDR para correlacionar la respuesta de la zona con las perturbaciones no intencionadas es aún más dudosa si se considera que no existía una unión rígida entre los soportes del puente líquido y los acelerómetros. Así pues, dado que no se conoce la respuesta en frecuencia del conjunto MSDR-FPM y ante el hecho de que estos registros de la aceleración son la única fuente de información respecto a las perturbaciones accidentales impuestas a la columna líquida (también están disponibles los registros de aceleración de un segundo sistema de acelerómetros, pero este segundo sistema estaba situado al otro lado del Spacelab, sobre el MEDEA, justo enfrente del MSDR) conviene señalar claramente que el análisis realizado de la señal de entrada tiene un valor fundamentalmente orientativo, y que su utilización posterior se basa en la hipótesis de que las perturbaciones sufridas por el puente líquido son estadísticamente semejantes a las registradas por los acelerómetros.

Dado que las señales proporcionadas por los acelerómetros en cada uno de los ejes u, v y w son análogas, al menos en los períodos de tiempo analizados (definidos en § 3.3), el análisis estadístico se ha centrado básicamente en las aceleraciones según el eje v, que es el de orientación más próxima a la del eje del puente líquido (nótese que salvo para valores

medios, el sistema de registro de aceleraciones del MSDR no permite calcular el vector aceleración ni, consecuentemente, la componente de la aceleración según una dirección distinta de los ejes u, v y w del triedro de referencia).

Para justificar la hipótesis de ergodicidad se ha calculado la función de autocorrelación sobre diferentes registros temporales del valor medio de la aceleración según el eje v*, comprobándose la invariancia de la misma. Por otra parte la apariencia general, tanto de los registros de máxima aceleración, como los de mínima o los de aceleraciones medias, es similar a la del ruido blanco, sin que aparezcan muestras significativas de la presencia de frecuencias privilegiadas.

Así pues, la perturbación puede ser considerada, de la manera más general, como suma de dos términos: un nivel medio de microgravedad sobre el que va superpuesta una señal aleatoria de valor medio nulo. El valor medio (o las frecuencias muy próximas a cero) sería debido a la proyección sobre el eje de medida de las aceleraciones producidas por las fuerzas que

---

* Aunque, formalmente, el sistema de registro de aceleraciones del MSDR (detección de picos) no permite calcular el valor medio de la aceleración según un eje ya que los picos registrados, máximo v^+ y mínimo v^-, en cada segundo se habrán presentado en instantes diferentes, al objeto de simplificar el manejo de los datos experimentales conviene definir un valor promedio, $v = (v^+ + v^-)/2$, estimación del valor medio real.

durante el vuelo orbital actúan sobre la nave o, más concretamente, sobre la parte de la nave donde están situados los acelerómetros (resistencia aerodinámica residual, efectos de gradientes gravitatorios y rotación del Orbiter (Hamacher, Merbold y Jilg, 1986)). Estas fuerzas son de período muy largo comparado con la longitud de los registros y, por tanto, aparecen como niveles constantes. Su presencia es por tanto determinística, y su estudio deberá realizarse aparte del estudio del resto de la excitación que, por el contrario, parece razonable considerarla como aleatoria al estar generada por un número grande de fuentes de ruido mecánico no coherentes entre sí, ruido que se transmite por la estructura de la nave y del MSDR hasta los acelerómetros.

La parte aleatoria de la señal de entrada puede suponerse isotrópica, es decir, independiente de la dirección y, en consecuencia, la misma en cualquier eje. Como comprobación, además del análisis que se describe a continuación sobre la componente según el eje v de la aceleración, también se ha realizado un análisis, más reducido, de registros de la componente según u, obteniéndose resultados que avalan la hipótesis de isotropía.

El cálculo de la estimación suavizada de la densidad espectral de la parte aleatoria de la señal $\hat{S}_{BB}(\omega)$ se ha realizado promediando los valores de estimaciones aisladas $\tilde{S}_{BB}(\omega) = |\mathbf{B}(\omega)|^2$ sobre ocho registros diferentes (cuatro de estos registros corresponden a períodos de tiempo coincidentes con los intervalos de evolución de la entrefase analizados, más otros cuatro, próximos al Run 5 definido en § 3.3, en los que no aparecen picos debidos a maniobras o actuaciones de los astronautas).

La densidad espectral suavizada, $\hat{S}_{BB}(\omega)$, así como la banda en la que la probabilidad de que se encuentre el valor real sea del 60 %, se muestran en la figura 7. A la vista de este gráfico se ha decidido aproximar el espectro de la parte aleatoria de la señal de entrada por una constante (línea doble) que es el valor medio de $\hat{S}_{BB}(\omega)$ en el intervalo. Así pues, se considerará la entrada como ruido blanco, ya que en la figura 7 no es posible discriminar frecuencias privilegiadas.

Falta aún por considerar la contribución al espectro de frecuencias de la parte determinística de la señal de entrada (nivel medio de la microgravedad), contribución que se manifiesta como un sumando en el origen $\hat{S}'_{BB}(0) = B_m^2$, donde B_m indica el valor medio del número de Bond según el eje de la columna líquida. El nivel medio real de microgravedad según el eje del puente líquido se obtendría de la suma vectorial de los niveles medios existentes según los ejes v y w (figura 5).

Desgraciadamente, los datos registrados durante el vuelo permiten calcular un cierto valor medio según el eje v, pero no según el eje w ya que faltan los registros correspondientes a la dirección w^+ (el valor real de la aceleración según este eje se mantuvo, durante las secuencias en consideración, acotado entre valores negativos y en consecuencia el detector de picos positivos, w^+, registraba constantemente el valor 0). Ante esta situación la solución adoptada ha sido utilizar el propio puente líquido como acelerómetro, calculando a partir del valor medio de la función A(t) en cada secuencia, el número de Bond que produce tal deformación de la entrefase. Para estos cálculos se han utilizado las expresiones de la aproximación de segundo orden de las formas de

equilibrio desarrollada en Meseguer, Mayo, Llorente y Fernández (1985), expresiones que, una vez subsanado el error tipográfico existente en la ecuación (A.9a) (la constante 1/4 debe ser remplazada por 1/2) permiten analizar la influencia en la forma de la entrefase de efectos tales como gravedad axial, volumen no cilíndrido y discos desiguales.

En la Tabla 1 se muestra, para cada una de las secuencias analizadas* el valor medio A_m de la función A(t), el número de Bond medio, B_m, calculado según lo descrito y, a título comparativo, el número de Bond medio según la dirección v calculado a partir de los registros de los acelerómetros del MSDR.

Tabla 1

Esbeltez, Λ, volumen de líquido, V, y valores medios de la deformación de la entrefase, A_m, la perturbación axial, B_m, y según el eje v, B_v, durante las secuencias analizadas.

Run	Λ	$V \pm 0.05$	$A_m \pm 5\times10^{-4}$	$B_m \pm 10^{-4}$	$B_v \pm 10^{-4}$
6	2.571	16.28	0.0303	0.0094	0.0146
3	2.714	16.82	0.0464	0.0089	0.0156
4	2.854	18.84	0.0574	0.0088	0.0160
5	2.857	17.92	0.0876	0.0100	0.0159

* Las distintas secuencias se numeran cronológicamente desde Run 3 hasta Run 6, de acuerdo con la descripción de la ejecución del experimento FLIZ presentada en Martínez y Meseguer (1986).

A la vista de los resultados de la Tabla 1 se puede destacar la proporcionalidad de los valores de B_m y B_v, y también la casi segura existencia de un error en el cero de los acelerómetros del MSDR (esta posibilidad es también apuntada en Hamacher, Merbold y Jilg (1986)). En efecto, de acuerdo con la orientación del eje del puente líquido respecto al triedro u,v,w, sería

$$B_m = B_v \cos 36^o - B_w \operatorname{sen} 36^o$$

y teniendo en cuenta que B_w, aunque desconocido, sería negativo, un límite inferior del segundo miembro sería $B_i = B_v \cos 36^o$, valor que es, atendiendo a los resultados de la Tabla 1, superior al de B_m.

3.3. Análisis de la señal de salida

Las diversas secuencias analizadas se muestran en la figura 8, donde se ha representado la función A(t), expresión (3.1), calculada a partir de las fotografías del puente líquido tomadas durante el experiento FLIZ (para una descripción del proceso de digitalización y filtrado de estas imágenes véase Martínez, 1986).

Estas secuencias corresponden, en general, al intervalo de tiempo que, en cada ensayo de rotación, transcurrió entre que se alcanzó la separación de discos y volumen de líquido estipulados en los procedimientos y el tiempo en que se inicia el ensayo de rotación correspondiente (excepto en el caso del Run 3 en el que el fin de la secuencia analizada lo marca el inicio de la rotura del puente líquido).

En la Tabla 2 se precisan, con más detalle, los límites de los intervalos analizados.

Tabla 2

Resultados del Experimento FLIZ (Spacelab-D1). Características y condicionantes de los límites de las secuencias analizadas.

Run	Límite inicial	Principio de la secuencia*	Duración [s]	Límite final
3	Esbeltez constante. La etapa anterior no está filmada	6/01:26:11	108	Inicio de la rotura del puente líquido
4		6/01:49:26	82	Disminución del volumen y de la esbeltez
5	La esbeltez y el volumen varían, aumentando hasta que se alcanzan los valores nominales	6/03:10:42	134	Inicio del ensayo de rotación
6		6/03:23:49	126	

* Los números indican el MET (Mission Elapsed Time) de acuerdo con el siguiente convenio: Dia/hora:minuto:segundo.

La densidad espectral de la señal de salida, $S_{AA}(\omega)$ se ha estimado mediante el cálculo de la transformada directa de Fourier de la señal A(t), ecuación (3.1), del registro correspondiente (véase el apéndice). Las longitudes de los registros (el número N de fotografías consideradas)

se ha seleccionado en cada secuencia de modo que, aproximadamente, el valor de A(t) coincida al inicio y al final del período en estudio, es decir, tomando, cuando los datos lo permiten, un número entero de ondas. Para estudiar la posible influencia del número de ondas de la señal en la estimación de la densidad espectral en cada secuencia se han analizado, al menos, registros de tres longitudes diferentes, con diferencias de una onda entre unos y otros. Obviamente, en cada caso la elección del punto final del registro influye en los coeficientes de la transformada de Fourier de la señal, como se muestra en la figura 9, donde se ha representado el módulo de la función de transferencia $|H(\omega)|$ correspondiente al Run 4. Como se observa en este gráfico aparece un pico en las proximidades de $\omega = 0.2$ que, al aumentar el número de puntos del registro se va agudizando hasta que sobrepasado el valor N = 24 ó 25 se vuelve a ensanchar (obsérvese en la figura 8 que A(t) alcanza el valor inicial precisamente entre los puntos 24 y 25). Este proceso se ha realizado para fijar las tres longitudes de registro de cada una de las secuencias analizadas, habiéndose establecido en cada caso la longitud de registro seleccionando el valor de N que proporciona el pico de la frecuencia de resonancia más agudo.

4. RESULTADOS

En las figuras 10 a 13 se ha representado la función de transferencia $H(\omega) = (S_{AA}(\omega)/S_{BB}(\omega))^{1/2}$ de cada una de las secuencias analizadas, ordenadas de menor a mayor esbeltez. En estas figuras se muestran también las funciones de transferencia teóricas obtenidas a partir de los modelos lineal, que supone volumen cilíndrico, y autosemejante linealizado,

presentados en § 2.1 y § 2.2, respectivamente.

Como se observa en los gráficos, en todos los casos el valor de $H(\omega)$ experimental resulta inferior a las estimaciones teóricas: el puente líquido parece responder con menos intensidad que lo que predice la teoría, y esto es así de una manera uniforme para todas las frecuencias. La razón de esta diferencia sustancial podría ser, aparte de las imprecisiones de las medidas y los errores de cálculo, la posible amortiguación de la perturbación por los apoyos del FPM. En efecto, los acelerómetros del MSDR están en su parte superior, mientras que el FPM está a una altura media, montado sobre guías telescópicas, de modo que, en operación, el FPM queda fuera del MSDR, sujeto a éste por un soporte no rígido que en cierta forma aisla al FPM de las perturbaciones sufridas, y registradas, por el MSDR. El conocimiento de la función de transferencia de este soporte permitiría relacionar adecuadamente las respuestas de los acelerómetros con la perturbación real a la que está sometido el puente líquido.

Según el fabricante del FPM (Alessio y otros, 1977), la placa base de este equipo está montada sobre seis apoyos de goma que ofrecen una rigidez grande en el caso de aceleraciones fuertes (lanzamiento y aterrizaje) y pequeña cuando las perturbaciones ambientales son pequeñas. En condiciones de rigidez pequeña las frecuencias naturales son 6.3 Hz, 6.5 Hz, 11 Hz, 16 Hz, 18 Hz y 20 Hz, la menor de éstas muy por encima del rango de frecuencias considerado en el estudio de la respuesta del puente líquido (de 0 Hz a 0.16 Hz).

A la vista de los resultados presentados en los gráficos se podría deducir que el conjunto MSDR-FPM introduce un factor de amortiguamiento del orden de 5 entre la perturbación registrada por los acelerómetros y la experimentada por la columna líquida.

A pesar de las diferencias entre resultados teóricos y experimentales, hay un punto de gran interés, la frecuencia de resonancia, que permite juzgar la bondad de las predicciones teóricas. En la Tabla 3 y en la figura 14 se compara la pulsación adimensional correspondiente a la

Tabla 3

Resultados del Experimento FLIZ (Spacelab-D1)

Run	Λ	V	V/V_c	ω_{re}	ω_{r1}	ω_{ra}	ω_{rs}
6	2.571	16.28	1.008	0.30	0.348	0.243	0.240
3	2.714	16.82	0.986	0.22	0.274	0.203	0.195
4	2.854	18.84	1.051	0.19	0.206	0.192	0.182
5	2.857	17.92	0.998	0.13	0.205	0.168	0.130

Λ: esbeltez

V: volumen adimensional del puente líquido

V_c: volumen cilíndrico, $V_c = 2\pi\Lambda$

ω_r: pulsación adimensional correspondiente a la frecuencia de resonancia; el segundo subíndice indica la fuente del resultado de acuerdo con la siguiente clave: e, experimental; 1, modelo lineal (§ 2.1); a, modelo autosemejante linealizado (§ 2.2); s, modelo autosemejante completo (oscilaciones infinitesimales).

frecuencia de resonancia según se deduce de los datos experimentales con la obtenida de los modelos teóricos, en la Tabla 3 se indican también los valores en cada secuencia de la esbeltez y el volumen del puente líquido, así como el cociente V/V_c, donde V_c indica el volumen de un puente cilíndrico de la misma esbeltez.

A la hora de comparar resultados debe tenerse en cuenta que la pulsación de resonancia obtenida del modelo lineal, ω_{rl} se ha obtenido suponiendo que el volumen de líquido es, en cada caso, el cilíndrico mientras que en los resultados derivados de los modelos autosemejantes, linealizado, ω_{ra}, y completo, ω_{rs}, el volumen del puente líquido es el real.

A la vista de los resultados se pueden extraer dos conclusiones principales. La primera es la fuerte dependencia de la frecuencia de resonancia con el volumen de líquido, comparable a la dependencia con la esbeltez del puente líquido (recuérdese que en variables de semejanza el parámetro importante no es la esbeltez sino la esbeltez equivalente, $\delta = 1 - \Lambda/\pi + (V/(2\pi\Lambda) - 1)/2)$. La segunda conclusión hace referencia al rango de validez de los modelos utilizados, que se puede fijar en $\Lambda > 2.7$ para los modelos autosemejantes (la acotación para el modelo lineal no es tan clara dado que se comparan configuraciones de distinto volumen).

En resumen, se ha analizado la respuesta en frecuencia de puentes líquidos sometidos a perturbaciones axiales aleatorias encontrándose que la respuesta de tales configuraciones queda razonablemente explicada, tanto cualitativa como cuantitativamente, con las teorías presentadas. El

punto más débil del estudio realizado se refiere sin duda a la precariedad de los datos experimentales y su consiguiente dificultad de análisis. Respecto a este punto, debe tenerse en cuena que las secuencias analizadas son marginales (no estaba previsto realizar estudios de esta naturaleza en los procedimientos del Experimento FLIZ) y, en consecuencia, la disponibilidad de estos datos experimentales ha sido, en cierta medida, casual.

5. APENDICE

5.1. Determinación de la densidad espectral

Sea la función Y(t) cuya densidad espectral $S_{YY}(\omega)$ se desea calcular. La transformada de Fourier $\mathbf{Y}(\omega)$ de la señal Y(t) viene dada por la expresión

$$\mathbf{Y}(\omega) = \frac{1}{\pi} \int_{-\infty}^{\infty} Y(t)\exp(-i\omega t)dt \quad , \tag{5.1}$$

y el módulo de $S_{YY}(\omega)$ es $|S_{YY}(\omega)| = |\mathbf{Y}(\omega)|^2$.

Para el cálculo de (5.1) se ha de conocer el valor de la función Y(t) para todo t. Como la duración de los registros es finita, en vez de $\mathbf{Y}(\omega)$ lo que se calcula es una estimación de la misma $\tilde{\mathbf{Y}}(\omega_k)$ en la forma

$$\tilde{\mathbf{Y}}(\omega_k) = \frac{2}{T} \int_{0}^{T} Y(t)\exp(-i\omega_k t)dt \quad , \tag{5.2}$$

donde $\omega_k = 2\pi k/T$.

Además, Y(t) es una señal muestreada, es decir, sólo se conoce para valores discretos de la variable t, lo que implica aproximar la integral por una suma evaluando las contribuciones elementales bien por la regla de los paralelogramos cuando los datos están equiespaciados (transformada discreta, Kay y Marple (1981)) o por trapecios cuando no lo están.

5.2. Errores en la estimación del espectro.

Las posibles fuentes de error a considerar en el proceso de estimación de la densidad espectral son:

1) Cuantización

Debido a que las medidas están tomadas con precisión finita. Este error puede ser considerado como un ruido en la señal cuya desviación típica es $\sigma_c = 0.29$ u, siendo u la unidad de la escala de medida (Bendat y Piersol (1971), pág. 232).

2) Aliasing

Según el teorema de Shannon, la máxima frecuencia determinable en una señal muestreada es la frecuencia de Nyquist, $f_m = 1/(2t_o)$, donde t_o es el intervalo de muestreo. En nuetro caso $t_o = 2$ s para la señal A(t) y $t_o = 1$ s para la B(t), es decir, $f_m = 0.25$ Hz ($\omega = 0.79$) y $f_m = 0.5$ Hz ($\omega = 1.57$) respectivamente.

3) Leakage

Si la longitud del registro no es un múltiplo del período de la señal armónica la potencia asociada a ese armónico se difunde a

las frecuencias próximas. Para corregir este efecto, en el caso de la entrada B(t), que es una señal aleatoria, se ha empleado un método habitual: dado que la contribución principal a este error se debe a los valores del registro en los extremos, se ha empleado el llamado filtro de Bingham con ventana de datos ahusada (Bendat y Piersol (1971), pág. 229, Newland (1975), pág 147) que consiste en multiplicar los datos originales por la función de ponderación

$$\begin{aligned} p(t) &= \frac{1}{2} K\left(1 - \cos\frac{10\pi}{T} t\right) && , \quad 0 < t < T/10 \\ p(t) &= K && , \quad T/10 < t < 9T/10 \\ p(t) &= \frac{1}{2} K\left(1 + \cos\frac{10\pi}{T} \left(t - \frac{9}{10}T\right)\right) && , \quad 9T/10 < t < T \end{aligned} \tag{5.3}$$

donde K = 1/0.875. Si la señal es armónica este error no se produce si se elige T de modo que coincida con algún múltiplo del período armónico. Este ha sido el caso de la señal A(t), como ya se explicó en § 3.3.

4) Limitación de resolución

La resolución en el campo de la frecuencia es del orden de la separación entre dos frecuencias consecutivas del espectro, de valor $\Delta f = 1/T$. La resolución puede mejorarse añadiendo ceros al registro, con lo que se aumenta el valor de T pero no se cambia el espectro, sólo se rellena al disminuir la separación entre frecuencias. En nuestro caso, sin haber introducido ceros, valores típicos son $T \sim 100$ s, $\Delta f \sim 0.01$ Hz ($\Delta\omega \sim 0.03$).

5) Carácter aleatorio de la señal

Enseña el análisis estadístico que para señales aleatorias

$$\sigma/m \simeq (ET)^{-1/2} \qquad (5.4)$$

donde σ es la desviación estándar de una medida cuya media es m, E es la anchura de banda efectiva de la ventana espectral (empleada en la transformada de Fourier) y T la duración del registro. Por otra parte, del análisis de un proceso aleatorio del tipo χ^2_j (donde j indica el número de grados de libertad estadísticos) se deduce que

$$\sigma/m = (2/j)^{1/2} \quad ; \qquad (5.5)$$

en consecuencia, $j \simeq 2ET$ (Newland (1975), pág. 108). Generalmente, y para una estimación aislada, es $E \simeq 1/T$, con lo cual resulta $j \simeq 2$ y $\sigma/m \simeq 1$ (la desviación es del orden de la media). El modo de mejorar la precisión, sin disminuir la resolución E, es promediar las estimaciones de registros adjacentes. Así, si es q el número de estimaciones espectrales aisladas $\tilde{S}_{YY_i}$, la estimación espectral suavizada (promediada) $\hat{S}_{YY}$ será

$$\hat{S}_{YY} = \frac{1}{q} \sum_{i=1}^{q} \tilde{S}_{YY_i} \; . \qquad (5.6)$$

Por otra parte, si la longitud de cada registro es T', la longitud total será $T = qT'$, la nueva anchura de banda efectiva $E' = 1/T' = q/T$, el número de grados de libertad $j' \simeq 2q$ y la desviación

$\sigma/m \simeq q^{-1/2}$ (Bendat y Piersol (1971), pág. 329). En nuestro caso, para la señal de entrada B(t), se han promediado ocho registros (q = 8) obteniéndose, de las tablas de distribución χ^2_j (Beauchamp y Yuen (1979), pág. 149), las siguientes acotaciones para intervalos de confianza del 50 % ($0.8 < \sigma/m < 1.4$) y del 80 % ($0.7 < \sigma/m < 1.8$).

Además de tener en cuenta las posibles fuentes de error señaladas, existe un parámetro de gran importancia para determinar la precisión de las estimaciones de la función de respuesta en frecuencia, y es la función de coherencia γ^2_{XY} (Bendat y Piersol (1971), pág. 339)

$$\gamma^2_{XY}(\omega) = \frac{|S^2_{XY}(\omega)|}{S_{XX}(\omega)S_{YY}(\omega)} \quad . \tag{5.7}$$

Para un sistema lineal es $\gamma^2_{XY}(\omega) = 1$, ya que la entrada y la salida están correlacionadas. Cuando en la ecuación (5.7) se emplean estimaciones de densidades espectrales, la función $\gamma_{XY}(\omega)$ indica para qué valores de el sistema presenta no linealidades o superposición de ruido en las señales.

Hay un error intrínseco en $\gamma_{XY}(\omega)$ que depende del número de grados de libertad estadísticos y que es adicional a los errores introducidos por sesgo en las estimaciones aisladas de las densidades espectrales (piénsese en el caso límite de una única estimación, j = 2, que proporcionaría el valor $\gamma_{XY}(\omega) = 1$ aunque las señales X e Y estuvieran totalmente desacopladas). Para minimizar este error sería necesario realizar un suavizado de las densidades espectrales aisladas (Bendat y Piersol (1971),

pág. 193). En nuestro caso el número de datos de la función A(t) para una misma esbeltez es insuficiente para obtener varios registros y realizar el suavizado (tendrían que ser registros muy cortos, con lo que disminuiría la resolución en frecuencia). Así pues, formalmente, los resultados obtenidos reflejan la forma de la función de transferencia de un modo cualitativo, caracterizada por la presencia de una frecuencia de resonancia cuya relación de amplificación es mucho mayor que la de las otras frecuencias, caso típico de los sistemas poco amortiguados.

5.3. Técnicas de excitación

El objetivo de este apartado es comparar las diversas posibilidades de excitación que se ofrecen para determinar la función de transferencia de puentes líquidos. Las técnicas de excitación más comunes (García de Jalón y otros (1981), pág. 219, Ewins (1984), pág. 125) se resumen en el cuadro siguiente. Las secuencias analizadas en nuestro caso podrían englobarse en el punto 7 que, a posteriori, resulta similar al punto 2.

TIPOS DE EXCITACION

Tipo 1: Barrido de frecuencias

Excitación: Armónica (frecuencia variando lentamente o en escalones)
Ventajas: Control preciso de la excitación (para estudiar no-linealidades del sistema).
Máxima SR, Mínima PE.
Equipo barato.
Desventajas: No aconsejable para sistemas no-lineales.
Lento.

Tipo 2: Aleatorio

Excitación: Aleatoria.
Ventajas: Los promedios sobre muestras con diferentes señales de excitación dan la mejor aproximación lineal para sistemas no lineales.
Apropiado para ajuste teórico de las funciones de transferencia.
Más rápido que el tipo 1.
Control de la amplitud global de la excitación.
Buena SR y PE.
Desventajas: Baja resolución en sistemas con baja amortiguación (se evita con zoom).
Errores de "leakage" (se evitan con ventana de Hanning pero esto perjudica la resolución en frecuencia y da un aumento aparente de amortiguamiento en sistemas poco amortiguados).

Tipo 3: Pseudo-Aleatorio

Excitación: Aleatoria con período T (espectro de la excitación generado por el analizador).
Ventajas: En sistemas lineales, con buena calidad de señal, no hace falta promediar.
Mejor control de la excitación que en el tipo 2.
Elimina errores de "leakage".
Rápido.
Elevada SR, energía concentrada en las frecuencias de análisis.
Desventajas: Por ser periódico, resalta las no-linealidades, dificultando la obtención de parámetros modales en sistemas no-lineales.

SR: Relación señal/ruido
PE: Relación pico-valor eficaz
T: Período de muestreo del sistema de medida
FT: Transformada de Fourier

TIPOS DE EXCITACION (Cont.)

Tipo 4: Periódico Aleatorio

Excitación: Conjunto de etapas pseudo-aleatorias, tomando una muestra en cada etapa.
Ventajas: Mejor señal para determinar parámetros modales.
Similar al tipo 2 para sistemas no-lineales. Los promedios eliminan las no-linealidades.
Control de la señal y el espectro.
Elimina errores de "leakage"
Buena SR, energía concentrada en las frecuencias de análisis.
Desventajas: Lento, porque hay que alcanzar el etado estacionario en cada etapa, pero menos que el tipo 1.
Requiere equipo adicional para producir las señales pseudo-aleatorias.

Tipo 5: Impacto

Excitación: Aplicación de percusión.
Ventajas: Tiempos de preparación cortos.
Equipos baratos.
Rápido (si el ruido de las medidas es pequeño).
Apropiado cuando es difícil fijar un excitador (elementos pequeños).
Desventajas: Alta PE, no aconsejable para sistemas muy no-lineales.
Poca energía comunicada, baja SR.
Precauciones para evitar saturación de los equipos de la cadena de medida.
Si el amortiguamiento es pequeño necesita T grandes.
Si el amortiguamiento es grande, el ruido es importante.

Tipo 6: Relajación de carga

Excitación: Descarga de fuerza aplicada.
Ventajas: Para pequeños y grandes elementos.
Fácil control de la magnitud y dirección de la excitación.
Elevada energía a bajas frecuencias.
Desventajas: Más difícil de aplicar que el tipo 5.
Difícil calcular FT.

Tipo 7: Fuerzas en funcionamiento

Excitación: Desequilibrios generados durante el funcionamiento.
Ventajas:
Desventajas: Dificultad de medida de las fuerzas excitadoras.
Existencia de varias fuentes de excitación.

SR: Relación señal/ruido
PE: Relación pico-valor eficaz
T: Periodo de muestreo del sistema de medida
FT: Transformada de Fourier

REFERENCIAS

ALESSIO, C., CERRATO, R., D'ADDA, C., LEVIZZARI, G., MARTINELLI, G., CERONETTI, G. & ANTONUCCI, G. 1977 Fluid Physics Module, ESA Contract 3122/77/F/HGE(SC), Final Report.

BEAUCHAMP, K. & YUEN, C. 1979 Digital Methods for Signal Analysis, George Allen & Unwing, London.

BENDAT, J.S. & PIERSOL, A.G. 1971 Random Data: Analysis and Measurement Procedures, Wiley-Interscience, New York.

DA RIVA, I. & MARTINEZ, J. 1986 Floating liquid zones. Naturwissenschaften 73, 345-347.

EWINS, D.J. 1984 Modal Testing: Theory and Practice, Research Studies Press, Letchworth, Hertfordshire, UK.

GARCIA DE JALON, J., GIMENEZ, J.G., FLAQUER, J., BASTERO, C., SERNA, M. & NO, M. 1981 Teoría y Práctica del Análisis Modal, E.S.I. Industriales, San Sebastián.

HAMACHER, H., MERBOLD, U. & JILG, R. 1986 The microgravity environment of the D1 Mission, 37th IAG Congress, Innsbruck, paper IAF-86-268.

HAMACHER, H., JILG R., & MERBOLD, U. 1986 Analysis of microgravity measurements performed during D1, 6th European Symposium on Material Sciences under Microgravity Conditions. Bordeaux.

KAY, S.M. & MARPLE, S.L. 1981 Spectrum analysis - A modern perspective. Proc. of th EIEEE 69, 1380-1419.

LANGBEIN, D. 1986 Physical parameters affecting living cells in space. XXVI Cospar Meeting, Toulouse, Paper F.3.4.

MARTINEZ, I. 1986 Stability of liquid bridges. Results of SL-D1 experiment, 37th IAF Congress, Innsbruck, paper IAF-86-272.

MARTINEZ, I. & MESEGUER, J. 1986. Floating liquid zones in microgravity, Norderwey Symposium on Results of Spacelab-D1 Mission, Norderwey, FRG.

MESEGUER, J. 1983a The breaking of axisymmetric liquid bridges. J. Fluid. Mech. 130, 123-151.

MESEGUER, J. 1983b The influence of axial microgravity on the breakage of axisymmetric slender liquid bridges. J. Crystal Growth 62, 577-586.

MESEGUER, J., MAYO, L.A., LLORENTE, J.C. & FERNANDEZ, A. 1985 Experiments with liquid bridges in simulated microgravity. J. Crystal Growth 73, 609-621.

MESEGUER, J., SANZ, A. & LOPEZ, J. 1986 Liquid bridge breakages aboard Spacelab-D1, J. Crystal Growth, en prensa.

NEWLAND, D.E. 1975 Vibraciones Aleatorias y Análisis Espectral, Editorial AC, Madrid.

RIVAS, D. & MESEGUER, J. 1984 One-dimensional self-similar solution of the dynamics of axisymmetric slender liquid bridges. J. Fluid Mech. 138, 417-429.

SANZ, A. 1985 The influence of the outer bath in the dynamics of axisymmetric liquid bridges. J. Fluid Mech. 156, 101-140.

ZIMMERMANN, P. 1979 The german microgravity laboratory for material science and space processing experiments. Growth of protein crystal by diffusion into Sodium solution. A material science experiment in Spacelab. 30th IAF Congress, Munich.

FIGURAS

Figura 1. Geometría y sistema de coordenadas del puente líquido. FD indica el disco de inyección (Feeding Disk) y RD el opuesto (Rear Disk).

Figura 2. Respuesta en frecuencia del puente líquido según los modelos unidimensionales autosemejante linealizado (líneas continuas) y lineal (líneas a trazos). ω es la pulsación adimensional y los números en las curvas indican la esbeltez de la columna líquida. En esta figura, por razones de escala, en vez de la función de transferencia $H(\omega)$ se ha representado su raiz cuadrada.

Figura 3. Influencia, en variables de semejanza, de la deformación inicial α_o y la perturbación media β en el período de oscilación Θ_T de puentes líquidos (oscilaciones infinitesimales). Resultados obtenidos mediante integración del modelo autosemejante completo. La línea de trazos indica, para cada β, el valor de α_o de equilibrio.

Figura 4. Resultados del modelo autosemejante: variación con la perturbación β de la deformación del puente líquido α_{oe} y del período de oscilación para amplitudes infinitesimales alrededor de la posición de equilibrio, Θ_{Te}. Las curvas a y b corresponden al modelo autosemejante completo mientras que en la curva c se ha representado la expresión (2.36).

Figura 5. Orientación de los ejes de medida (u,v,w) y posición relativa de los acelerómetros del MSDR respecto al puente líquido. Obviamente en esta figura la columna líquida no está dibujada a escala.

Figura 6. Variación con el tiempo del valor medio de la perturbación B(t) según el eje v en un caso típico. El registro mostrado cubre un período de tiempo que incluye una de las secuencias analizadas (Run 5).

Figura 7. Densidad espectral de la parte aleatoria de la perturbación según el eje v, $\hat{S}_{BB}(\omega)$, calculada promediando ocho estimaciones aisladas. Los círculos corresponden a los valores nominales calculados y las líneas quebradas inferior y superior indican el margen de error. La línea doble señala el valor medio de la densidad espectral.

Figura 8. Variación con el tiempo de la deformación de la entrefase, medida con la función A(t), ecuación (3.1), para cada una de las secuencias analizadas (véase la Tabla 2). En los gráficos se indica también la velocidad de rotación de los discos, Ξ, adimensionalizada en la forma $We = \rho \Xi^2 R_o^3/\sigma$ (líneas gruesas).

Figura 9. Dependencia de la función de transferencia de la longitud del registro de la función A(t). Los resultados corresponden al Run 4. Los símbolos indican el número de datos del registro según la clave indicada en la figura.

Figura 10. Función de transferencia $H(\omega)$ de un puente líquido de esbeltez 2.571 y volumen 16.28. Los símbolos indican el número de puntos del registro de la señal A(t) de acuerdo con la siguiente clave: 54 (△), 59 (□), 64 (○). Las curvas indican resultados teóricos obtenidos con el modo autosemejante linealizado (línea continua) y lineal (línea de trazos).

Figura 11. Función de transferencia $H(\omega)$ de un puente líquido de esbeltez 2.714 y volumen 16.82. Los símbolos indican el número de puntos del registro de la señal A(t) de acuerdo con la siguiente clave: 40 (△), 47 (□), 53 (○). Las curvas indican resultados teóricos obtenidos con el modo autosemejante linealizado (línea continua) y lineal (línea de trazos).

Figura 12. Función de transferencia $H(\omega)$ de un puente líquido de esbeltez 2.854 y volumen 18.84. Los símbolos indican el número de puntos del registro de la señal A(t) de acuerdo con la siguiente clave: 24 (△), 32 (□), 40 (○). Las curvas indican resultados teóricos obtenidos con el modo autosemejante linealizado (línea continua) y lineal (línea de trazos).

Figura 13. Función de transferencia $H(\omega)$ de un puente líquido de esbeltez 2.857 y volumen 17.92. Los símbolos indican el número de puntos del registro de la señal A(t) de acuerdo con la siguiente clave: 88 (△), 98 (□), 108 (○). Las curvas indican resultados teóricos obtenidos con el modo autosemejante linealizado (línea continua) y lineal (línea de trazos).

Figura 14. Variación con la esbeltez Λ de la frecuencia de resonancia, ω_r. Los cuadrados indican resultados experimentales y los círculos resultados teóricos obtenidos con el modelo autosemejante completo (●) y linealizado (○) para configuraciones con la misma esbeltez y volumen que las experimentales. La curva indica resultados del modelo lineal (volumen cilíndrico).